UNIVERSITAT POLITÈCNICA DE CATALUNYA
BARCELONATECH
Escola Superior d'Enginyeries Industrial, Aeroespacial i Audiovisual de Terrassa

Titulació:

MÀSTER UNIVERSITARI EN ENGINERIA AERONÀUTICA

Alumne:

ORIOL ALMIRALL TORIBIO

Enunciat TFM:

ESTUDI: DISSENY I MESURA DE TÈXTILS APANTALLANTS/ANTIRADIACIÓ ELECTROMAGNÈTICA PER A PROTECCIÓ

Director del TFM:

IGNACIO GIL GALI

Convocatòria de lliurament del TFM:

QUADRIMESTRE PRIMAVERA 2018-2019

Universitat Politècnica de Catalunya

ESEIAAT

Disseny i mesura de teixits apantallants/antiradiació electromagnètica per a protecció

Author:
Oriol Almirall Toribio

Supervisor:
Prof. Ignaci Gil Gali

A thesis submitted for the degree of

MSc Aeronautical Engineering

June 20, 2019

Abstract

Durant els darrers any s'han desenvolupat diversos estudis relacionats amb els metamaterials. La possibilitat d'aconseguir noves propietats més enllà de les pròpies dels materials convenvionals ha obert noves vies d'estudi. D'entre els diferents camps d'investigació en els quals els metamaterials i les superfícies selectives de freqüència estan involucrats, la seva aplicació en metamaterials tèxtils per tal de crear peces de roba i elements portàtils és un dels més nous i sobre els quals menys s'ha investigat.
Per aquesta raó, i per tal de demostrar que es tracta d'un camp important en el qual es poden obtenir resultats molt interessants mitjançant mètodes convencionals, en aquesta tesi es dissenya una superfície selectiva de freqüència a base de teixit i fil conductor.

Per aconseguir-ho, el primer pas és optimitzar la geometria mitjançant simulacions informàtiques fins a aconseguir les propietats electromagnètiques desitjades. Una vegada fet això, la cel·la unitat dissenyada és emprada per fabricar una superfície més gran, la qual és provada i els resultats obtinguts comparats amb els de la simulació.

Mitjançant aquest experiment, es demostra que malgrat que la superfície fabricada no és exactement idèntica a la simulada a causa de les imperfeccions i irregularitats inherents a qualsevol procés mecànic real, les propietats aconseguides són gairebé les mateixes que les simulades, obtenint nivells similars d'absorció i un petit desplaçament en freqüència.

Degut a que la superfície emprada en aquesta tesi és relativament petita, provar superfícies més grans per aproximar millor la hipòtesi d'extensió infinita i millorar el procés de fabricació són els següents passos a seguir per tal de millorar una tecnologia que es demostra útil, possible i a l'abast.

In recent years several studies regarding metamaterials have been carried out. The possibility of reaching new properties further from the ones offered by conventional materials has opened new ways of study. Among the different fields of investigation in which metamaterials and frequency selective surfaces are involved, applying them on fabrics and creating wearable structures is one of the newest, and still few investigation has been done on it since, although its potential applications, it is still difficult to reach good results.
For this reason, and in order to prove that this is an important field in which very interesting results can be obtained by means of conventional procedures, in this thesis a FSS based on fabric and conductive thread is designed.

To do so, the first step is to optimize the geometry using computer simulations until reaching the desired electromagnetic properties. Once done that, the designed unit cell is applied in a larger surface, which is tested and the obtained results compared to the ones given by the simulation.

By doing this, it is proved that, although the final crafted surface is not exactly the same that the designed one because of the imperfections inherent in any construction process the properties reached are almost the same, offering similar levels of absorption and a small shift of frequency.

Since the surface tested in this thesis is relatively small, testing bigger surfaces in order to better approximate the infinite extension hypothesis and improve the construction process are the logical steps to follow in order to improve a technology which has already been proved to be useful, possible and within reach.

Contents

List of Figures

List of Tables

Nomenclature

A	Absorption Factor / Absorbance / Absorptivity
AD	Artificial Dielectric
AFA	Antenna-Filter-Antenna
AM	Amplitude Modulation
AMC	Artificially Magnetic Conductor
A-SBFA	Advanced Short Backfire Antenna
C	Capacitance
BW	Bandwidth
BWM	Backward Wave Media
CRLH	Composite Right-/Left-handed
CST	Computer Simulation Technology
d	distance
DANL	Displayed Average Noise Level
DNG	Double Negative Media
E	Electric Field
EBG	Electromagnetic Bandgap
EMC	Electromagnetic Compatibility
EMI	Electromagnetic Interference
E_i	Incoming Wave
E_r	Reflected Wave
E_t	Transmitted Wave
EM	Electromagnetic
ERTA	Extended Range Transmission Analysis
ESA	European Space Agency
EUT	Equipment Under Test
f	frequency
FM	Frequency Modulation
f_r	Ressonance Frequency
FSS	Frequency Selective Surface
FWHM	Full-width at half-maximum
H	Magnetic Field
IR	Infrared
k	Phase Vector
L	Inductance
LH	Left Handed Material
LWA	Leaky Wave Antenna
MoM	Method of Moments
MTM	Metamaterial
MW	Microwave
n	Index of refraction
NIM	Negative Index Material
OTA	Over-the-air
PBC	Perfect Boundary Conditions
PBG	Photonic Bandgap
PEC	Perfect Electric Conductor

R	Resistance
RF	Radio frequency
RFID	Radio Frequency Identification
RSE	Radiated Spurious Emissions
rx	Receiver
S	Poynting Vector
$\hat{s}$	EM wave propagating direction
t	thickness
T	Transmission Coefficient
TE	Transverse Electric
TDR	Time-domain Reflectometer
TM	Transverse Magnetic
TOI	Third Order Intercept
tx	Transmitter
VSWR	Standing Wave Ratio
WLAN	Wireless Local Area Network
ε	Electric Permittivity
Γ	Specular Reflection Coefficient
λ	wavelenght
μ	Magnetic Permeability
θ	look angle

Chapter 1

Introduction

1.1 Objectives

The main objective of this thesis is to design, set up and test a frequency selective surface based on fabric and conductive thread in order to assess its feasibility and compare the results obtained in the testing phase with the simulated ones.

At the same time, some secondary objectives have been established. These are obtaining a deeper knowledge on metamaterials and their state of the art and become proficient in the use of the professional software Computer Simulation Technology (CST).

1.2 Scope

In this project a brief state of the art on metamaterials is presented. In this section a breakdown on the different kinds of existing metamaterials is given and, later on, the focus is centered on the ones of interest for this project, the electromagnetic metamaterials. At this point some information about their functioning, properties, history and current and future applications is given.
The last part of this section is devoted to the current state and properties of the wearable metamaterials for electromagnetic shielding, being the most important issue how do they work, why are they useful, how are they designed and which are their properties. It is part of the project determining how the different sizes affect the final performance. However, falls out of the scope of the project everything strictly related with the embroidering part, like the weaving technique or the thread used.

With the information obtained in the first part a first sample case is done. This case is extracted from a paper and its purpose is, on one hand, to help gaining expertise on the use of the required software and, on the other hand, obtaining similar results to the ones offered in the paper serves as a validation of the simulation process done. This section is also useful to set the final parameters of the solver to optimize the precision and the computational time.

Once clear how to simulate the desired type of metamaterial the optimization is done. To do so, a first approximation to the optimal sizes is done using bibliographic sources and, after that, several sweeps around the expected optimal values are done until reaching the best one. This procedure is repeated for different geometric combinations at two different frequencies and using two different unit cells.

Finally, the most optimal combinations are built and tested and the obtained results compared with the ones from the simulations.

Is out of the scope of this project the study of the embroidering process and weaving technique, as well as the optimization of the measuring process.

1.3 Requirements

In order to obtain satisfactory results some basic requirements are set:
In the first place, design has to be done considering only conventional and available fabrics and materials, without the consideration of any other element.

It is also mandatory that the tested results agree with the ones from the simulations, allowing just differences that can be explained considering the differences that always exist between the reality and the simulations.

Finally, it is important to note that, since computational power is limited, it is an important parameter to be taken into account when setting the simulations.

1.4 Contributions

The amount of electromagnetic radiation to which humans are exposed is increasing every year due to the uses and necessity of electrical energy, since all electrical equipment emit electromagnetic field in various frequency bands.

Then, although the use of EM waves is increasing day by day, the negative effects on the human health result from the establishment of many stations are being discussed. For this reason, some way of protecting people from electromagnetic radiation more feasible than heavy suits or other rigid elements is needed and, since clothes are the only element that humans always have on us, they happen to be the best option.

Tiny electrical currents exist in the human body due to several chemical reactions happening on it as part of the normal body functions (nerves transmitting electric impulses, digestion...). Apart from that, existing electric fields influence the human body inducing circulation currents within. To date, no adverse health effect produced by low-level long term exposure radiofrequency has been demonstrated, although this is an issue that concerns population and on which scientists are still investigating.

Nevertheless, what is true is that electromagnetic fields above certain levels can trigger biological effects. In addition, a look at the news headlines of recent years allows to understand how important the effect of radiation is becoming to people. Television, Wi-Fi, mobile phones, microwaves oven... all these devices have been, at some point, at the focus of health concern. For this reason, several international programs have been carried out in order to quantify these effects, being the most important of them the International EMF Project. This project did not confirm the existence of any health consequences from exposure to low-level electromagnetic fields. However, some gaps in knowledge about biological effects exist and need further research [17] [18] [19] [20]. Apart from this possible biological hazard, as the number of electromagnetic signals is increasing, interference is becoming an issue. Cost and complexity for isolation/shielding mechanisms is one of the main points when designing electronic devices [21] [3].

So, to sum up, electromagnetic shielding is necessary for both reducing the interference among the different near devices and to protect some systems for security issues. At the same time, since electromagnetic radiation has some effects on the human body protecting humans of it is also a key point and, maybe, the most difficult one, since humans have complex and variable shapes, non-constant humidity degree... In addition, inside this group there are two main types of electromagnetic radiation: the one with high energy and that directly produces changes in human biology and the low energy one, which is still not proven to have negative effects on the human body, although the concern on this aspect is growing fast among the population.

To fight against this, the use of frequency selective surfaces has appeared as an excellent method in most of the cases. However, when it comes to protecting people, the rigid and expensive materials usually used to produce them make it non-viable. With this in mind, in this thesis the use of this technology applied to fabrics is presented. Although some research has been already done is still a very new and promising field of investigation. By applying the frequency selective surfaces concept to fabrics, apart from the conventional applications, a whole new world of clothes, curtains and other low-weight, high-versatility applications opens up. For this reason, this project offers a methodology and a prove of a simple and low-cost method to do it.

Chapter 2

Background

In this chapter a first description for the word metamaterial is given along with some basic principles and applications. After that, and once having broken down the different kinds of metamaterials the focus is centered in the frequency selective surfaces (FSS) kind, more specifically in the ones of interest for the desing proposed in this thesis: Basic element, single layer, absorber, wearable and textile FSS.

After that, some basics of electromagnetics and CST Studio Suite are given, in order to make the further analysis and discussions fully understandable.

2.1 Metamaterials and FSSs

2.1.1 Metamaterials

A metamaterial is a synthetic composite material with a structure such that it exhibits properties not usually found in natural materials [22]. That is, a class of material engineered and designed to produce properties that do not occur naturally. In addition, these properties are more usually derived from the periodic structure rather than from the components themselves.

Although there exist different kinds of metamaterials (elastic, acoustic, structural...) the main interest is focused in the **electromagnetic metamaterials** (from now on, for the sake of simplicity referred simply as metamaterials).
While almost all the materials that can be found in nature have positive electrical permittivity, magnetic permeability and index of refraction (some exceptions could be low loss plasmas, metals and semiconductors at optical and IR range for negative permittivity [3]), these new artificially created materials (catalogued as negative index materials (NIM) or double negative (DNG) media or left handed (LH) materials or backward wave media (BWM)) exhibit negative values for these parameters [23].
Along with metamaterials, a wide number of new concepts has appeared [24]: Frequency Selective Surfaces (FSS), electromagnetic/photonic bandgap materials (EBG/PBG), plasma structures, left-handed medium (LHM), Artificial Magnetic Conductors or fractal elements. In Fig. 2.1 the different kinds of existing metamaterials are presented.

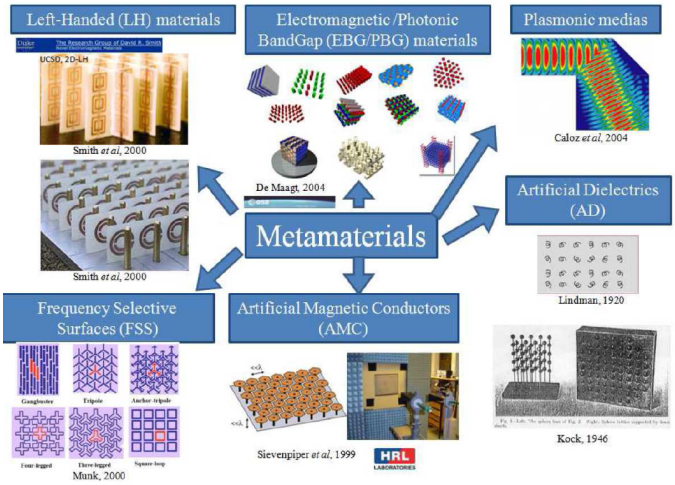

Figure 2.1: Scheme of the existing types of metamaterials [1].

2.1.2 Properties of the electromagnetic metamaterials

The main determinants of the response of a material to electromagnetic waves are the electric permittivity ε and the magnetic permeability μ, that determine its response to the electric and the magnetic field respectively. Then, as the refractive index is defined as $n = -\sqrt{\epsilon\mu}$, it also becomes negative. Hence, when light enters from the vacuum to the metamaterial, it bends in the opposite direction, as can be seen in Fig. 2.2.

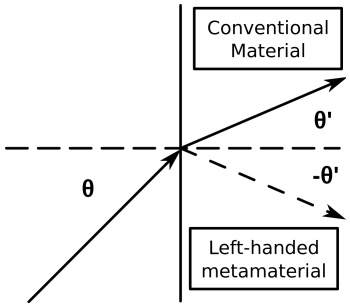

Figure 2.2: Refraction in a normal material and in a metamaterial (LH) [2].

Due to this property, when there is a change in the sign of ϵ and μ in the Maxwell's equations it appears a left-handed triplet of electric field **E**, magnetic field **H** and phase vector **k**. So, as for the normal materials it is a right-handed vector, this fact implies that the Poynting vector **S** and the group velocity are in the opposite direction. As a result of that the waves move in a backwards fashion (the wave phase appears to undulate backward while the energy propagates along the incident in a forward direction). The phase vector specifies the direction of the phase velocity, while the direction of the propagation of the energy is given by the Poynting vector.

Apart from that, the reverse Doppler effect is another strange property of metamaterials which is still under investigation for its application in mobile wireless communication [23]. Also, reverse Cherenkov effect can be appreciated. This means that, in a metamaterial, a charged particle passing through it emits light from a cone behind the particle instead of in front of it, as happens in regular materials. As Cherenkov radiation occurs when a charged particle moves in a medium faster than the light in this same medium, one possible application in particle physics could be the construction of a Cherenkov detector to indentify charged particles of different velocities[25].

2.1.3 Applications of Metamaterials

The following section is devoted to some of the main current application of the Metamterials as a concept, in order to give a first look at the State of the Art of the technology.

Guided Wave Application

Some guide-wave components that are currently being developed using MTM are: couplers, phase shifters, power dividers and mixers.
Arbitrary coupling-level impedance and phase couplers, multilayers super-compact structures, zeroth-order resonators with constant field distribution and tight coupled-line phase or impedance couplers are also under investigation.
For example, in Fig. 2.3 can be seen a CRLH impedance coupler where arbitrary coupling level is based on a new principle of even/odd modes coupling with unbalanced CRLH gaps [26]. Coupling depends on the length of the structure which is not $\pi/2$.

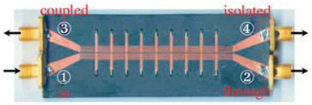

Figure 2.3: Arbitrary coupling-level-edge-coupled impedance microstrip coupled-line coupler [3].

Radiated Wave Application

Some 1D and 2D Leaky-wave antennas and reflectors with unique functionalities have been designed [27]. For example, Fig. 2.4 shows the example of 1D frequency-scanned back-fire-to-endfire antenna [26] and Fig. 2.5 corresponds to an electronically scanned backfire-to-endfire antenna [28].

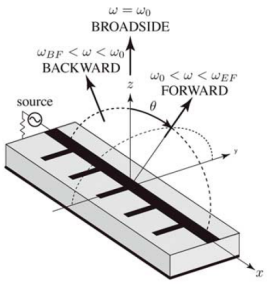

Figure 2.4: Frequency-scanned back-fire-to-endfire 24-cell LW antenna [3].

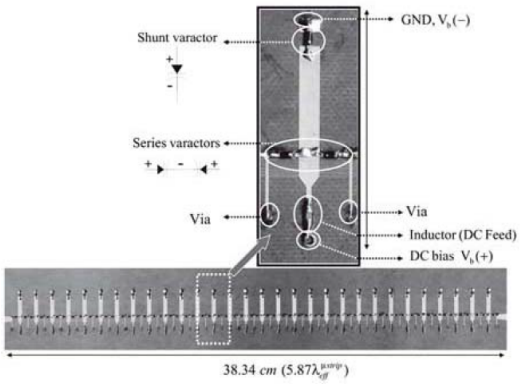

Figure 2.5: Electronically-scanned back-fire-to-endfire 30-cell LW antenna including reverse-biased varactor diodes for beem-steering [3].

The conventional configuration of a LH LWA (Leaky wave antenna) for microwave applications is a series of interdigital capacitors and shunt stubs connected with vias to the ground.

Refracted Wave Application
By now this domain of application is conceptual but promising [29] [30].

Future Applications
According to [26], some of the countless envisioned applications for MTMs and CRLH structures are:

- Versatile tunable MTM devices including distributed thin-film ferro-electric and ferro/i-magnetic materials such as filters, resonators, antennas.
- Anisotropic minimum-impedance-path metamaterials inspired from the Fermat's principle in optics, to mold the flow of electromagnetic energy.
- Miniaturized devices based on CRLH zeroth-order resonance or super slow-wave effect.
- Nonlinear MTM devices.
- Full-space scanning 2-D LW antennas.
- Active MTMs (this is a totally unexplored area to date).
- Refracted-wave applications.

Other Applications of Metamaterials

Apart from the already mentioned applications for high-frequency, some other applications are discussed in [3] for different fields:

- **Perfect Lens**. Since lens are based on curved surfaces and these surfaces focus light by means of the refractive index contrast, no lens can focus light onto an area smaller than a square wavelength. Then, as an unconventional approach, in a parallel side slab of MTM both the propagating and evanescent waves contribute to the resolution of the image.
- **Application in Automotive**. These new types of electromagnetic devices and components will open up a new field of automotive electronic devices such as beam scanned antenna for radar and mobile communications, novel magnetic materials for electric motors, the high performance absorbing and shielding materials for electromagnetic compatibility, and optical devices like LED headlights and night vision using infrared cameras [31].
- **Cloaking Effect**. Making a device invisible to the eye. There is a lot of research in this area. An object is invisible if it does not reflect waves back to the source and does not scatter them in any other direction. Current studies are based in both shape and metamaterials to accomplish so [32].

Space Applications

Special attention deserve the latest applications on Space, since the use of metamaterials for applications in space has been one of the main fields of study of the ESA for the last 20 years. Among the most notorious proposed applications the most outstanding and suitable for future application in real projects are the ones related with cloaking and antennas.

For instance, in [33] an electromagnetic cloaking device working at microwave frequencies is presented and, once studied the results, this system is extended to optical frequencies for cylindrical and spherical electomagnetic cloaks. To do so, the design is based on the use of layered structures of alternate plasmonic and non-plasmonic materials in order to reach the collective behavior of an effective epsilon-near-zero material.
The application presented in [34] is also related to the electromagnetic cloaking but, in this case, the approach is by means of the magnetization and the radar cross section. In addition to a transformation optics for achieving magnification and high resolution in hyperlenses.
At its turn, in [35] a detailed study of the different metamaterials for cloaking purposes is presented. Then, the obtained results are compared with the ones that can be found in literature in order to assess the suitability of its application on space, leading to interesting conclusions related with the design of metamaterials that transform fields in a desired way.

Apart from cloaking, the other major field of application in space is in antennas for augmentation purposes. As an example, in [4] an Advanced Short Backfire Antenna (A-SBFA) augmented with metasurfaces is presented. This system allowed to achieve a very high aperture efficiency across two frequency bands, achieving a performance unprecedented for any antenna of widespread use. This is a very illustrative example of how metamaterials, when applied to conventional technology, can provide significant performance enhancements.
In Fig. 2.6 a 3D view of the assembled A-SBFA is shown, presenting the 3D-printed aluminum cavity, feed antenna and subreflector, as well as cooper metasurfaces etched on a thin substrate and separated from cavity walls by a low permittivity foam layer.

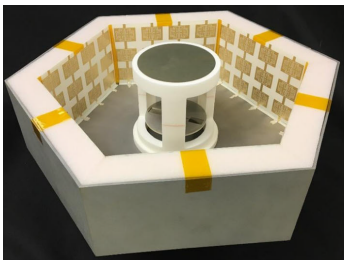

Figure 2.6: View of the assembled A-SBFA [4].

2.1.4 Frequency Selective Surfaces FSS

A frequency-selective surface (FSS) is a structure consisting most typically of two-dimensional periodic elements, as depicted in Fig. 2.7. Here the periodic array of slots (or apertures) in a perfect conducting sheet act as a *bandpass* filter, namely, *passing* waves at the resonant frequency of the slots but rejecting them at higher and lower frequencies. On the contrary, the array of conducting patches act as a *bandstop* filter, namely, *rejecting* waves at the patches resonant frequency but passing them at higher and lower frequencies, as can be seen in Fig. 2.8. In the case of freestanding and thin grids without dielectrics, the filtering performances of the patch element FSS and aperture FSS are exactly complementary to each other [6]. However, when the area of the aperture is equal to the unit cell (a wire-mesh type), there is a limitation for the aperture-type FSS [36].
The existence of the resonating size of array element causes the emergence of the side lobes in the transmitted and reflected fields (see 2.1.7), which are the defining feature of FSSs. However, as compared to the FSSs, the resonating element and unit cell of metasurface is relatively much smaller than the wavelength and it helps to eliminate the grating lobes in the frequency response. Therefore, FSSs in the terahertz domain are usually termed as metasurfaces [37].

Low profile, reduced periodicity, dual polarization, angular stability, multi-pole frequency response with higher out-of-band rejections, and easy manufacturability are some of the desired properties of FSSs. Nevertheless, achieving all the aforementioned characteristics for an optimized design has been a challenge for the FSSs designers [9].

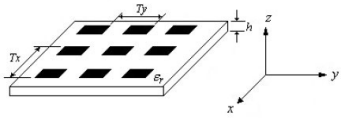

Figure 2.7: FSS structure [5].

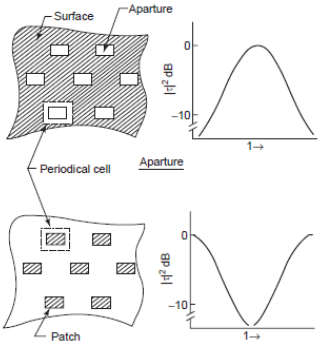

Figure 2.8: Typical filtering characteristics of aperture and patch elements FSS [6].

2.1.5 Principle of Periodic Structures

A periodic surface is formed when identical elements are arranged in an infinite array of one or two dimensions [9].
There are two basic ways of exciting a periodic array: by means of an incident plane wave (passive) or by the attached generators to individual element (active). In this thesis only the passive way will be considered. With this kind of excitation, the incoming plane wave (E_i) will be partially transmitted (E_t) in the forward direction and in part reflected (E_r) specularly. In the ideal condition of resonance and without grating globes (see 2.1.7), the amplitude of the reflected wave should be equal to the incident wave, while the transmitted signal should be equal to zero. The specular reflection coefficient (Γ) can be defined by (2.1).

$$\Gamma = \frac{E_r}{E_i} \tag{2.1}$$

In a similar way, the transmission coefficient (T) can be defined by (2.2).

$$T = \frac{E_t}{E_i} \tag{2.2}$$

The appropiate selection of FSSs array elements, shape, dimensions and substrate material is the most important part of the design process.
In [9], Munk explains the operational theory of FSS based structures: when EM waves incide a FSS structure, they incite electric currents into the array elements. The level of coupling energy defines the amplitude of the produced currents. However, these generated currents also work as EM sources and they create additional scattered fields. Incident EM fields combined with these scattered fields make up the resultant field in the surrounding of FSS. Consequently, the required currents and field characteristics can be obtained by properly designed elements that create the filter response.

Physically, when a unit cell of an FSS is illuminated by the EM wave, it can be converted to an equivalent resonance circuit. The resonance frequency can be found by (2.3), in which L and C represent the equivalent inductance and the capacitance of an FSS unit cell, respectively.

$$f_r = \frac{1}{2\pi\sqrt{LC}} \tag{2.3}$$

Choosing an appropriate array element is very crucial in designing FSS [7]. While various unit cell geometries have been implemented, out of which some are easily controllable and so more famous in FSS community. A classification of frequently used FSS elements types is summarized in [37] based on their resonant properties. For example, non–resonant element (patch, wire grid) can be modeled by a capacitance, whereas single resonant element (like loop, cross, dipole) can be represented by a series combination of capacitor and inductor. It is to note that the number of resonances has a direct relationship with the count of lumped elements.

There are two main ways to find the impedance and scatering properties of periodic structures [9]. The first one is mutual impedance method, which is linked to MoM, and the second one is the plane wave expansion approach, also called the spectral method. Periodic FSS structure can be

designed based on **Floquet theorem**, since by definition a periodic structure must be infinite in extent. A planar array which is infinite in x- and z- direction with identical inter-element spacing ($D_x = D_z$) as shown in Fig. 2.9 is termed as a truly periodic configuration (infinite $\times$ infinite). Then, the array is incident by an incoming EM wave propagating in certain $\hat{s}$ given in (2.4).

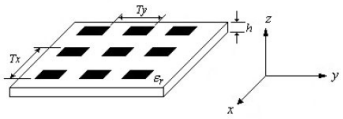

Figure 2.9: A true periodic structure showing inter-element spacing and element length of L [7].

$$\hat{s} = \hat{x}s_x + \hat{y}s_y + \hat{z}s_z \tag{2.4}$$

The amplitude of currents on the entire element will be equal, while the phase of the incident EM field will match with the phases of these currents. By Floquet's theorem, the element currents in column m and row n are given (2.5) [38].

$$I_{mn} = I_{0,0}e^{-j\beta mD_x s_x}e^{-j\beta nD_z s_z} \tag{2.5}$$

Then, using Ohm's law for reference element 0,0 gives (2.6)

$$V^{0,0} = \left[Z_L + \sum_{m=-\infty}^{\infty}\sum_{n=-\infty}^{\infty} Z_{0,mn}e^{-j\beta mD_x s_x}e^{-j\beta nD_z s_z}\right] I_{0,0} \tag{2.6}$$

and, array scan impedance is given by (2.7)

$$Z^{0,0} = \sum_{m=-\infty}^{\infty}\sum_{n=-\infty}^{\infty} Z_{0,mn}e^{-j\beta mD_x s_x}e^{-j\beta nD_z s_z} \tag{2.7}$$

2.1.6 Dielectric Loading Effects

Dielectrics are often used for stabilizing the drift of FSS resonant frequency with the steering of incident angle or for structural support [6], and has been proven that resonant frequencies decrease as the dielectric thickness increases [39].

The dielectric loading effect of a slot array is also dependent on the incident angle and the wave polarization. For TE incidence, the resonance decreases as the dielectric thickness increases (similar to the case of normal incidence). For TM incidence, a significant reduction in the dielectric loading effect is noticed as the Brewster angle (63°) is approached. At this angle the air/dielectric interface does not reflect incident waves, and the resonant frequency behaves similarly to that of the patch array. In fact, the angular stability of the slot arrays is lost for dielectric thickness greater than 1mm. However, if the dielectric is a multiple quarter-wavelength thick the resonant frequency becomes stable again [6].

One of the most important applications of dielectric loading is the multiband FSS design. For a multiband FSS application, the highest frequency generally determines the element spacing or lattice size [6].

In addition, for the FSS applications, the high-dielectric-constant substrate should be kept thin enough to prevent the generation of surface waves, especially at large incident angles. It should be noted that the surface wave (or Wood's anomaly; see 2.1.8) of an FSS grid embedded in dielectrics will not be eliminated, but only pushed higher in frequency, if the dielectric is thin. Furthermore, the occurrence of grating lobes is dependent on the physical size of the lattice and not of the presence of the dielectrics [40].

2.1.7 Grating Lobe Phenomenon

Grating or Bragg lobes are undesired secondary mainbeams occurring at angles with higher-order constructive interference when the lattice size becomes electrically large [7]. Since the periodic array elements behave similarly to the conventional array, the largest lattice size to avoid grating

lobes should obey the same rule that governs a conventional array antenna. A general rule to avoid grating lobes is that the lattice size should be less than one wavelength for the normal incident case (0° incident angle). For large incident angles, the spacing should be kept below half free-space wavelength.
Maximum spacing would depend, among other things, on the lattice type, as well as the incident frequency. As a general rule, this inter-element spacing can be found by means of the Grating Lobe Condition (2.8) [8], although the shape of the lattice has also a huge influence. In Fig. 2.11 some specific shapes are shown, demonstrating that the square lattice has the most closely packed elements, while the triangular lattice has the largest element spacing. The spacing requirements given in this figure prevent the peak of the grating lobe from entering real space. To avoid wasted energy, not even the shoulder region of the grating lobe should enter real space; therefore, the lattice size should be approximately two-thirds or less of that given in Fig. 2.11.

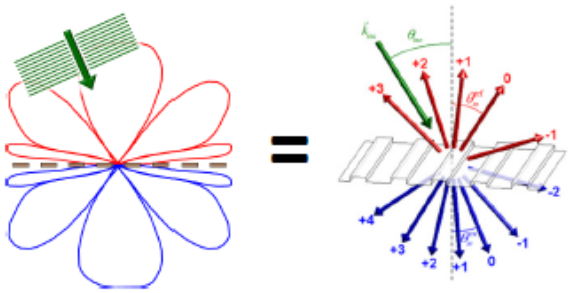

Figure 2.10: Schematic representation of the Grating Lobe Phenomenon [8].

$$k_0 n \sin\theta_m = k_0 n_{inc} \sin\theta_{inc} - \frac{2\pi m}{d_x}$$
$$n \sin\theta_m = n_{inc} \sin\theta_{inc} - m\frac{\lambda_0}{d_x} \tag{2.8}$$

where, according to Fig. 2.10,

n = refractive index around diffracted order
n_{inc} = refractive index around applied wave
d_x = interelement spacing (grating period)
m = ...,-2,-1,0,1,2,...

Lattice Type	Maximum Spacing	$\theta_0 = 0°$	$\theta_0 = 45°$
Square spacing	$\frac{a}{\lambda_0} < \frac{1}{1+\sin\theta_0}$	$\frac{a}{\lambda_0} < 1$	$\frac{a}{\lambda_0} < 0.59$
Triangular spacing	$\frac{a}{\lambda_0} < \frac{1.15}{1+\sin\theta_0}$	$\frac{a}{\lambda_0} < 1.15$	$\frac{a}{\lambda_0} < 0.67$
Brick spacing	$\frac{a}{\lambda_0} < \frac{1.12}{1+\sin\theta_0}$	$\frac{a}{\lambda_0} < 1.12$	$\frac{a}{\lambda_0} < 0.65$

Figure 2.11: FSS Lattice Types and Grating Lobe Criteria [7].

2.1.8 Wood's Anomaly Phenomenon

Wood's anomalies were first observed in the diffraction spectrum of optical gratings in 1902 [9]. These anomalies exhibit themselves as rapid variations in the intensity of the various diffracted spectral orders in certain narrow frequency bands, which could not be explained by the grating theory at that time [7]. These anomalies usually occur at frequencies near or higher than the resonant frequency of any periodic structure [40]. The frequency of Wood's anomaly is decreased

with an increase in the dielectric thickness. Further, for a slot array in free space, the Wood's anomaly will occur just below the frequency at which the grating lobe starts to propagate in real space, which for normal incidence on a rectangular grid array will first occur when the lattice size is one wavelength. It has been shown that these nulls are associated with a surface wave propagating along the surface of the array [40].

2.1.9 Types of FSSs

There are different ways of categorizing the FSSs on the basis of array element, structure design and application. Fig. 2.12 gives the taxonomy of the FSSs classification. Since there are so many different types of FSS and the aim of this study is not to present a full in-detail State of the Art of each one only the types of interest for the proposed design will be studied: **Basic Element Type**, **Single Layer**, **Absorber FSS**, **Wearable FSS**, **Textile FSS**, and only referring to other types when necessary for the full comprehension of the expressed ideas and/or decisions made.

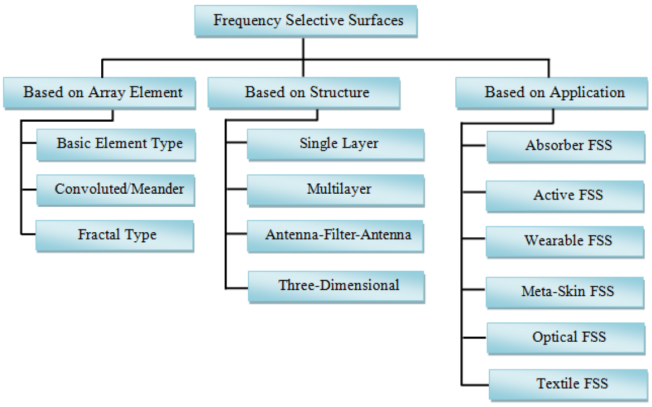

Figure 2.12: Classification of the different types of FSS [7].

2.1.10 Array Element: Basic Element Type

In general, four basic types of FSS element groups have been classified [9] and are illustrated in Fig. 2.13.
Depending on the potential application, FSS designers select an array element from any of these groups and/or use a combination of these as well. A good element should present a stable resonance response with the variation in incidence angles. Commonly, selecting a group-2 element with a larger loop area is beneficial and it enhances the bandwidth [9].

Square loops, simple circular loops to advance loaded elements with three or four legs have been utilized; especially hexagonal loop structures are useful for wideband applications. When circumference (perimeter) of the loop element becomes equal to a full wavelength, FSS reaches the resonance. It is found that an ample range of bandwidth can be achieved by changing the shape of these loop elements.

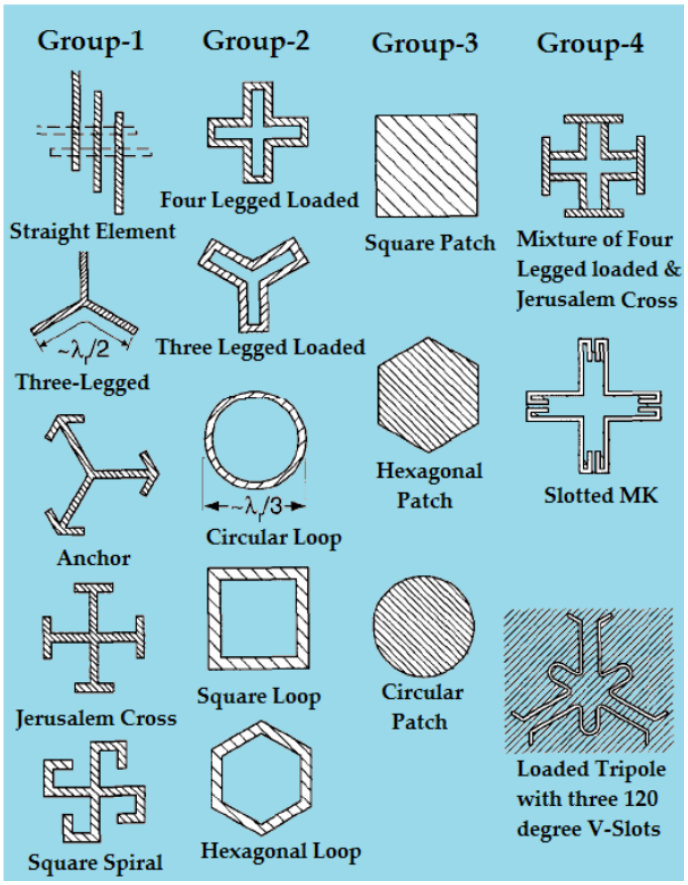

Figure 2.13: Typical shapes of FSS elements [9].

Nevertheless, the bandwidth of almost all types of FSSs can be varied by altering the inter-element spacing, which must be small in terms of the wavelength. If the inter-element spacing is greater than half of the wavelength, it will result in the early onset of the grating lobes, pushing the main resonance towards downside with varying incidence angles [7].

Such FSS resonates when the circumferencs is equal to the wavelength, depending on the effective permittivity and with convincingly large inter-element spacing [9]. The bandwidth increases when the inter-element spacing is reduced. On the other hand, at a certain closer distance, this increases the inter-element capacitance as well, thereby pushing the resonant frequency towards the lower side. To overcome this discrepancy and regain the desired resonant frequency, the circumference of an element should be reduced. Group-1 stands next to loop family. With proper design of elements in this group, inter-element spacing can be reasonably reduced to experience extremely large bandwidth. This way, the inception of grating lobes is significantly delayed. Group 3 consisting of solid interior elements are mostly used in combination with complementary elements that are adjacent to it.

Conventionally, the general attribute of FSSs is that they reach resonance at the desired frequency only when the patch or slot size in the unit cell becomes at least in the order of half of the wavelength. However, this limitation can be overcome by minimizing the electrical dimensions of the constituting element/inclusions at subwavelength level to ensure insensitivity to variations of incident angle and polarization [7].

Convoluted or Meandred FSSs and Fractal Based FSSs

Apart from basic elements other types of array elements exist. For applications demanding miniaturized FSS, especially where flexibility is a challenge like in radomes, convoluted FSSs are used. These FSSs offer the same electrical properties without affecting the angular stability with a much smaller dimensions. In addition, it is proved in [21] that the convoluted square loop FSS structures can present better stability in polarization as compared to the simple element. The concept of convoluting the elements to reduce the unit size is a constructive approach to tighten the curved

structures and evidently isolate the grating lobes effect from the fundamental resonance. However, manufacturing limitation falls on the way as a penalty to pack the resonating length to diminish the unit cell of a particular area.

Current applications of convoluted or meandred FSSs are for selective frequency isolation in office windows and increasing the reliability of mobile communications [41]. Despite all the advantages presented that make this kind of array such an attractive choice for smart applications requiring high stability in dual/multi band performance, the reduced independent controllability, high insertion loss and fabrication/implementation difficulties are some of the main problems faced in the use of convouted or meandred FSSs.
Some examples of convoluted and meandred FSSs are presented in Fig. 2.14, where (a) is a convoluted square loop FSS, (b) is an array element with interwoven geometry and (c) is the geometry of the miniaturized element based on meandred lines showing 2 × 2 unit cells presenten in [42].

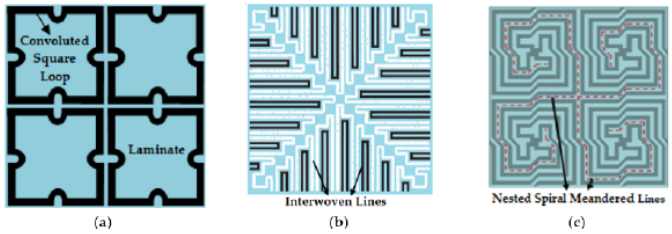

Figure 2.14: Some examples of convoluted and meandred FSSs [7].

Another type of array elements are the fractal ones. Fractals occupy a much smaller area because of their efficient space usage. Nowadays, significant research in microwave engineering is being done in the desing of new FSS based on the theory of fractal geometry, due to its attractive properties [43]. Fractal FSSs are famous for their self-similarity nature, thereby creating multi-band response and compactness. The multi-band frequency response of Sierpinski fractals has lucratively been used in the past for designing dual-band FSSs [44]. It is proved that with the increase in the electrical length of the fractal patch, a decrease of the working frequency is achieved, and for that reason, a lessening in the structural dimensions is observed. Fig. 2.15 gives an overview of some of the fractal shapes used in recent researches.

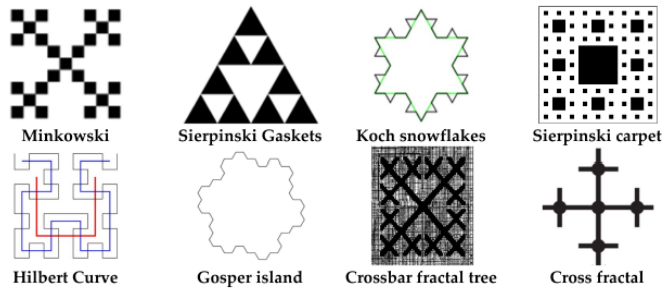

Figure 2.15: Some typical fractal FSS geometries investigated in different applications [7].

Since fractal-based FSSs is still a very new topic its use in actual applications is very limited and its complexity makes further explanation on this topic to fall out of the scope of this project, although a lot of research is being done like in [43] [44] [45] [46] [47] among others.

2.1.11 Structure: Single Layer

Single layer FSSs are composed of two-dimensional array of periodic resonant elements. Hence, their potential use is restricted by the limited space available for the unit cell. Then, arranging a huge number of large-sized array elements and creating a better performing finite FSS is exigent, especially taking into account the difficulty that the large inter-element spacing and element size add, particularly when crafting curved surfaces [42]. Because of that, miniaturized array element FSS have emerged and enhanced the angular stability of the whole structure. In addition, these

miniaturized elements cause the working bands to be separate from the grating lobes region as defined by the period of the array. In the last years miniaturization has been achieved for simple elements such as simple loops, multi-poles, patches, convoluted, meandred and fractal elements [48] [49].

In short, FSSs are efficient structures with less mass, volume, and cost and therefore, easily integrable and mountable to many EM structures such as bigger antenna apertures, to be used in multitude of applications for advanced and complex communication systems, including radar configurations [7].

Since one of the most significant challenges when working with FSSs is the limitation of its operating bandwidth, several solutions have been proposed to overcome this problem, being the use of **multilayer FSSs** the most notorious of them, since even the use of fractal elements in single layer FSSs has been shown to be insufficient [43]. It has also been tried to use resonating elements of very complex geometry, but it typically results in multiband response and overall enhanced BW without improving it for single resonance and occasionally decreasing it in some cases. For this reason, the use of multilayers is more suitable **to increase the BW of single resonance**. Then, a broadband response in the desired frequency range is achievable by multilayered FSS structures due to the discontinuity provided by the layers.

However, for the wider BW demands traditional FSS or first-order FSS (even when multilayered) are insufficient and also size (despite the use of fractal elements) may be a problem.
For these reasons, recent studies have proposed FSSs based on the array of Antenna-Filter-Antenna (AFA), considered as low profile and high frequency selectivity constructions [50] [51].

The most usually required qualities of an FSS include wide passband, fast roll-off (sharp edges), and insensitivity to incident angles and polarizations of an incoming EM wave in applications such as RCS reduction, terahertz sensing, EM compatibility, and telecommunication [7]. Unfortunately, the previously mentioned two-dimensional structures are not able to carry out all these functions at the same time. To overcome these limitations, in the recent years 3D FSSs structures have appeared [52]. These structures introduce inter-surface additions such as periodic arrays of microstrip line board, metal plate bits, holes or some resonating metal lines, granting this way superfluous choice of design methods, and therefore, adaptable for advanced performance applications.
The main obstacle in the application of this kind of structures, however, is the complication in manufacturing and realization, although a lot of research is being done on this field. Superior performance and ground-breaking implementations are envisaged by future explorations in 3D FSS design scenarios [7].

2.1.12 Application: Absorber Textile

FSSs have been used in various application in different frequency bands and in fields as diverse as radio frequency identifications, wireless communications, shielding purposes/EMI/EMC problems, polarization transformation, stealth radomes, EMI protection from portable electronics/wireless charging pad, directional multi-band antenna, polarization direction and sensing, etc. [7]. Although it is possible to categorize FSS according to their applications or purposes, here only the main characteristics of the FSS studied in this thesis must have are explained.

In general, a FSS produces good reflection in a specific range of frequencies in its stopband. However, for some applications such strong reflection must be reduced, which determines the terminology of frequency selective absorber. In this kind of FSS, the reflected signals ara absorbed in the stopband by introducing some absorbing array elements. Therefore, instead of reflecting the incident EM waves back, microwave absorbers are chiefly used to absorb them. Among the applications of this kind of materials the most extensively studied is making military aircraft/-targets undetectable from the radars. If Γ and T are the reflection and transmission coefficients, respectively, the absorption factor A can be calculated using (2.9).

$$A = 1 - |\Gamma| - |T| \tag{2.9}$$

In the last years it has become common to install FSSs with reflect/transmit characteristics integrated into the walls of the buildings to secure the wireless local area network (WLAN). These FSSs allow the mobile phone signals to pass while blocking the WLAN signals. However, this solution has presented several problems such as stopband reflections from FSS plane that causes extra delay spread and multi-path fading in WLANs.
As it has been seen, a stable response at high angles of incidence and achieving a compact design

with reduced space between the FSS and the resistive sheets are two of the main challenges when designing absorbers. For this reason, lossy FSSs as absorbers have been resently been investigated [53].
Since polarization insensitivity features are also impertive for most of its applications, microwave absorbers are usually constituted by good symmetric unit cells in which periodic resonating elements resonate equally at the different polarizaztion of incident wave.

Textile FSS is a pretty new topic and rare good researches are found in literature [7]. However, it is another emerging class after wearable FSS.
Fabric production techniques have been used to produce conductive components [54], and fabrics able to control the propagation of EM waves at microwave frequency regime have been embeded into buildings [55].

One of the main challenges that the research on this topic is facing is the difficulty of reaching the fully integration of the circuit in the textile. Traditional methods like ink-jet printing, emboidering and other non-woven based processes have appeared to be unable to obtain fully intergation giving a circuit which is simultaneously flexible, wearable, washable and fully integrated. For this reason, last researches are focused on the weaving technology. Although in this methodology the way of weaving the warp and the weft has influence on the final performance of the circuit, the study of this phenomenon falls out of the scope of this project and a full study on this topic can be found in [56].

2.1.13 Future Challenges and Potential Applications of FSSs

Once seen what an FSS is and what its most current application are, it is time to see what challenges are this kind of materials facing in the future, as well ass, once overcome, what are the most suitable future applications for them.

- **Pragmatic FSS design**. Achieving constant BW with the variation of incidence angle, low dielectric constant substrates and wavelength thickness are required on the outer layers for some applications in planar elements. However, such low dielectric materials are not available with mechanic properties high enough to deal with the other loads.

- **Design tools**. A lot of commercial softwares are nowadays available providing accurate analysis for all types of FSS geometries. They are very reliable analyzing periodic surfaces, since the structure is presented by a global unit cell. This technique, however, is very limited when it comes to analyzing other types of complex or uneven geometries because of the impossibility of applying approximation rules that work with the global unit cell.

- **Optimization Dilemma**. Although a lot of different optimization processes have been studied so far, none of them works always and each process should be utilized at the appropriate occasion and right place.
  Checking the dielectric profile, geometric parameters, being aware of the effect of the grating lobes, cross-polarization, and instability of the resonating frequency. It is a real challenge to sort the chaos that is created by such optimization computer program, becoming the task of appropriately defining parameters during the optimizing process about the good and the bad result a huge challenge for the designer.

- **Accurate Analysis**. Generally, a good estimated FSS analysis yields very accurate response and is reliable, as predicted [9]. However, for some designs this is not always true, since it is assumed that the distribution of current on the array elements remains constant and only amplitude and/or phase vary with the incidence angle. On the contrary, in some cases, the odd-modes may alter the current distribution for oblique incidence angle, and so the BW is no more constant, thereby failing the analysis. A solution to this problem might be using compact array elements such that only the primary current distribution lies in the resonant area. However, there is a limitation to reduce the element size and inter-element spacing. Also, this may impact the flatness of the transmission curve's top. Therefore, a trade-off needs to be made between constant bandwidth and flat top of the frequency response [7].

- **Miniaturized Design**. Especially for curved surfaces where flexibility is a requirement reduced unit cell with fairly small electrical dimensions and higher angular stability is a must.

- **Higher operating bandwidth**. It is especially important for single layer FSS structures. As has already been seen, despite the fact that multilayer build helps to achieve higher BW, especially at low operating frequencies it is the foremost challenge for the FSS designers.
- **Fabrication challenges in 3D structures**. Although 3D structures alleviate some of the problems that 2D structures encounter and its promising future the complexity of realization and fabrication is still an unsolved issue.
- **Transmission through energy saving Glass**. Coating of FSS can degradate the thermal insulation of current energy saving glasses used in some buildings.
- **Active FSS issues**. Although they have been not considered in this thesis Active FSS solve the problem of permanent constituent characteristics in the performance of conventional FSS, since they allow the control of the EM response by dynamically tuning through external excitation. However, various issues arise when talking about this kind of FSSs. Sometimes, they suffer from degradation, they are more difficult to create and more expensive than traditional FSSs and power consumption is extremely high due to the number of active devices.
- **FSS for smart cities applications**. Wireless mobile communication takes place mostly in the 6 GHz and below frequency bands, while some other smart cities applications take place at frequencies higher that 24 GHz. Then, a proper performance in such low and high frequencies is a challenge for FSSs, at the same time that dealing with the interference that occurs in the overloaded WiFi band is also complicated.
- **Problem of Transmission losses**. Although FSS structures have been designed to exhibit lossless transmission response, this does not happen in real scenarios.

2.2 Electromagnetics and CST: Sample Case

The aim of this section is to provide the basics to understand the simulations done and the results obtained in this project. As all the simulations will follow the same procedure, it will be explained only here and just the specifications or relevant modifications done through the project will be explained in the future. In addition, it will serve as a validation of the procedure and methodology applied, since the results obtained in this sections will be compared to the reliable ones given in [11].

2.2.1 CST: A brief introduction and Workspace configuration

The software used in this thesis is CST (Computer Simulation Technology) by Dassault Systemes. This software offers accurate, efficient computational solutions for electromagnetic design and analysis with a user-friendly interface and enabling the user to chose the most appropriate method for the design and optimization of devices operating in a wide range of frequencies. In this case, CST will be run using an intel® Core™ i7-7700HQ with a Processor Base Frequency of 2.80 GHz and 16.0 GB of RAM.

Inside the program the module that will be used in this case will be the **MW & RF & Optical** and, inside this module, the **Periodic Structures** option will be selected. Among the different workflows offered then, first of all the **Metamaterial - Unit cell** option is selected (it is important to point out that all this initial selections are for the program to open a pre-stablished workspace optimized and most suitable for the desired simulation, and everything may be modified later).
Finally, there are two possible solvers: Frequency Domain and Time Domain, being the second just useful for normal incidence waves. Then, since the study carried out is centered in the frequencies the selected solver will be the **Frequency Domain** one.
In addition, according to the CST developers, although both solvers may work for the desired application and sometimes the Time Domain may become more efficient [10], the use of the Frequency Domain solver allows more versatility that will be useful in future calculations.

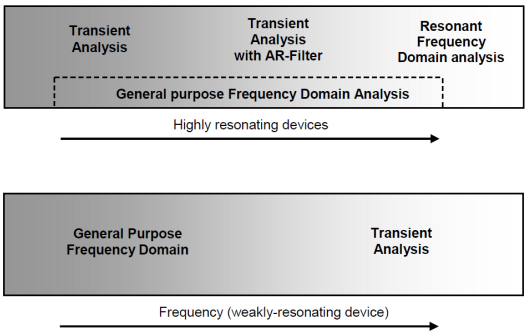

Figure 2.16: Rough guideline for the application ranges of the solving methods [10].

Once done that, the last step to finish the set up is to select the units, which are shown in Table 2.1 and select the frequency span considered, that in this case goes from 8 GHz (λ = 37.5 mm) to 11 GHz (λ = 27.3 mm).

Dimensions	mm
Wavelenght / Frequency	mm / GHz
Time	s
Voltage	V
Current	A
Resistance	Ohm
Capacitance	S
Inductance	H
Capacitance	F

Table 2.1: Units used in the CST

With the workspace properly defined the next step is creating the geometry.

2.2.2 Geometry definition

CST has its own geometry creation palette, which is shown in Fig. 2.17. The main features of this palette are the constant use of the local frame of reference, the picking options and the boolean operations.

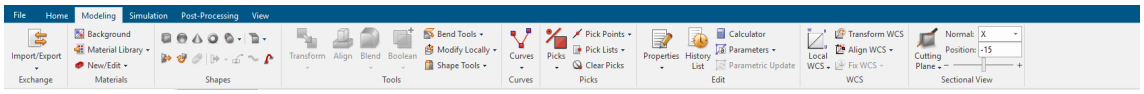

Figure 2.17: CST geometry creation palette.

The creation of the geometry starts with the basic structure, the unit cell, since as will be seen later CST has its own procedure to simulate the whole structure from the unit cell. The geometry chosen and given in [11] is shown in Fig. 2.18, where (a) is a magnified view of the unit cell and the periodic structure and (b) is a side view where the direction of the incident waves are given. It is important to note that all distances are given by means of parameters (whose initial values can be consulted in Table 2.2) since as the CST also allows to work with parameters in its geometry module (see Fig. 2.19) it is the easiest and fastest way to modify the geometry in an ordered way to optimize it.

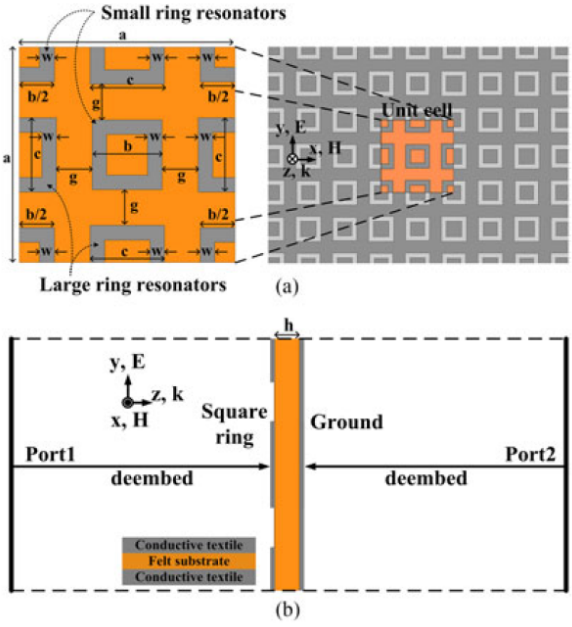

Figure 2.18: Geometry of the sample [11].

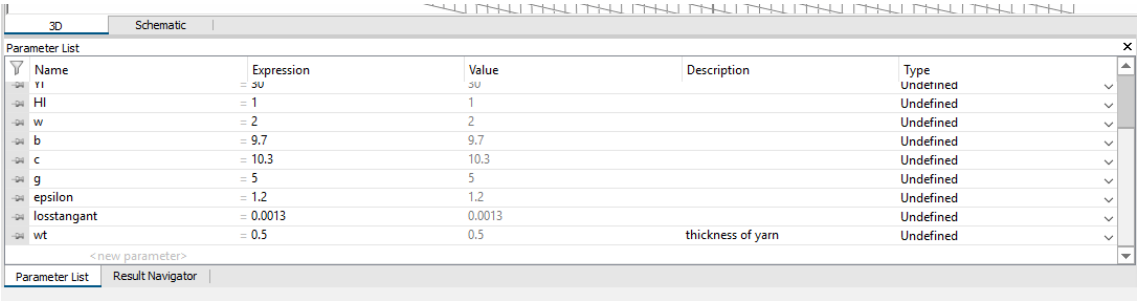

Figure 2.19: Dimensional parameters introduced to CST.

So, roughly explained, the procedure is as follows: The felt is created using the brick command and, after that, the resonator rings are created using the same command as solid squares. Following, the wholes inside the squares are created using the same brick command, defining the material as vacuum and using the boolean operation subtract.
To finish with, the ground is inserted.

a	30 mm
b	9.7 mm
c	10.3 mm
w	2 mm
g	5 mm
h	1 mm

Table 2.2: Dimensions of the sample unit cell.

Finally, in order to fully determine the physical properties of the unit cell it is only left to say that the thickness of the substrate is of 1 mm and made of felt ($\epsilon_r = 1.2$, $\tan\delta = 0.02$) while the material considered for the resonator ring is PEC (Perfect Electric Conductor).
Since the dimensions of the conductive thread are not given, some reasonable dimensions will be tested, which will give, in addition, an idea of the effect of this dimensions on the results.

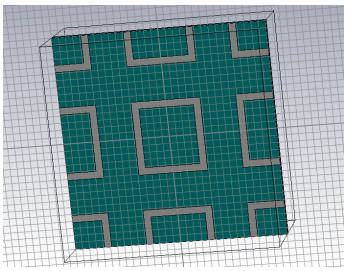

Figure 2.20: Geometry of the sample created in CST.

2.2.3 Create Structure

Once created the unit cell the next step is the creation of the ports and the whole structure. In the chosen template these are already existing and located at Zmax and Zmin.
After the ports, it is time to define the incident wave. In the boundary conditions definition, it is possible to specify the incident angle of the incoming plane wave by setting angles Theta and Phi. Also different periodicity can be assigned in the x- and y-directions to configure the periodicity of the FSS in the section Unit Cell of the boundary conditions. Finally, in the section Boundaries the x- and y- directions are defined as unit cell, while the direction of the wave is left as Open (add space) to ensure distance between the boundary and the structure.

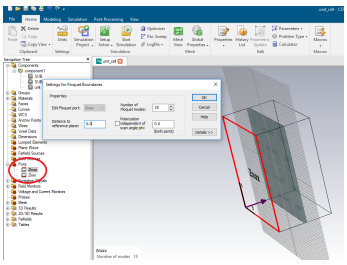

Figure 2.21: Ports used in the simulation.

In this case a plane wave travelling along the z-axis from the Zmax to Zmin is simulated. For off-normal incident angles the Floquet port modes ensure that the reflected wave is recorded in the direction of optical reflection, while the transmission is in the same direction as the incident wave. This is elucidated by the figure below.

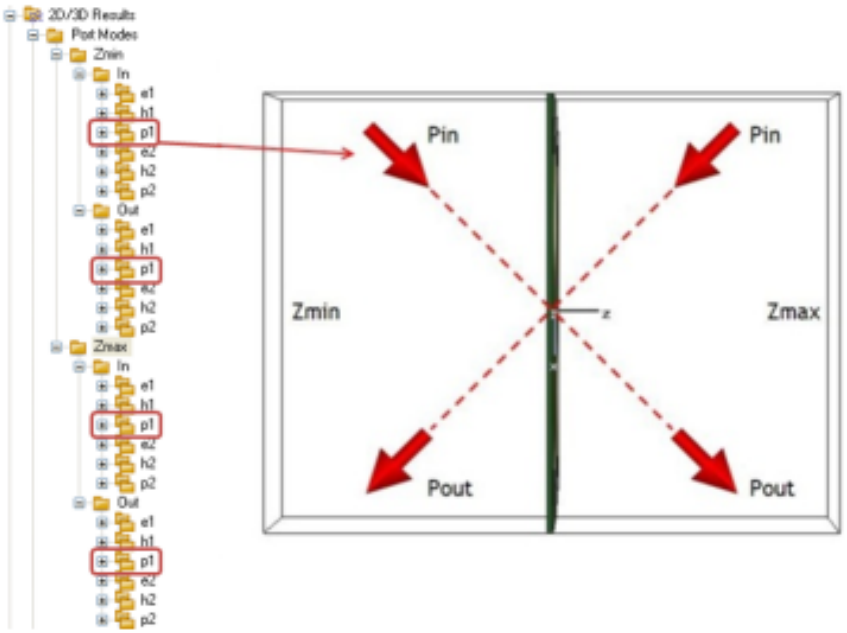

Figure 2.22: Incident and transmitted directions are automatically set by the Floquet modes [12].

The default Floquet port settings excite two plane waves with orthogonal electric fields as shown in Fig. 2.23 (TE(0,0) and TM(0,0) modes), but higher order may also be specified. Co-polar and cross-polar coupling between the modes, both reflection and transmission, are represented in terms of S-parameters. The co-polarised reflection of mode 1 at port Zmax would thus, for example, be named SZmax(1),Zmax(1), and the cross-polarised transmission between modes 1 and 2 SZmin(2),Zmax(1) [12].

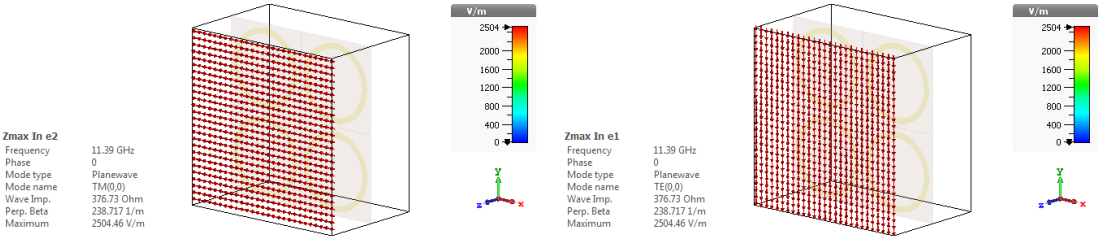

Figure 2.23: TE(0,0) mode, electric field (right) and TM(0,0) mode, electric field (left) [12].

2.2.4 Solver Configuration

After creating the geometry and once the simulation conditions established, the frequency solver can be started.
As can be seen in 2.24, here only the Zmax port has been used as a source, since is not of interest for the simulation an incident wave coming from the opposite side of the resonator rings.

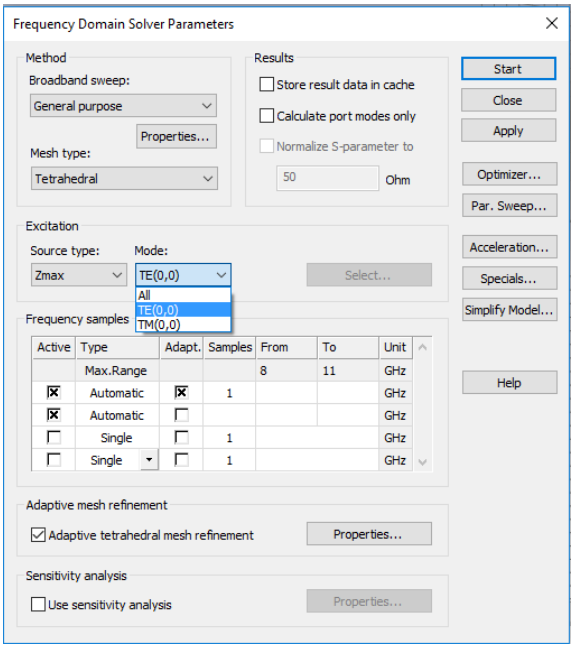

Figure 2.24: Parameters used for the Frequency Domain Solver.

Respect to the mesh, Tetrahedral elements are used, since some corners or acute angles may not be properly catched by Hexahedral elements. In addition, the Adaptative tetrahedral mesh refinement is selected to improve the accuracy giving to these a minimum of 3 and a maximum of 10 passes and 3 checks to the convergence criteria of all S-Parameters.
About the solver, the accuracy is set to 10^{-5} and a 2nd order solver is used. These parameters, set by default, ensure good results with a reasonable computation time, although their effect on the results will be also studied later.

2.2.5 Analysis of the Results

First and foremost it is important to study the scattering parameters or S-parameter results, which represent the reflection from and transmission through the FSS, which are shown in Fig. 2.25.
The co-polar reflections and transmissions of both modes are almost identical due to the symmetry of the unit cell (the slight difference is due to the tetrahedral mesh). The transmission is almost completely blocked at 9.8 GHz, as seen from the SZmin(1),max(1) of about near 0, and the reflection is almost complete, as SZmax(1),Zmax(1) is of about -17.7 dB.

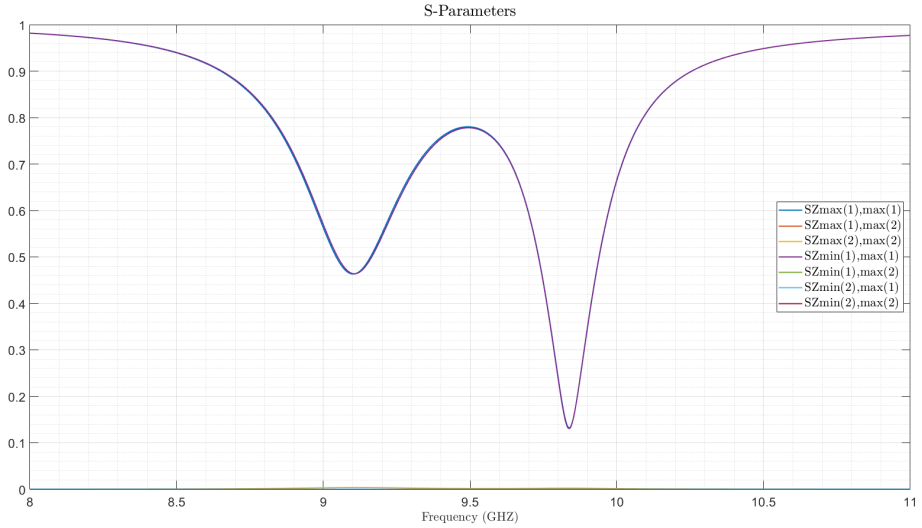

Figure 2.25: Simulated S-Parameter.

Comparison with the Sample Results

In order to properly compare the obtained results with the ones given in the paper it is necessary to obtain the absorption factor or absorbance. To do so, it is necessary to recall (2.9) and knowing that $\Gamma = S_{11}^2$ and $T = S_{21}^2$ one can rewrite:

$$A = 1 - \Gamma - T = 1 - |S_{11}|^2 - |S_{21}|^2$$

where, in the simulation, the index 1 refers to Zmax and 2 refers to Zmin. As the CST already does this calculations the obtained results are shown below.

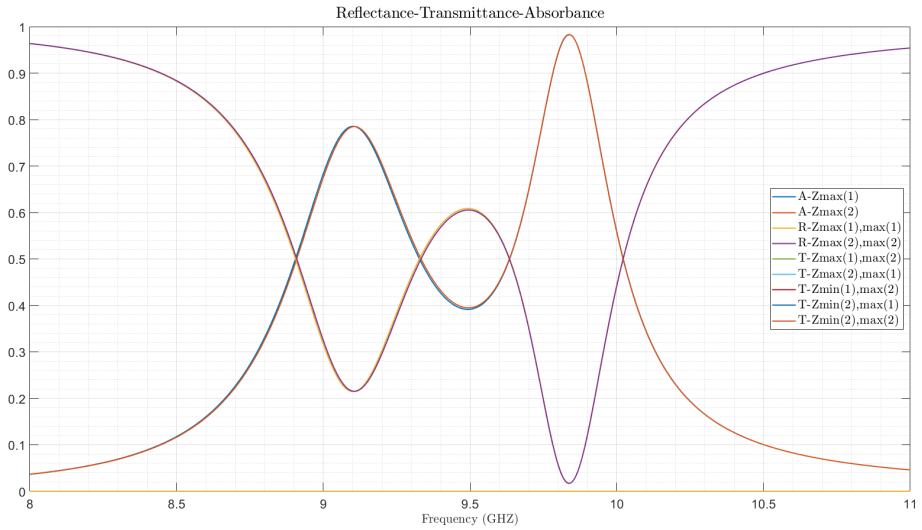

Figure 2.26: Simulated Absorbance Reflectance and Transmittance.

While the ones given in the [11] are shown in Fig. 2.27

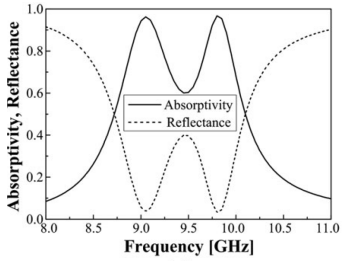

Figure 2.27: Simulated absorptivity given by [11].

Comparing both results it is possible to see that they present an identical peak at 9.8 GHz ($\lambda = 3.057 \times 10^7$ nm), but while in the simulated results the absorbance peak is of about 96-98%, in [11] this peak is of 97.2%, which is almost the same. The main difference, however, appears in the second peak. While in [11] this peak is allocated at around 9 Hz and has a height of 96.7%, in the simulations carried out it is slightly deviated to 9.08 GHz, which is also good, being the main difference the value of this peak, which in the simulation done is only of 78%.

To sum up, the simulated results are almost the same in the carried out simulation than in the results given by [11], being the main differences due to some of the following reasons:

- The programm/solver used in [11] is the one given in ANSYS, while the one used in the simulations presented in this thesis is CST. Although the results should be the same the internal procedure and the created mesh may lead to some numerical inaccuracies.

- Dimensions of the thread. Since the dimensions of the thread were not given some reasonable values have been tempted. In Fig. 2.28 it is easy to see how its dimension has a huge effect on the results up to when it is really small in comparison with the felt. In addition, the woven technique is also very important, as stated in [56], and in none of both simulations it has been taken into account.

- The material used as a conductor has been PEC, while in real life and simulations carried out in [11] it is different, although not specified.

- The weaving technique or disposition of the different materials are not given. In Fig. 2.28, the last value of $t = 0.004$ mm has been tested considering that the conductive material goes from $-t/2$ to $t/2$ instead of from 0 to t. Doing so, the absorbance on the lower frequency has increased, validating the idea that some discrepancy from [11] may come from the representation of the thread.

- Other parameters related with the solver or the construction of the metamaterial that have not been considered.

Then, the procedure that will be used through the process in order to set the simulations has been validated.

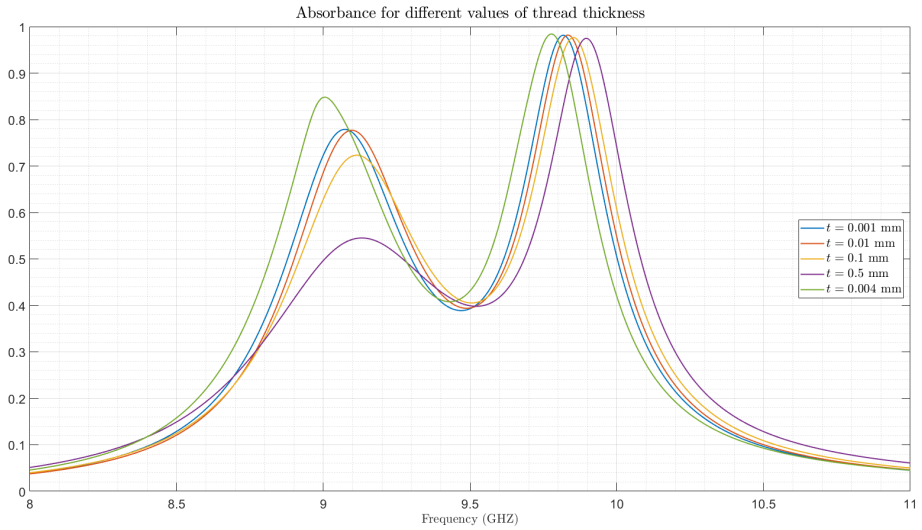

Figure 2.28: Absorbance for different values of thread thickness.

Effect of the addition of more Floquet Modes

During the launch of the simulation the CST solver gives a warning indicating that some Floquet modes are not being considered when only using TE and TM modes, which may lead to a miscalculation of the S-Parameters. The number of appropriate Floquet modes depend on the number of orders diffracted by the structure, and for optimization it is recommended to start with a small number of modes and increase it until the results do not change anymore and the warning given by the software disappear.

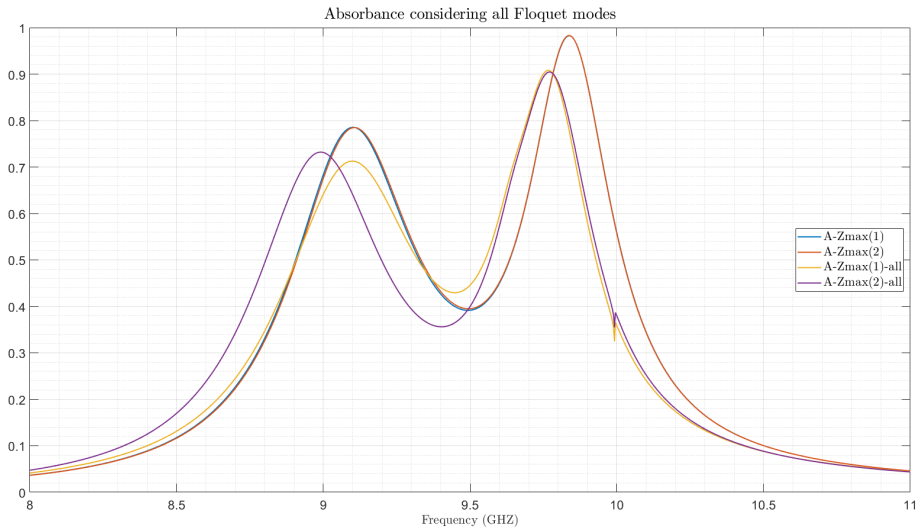

Figure 2.29: Absorbance for Floquet modes 1 and 2 when all modes have been considered.

In Fig. 2.29 it is possible to appreciate how, when 16 Floquet modes have been considered, the value of the absorbance and the resonance frequency for a given mode (in this case co- and cross-polarization) have been modified. This is due to the fact that the S-Parameters are computed considering all the data available, which may vary when including some Floquet modes. Then, although in this case using just two modes is enough to prove that the results are the same than

in [11] in future calculations it will be necessary to use the appropiate number of Floquet Modes in order to obtain the desired level of accuracy.

Effect of some Solver Parameters

For the calculations done so far the solver set up given by default by the chosen template has been used, for being already optimized to give accurate results with a reasonable computation time. However, in order to more properly asses the effect of these parameters on the results a new calculation has been done modifying the main parameters, in order to see how the results and the computation time change.

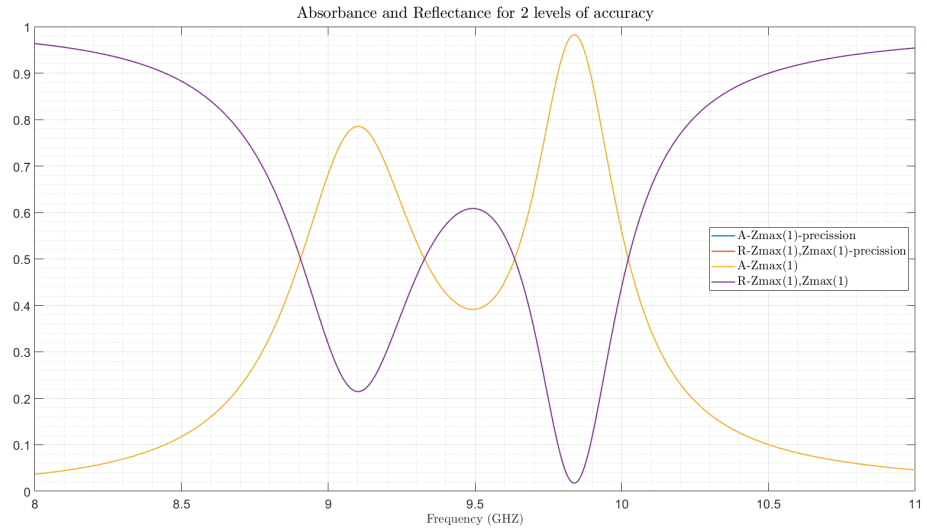

Figure 2.30: Absorbance and Reflectance considering two different solvers configurations.

Case	Standard	High Accuracy
Passes for Mesh Refinement	Minimum: 3, Maximum: 8	Minimum: 5, Maximum: 20
Check of discrete S-Parameters	3	10
Accuracy of Equation System Solver	10^{-5}	10^{-6}
Solver order	2nd (good accuracy)	3rd (high accuracy)

Table 2.3: Configuration of the solver for different levels of accuracy.

Table 2.3 gives the main parameters for the two considered options. Standard case refers to the values given by default, while High Accuracy Case is the one carried out with a more strict configuration for the solver.
The main difference between the two cases is that for the first one the passes for creating the Adaptative Hexahedral Mesh is set between 3 and 8, while in the second one these numbers have been increased to 5 and 20. Also the checks done in the results obtained for the S-Parameters have been modified from 3 to 10 and the accuracy increased from 10^{-5} to 10^{-6}. Finally, the solver used has passed from a 2nd order to a 3rd order one.

Once done that, while the computation time has increased form a few minutes to several hours the results, which are shown in Fig. 2.30 (the appendix -precission refers to the High Accuracy Case) have remained the same, so the solver set up given by default has proven to be optimal and accurate enough for the required calculations.

Variation of the Angle of Incidence

It has already been seen that the performance of the FSS may be affected by the angle of incidence of the wave. In [11] the performance of the unit cell is given as a function of the polarization angle

θ and is shown in Fig. 2.31.

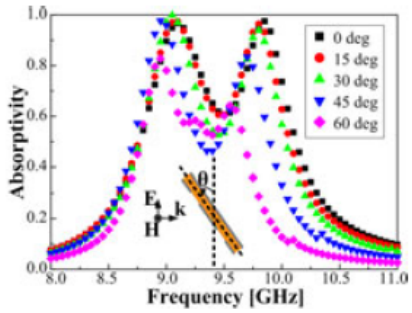

Figure 2.31: Simulated absorptivity characteristics at different polarization angles ranging from 0° to 60° [11].

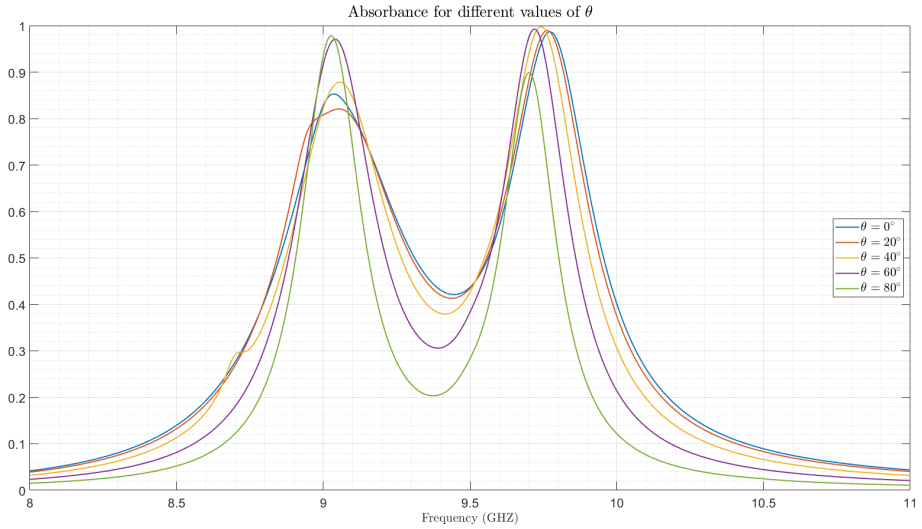

Figure 2.32: Simulated absorptivity characteristics at different oblique incident angles, θ ranging from 0° to 60°.

When comparing Fig. 2.31 with Fig. 2.32 it is possible to appreciate how in both cases the polarization angle has a small effect on the absorptivity. In both simulations the main effect of this angle is the decay of the highest frequency, while the peaks remain almost constant, just decreasing a bit at high angles of incidence.

Geometry Modifications

Finally, CST also allows to do geometrical sweep along the defined parameters, feature that will be really helpful for optimization purposes, since it will be necessary to test every considered dimension along feasible values in order to find the more appropriate one.
In [11] different values of b and c (with respect to the geometrical frame of reference given in Fig. 2.18) have been considered and the obtained results are shown in the Figure below.

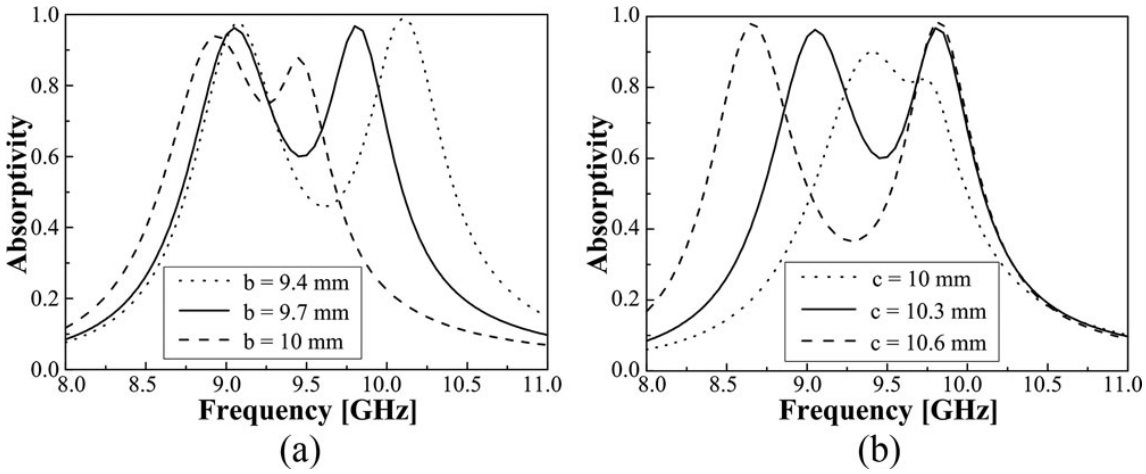

Figure 2.33: Simulated absorptivity characteristics for various (a) b and (b) c values [11].

When this same sweep of the geometrical variables have been done using CST the results can be seen in Fig. 2.34 and Fig. 2.35.

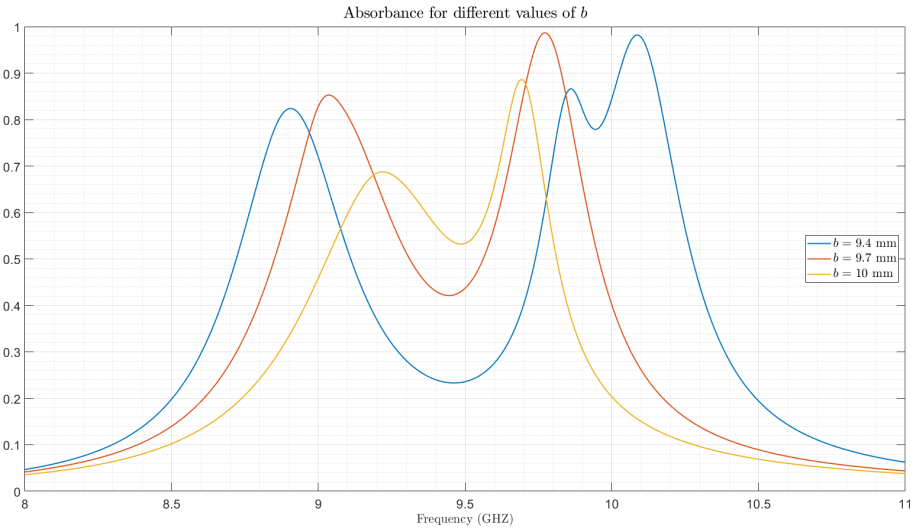

Figure 2.34: Simulated absorptivity for different values of b.

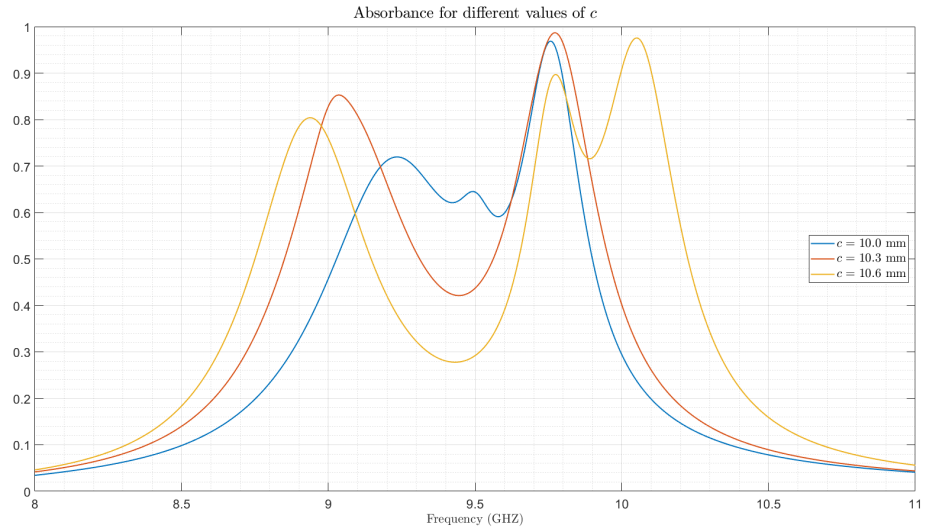

Figure 2.35: Simulated absorptivity for different values of c.

When analyzing all the pictures some conclusions can be drawn. In Fig. 2.33 it can be seen that as b increases, the high frequency absorptivity band shifts toward the low-frequency side, while the low-frequency absorptivity band is not affected. On the other hand, as c increases, the low-frequency absorptivity band shifts toward the low-frequency side, whereas the high-frequency band is not changed.
In Fig. 2.34 and 2.35 the same tendencies are observed, although more variation on the theoretically stationary frequency band also appeared.

2.2.6 Final Considerations

In conclusion, in Section 2.2 the main ideas necessary to understand how CST works and the simulations are carried out are presented. In addition, some of the main ideas that will be used later have been proven:

- Absorbance frequency depends on the dimensions of the unit cell, being possible to combine more than one shape to make it wider, although it may cause a small decrease on the peak values.
- The relative size between the felt and the thread has a huge effect on the performance. This will be a limiting factor during the design process since this dimension will be fixed.
- In spite of not being considered in this thesis, the weaving technique also affects the performance of the FSS.
- Due to its symmetry, the response of the FSS is the same in TE and TM mode.
- Although the influence of the incidence angle is important, it can be reduced in small angles with the proper design.
- Simulations have to be set up carefully, since the program is actually pretty optimized for this kind of simulations and increasing the precision makes the computation time to rapidly increase without offering more accurate results. In addition, choosing the correct number of Floquet Modes is also mandatory.

Chapter 3

Development

3.1 Case Study

Dimensions of the unit cell will strongly depend on the frequency chosen. For this reason, although there exist a lot of applications in different ranges of frequency that could be interesting, this study will focus on the frequency range of the Microwaves, for being the ones that offer the best compromise in size, being big enough for its construction to be feasible using a conventional embroidering machine and small enough to allow the inclusion of a huge number of unit cells without the need of an extremely big surface.
Some interesting applications at higher frequencies for a wearable metamaterial for electromagnetic shielding could be as an X-ray shielding for medical X-ray examinations or some kind of shielding for space applications on UV or Gamma ray frequencies. However, frequencies are so high that it is impossible to sew the required unit cells by means of conventional methods.
On the other side of the spectrum, infrared frequencies are also very interesting for applications like, for instance, military vest to avoid night detection or to hide marijuana plantations from satellites images at near infrared channel.

However, the most suitable frequencies for this project are around between 5 and 15 GHz for the reasons mentioned before. In this range of frequencies, two are chosen. First of all, the frequency of 5.55 GHz will be considered since it is the frequency in which most of the radars, mobile phones and Commercial Wireless LAN operate. For this reason, creating a wearable metamaterial optimized at this frequency could be helpful for radar invisibility, human protection against radiation or LAN isolation/protection. Nevertheless, this frequency is still a little bit low and dimensions may become too large, so another frequency, 10.64 GHz, is considered. This frequency is the one used by fixed mobile services and Earth exploration-satellite service [57].

Nonetheless, it is important to note that the aim of this project is to demonstrate the feasibility of the proposed technology and the considered frequencies are just to give to it a direct application, but have no further effects on the development of the project.

3.2 Initial Geometry Proposal

The first step to properly optimize the structure is choosing the appropriate geometrical representation. In Fig. 2.18 the representation offered in [11] has been used. However, when studying the actual configuration used for this project it is easy to appreciate how a conductive textile completely placed over the substrate is not realistic, since the weaving technique implies that the conductive textile is placed inside the substrate. For this reason, the approach used is the one proposed in [56] and depicted in Fig. 3.1, where two pieces of fabrics are stacked, and the conductive textile is stitched on the one on the top.

Although this is a much more realistic representation this will still be a source of error since, as proven in [56] how the thread is placed may cause the performance of the structure to vary. Then, although this feature is not considered in this thesis it will be a point to be taken into account when drawing the last conclusions.

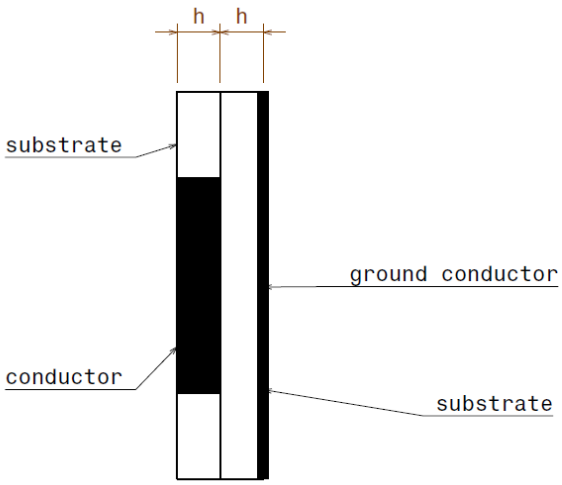

Figure 3.1: Schematic representation of the disposal of the layers forming the FSS.

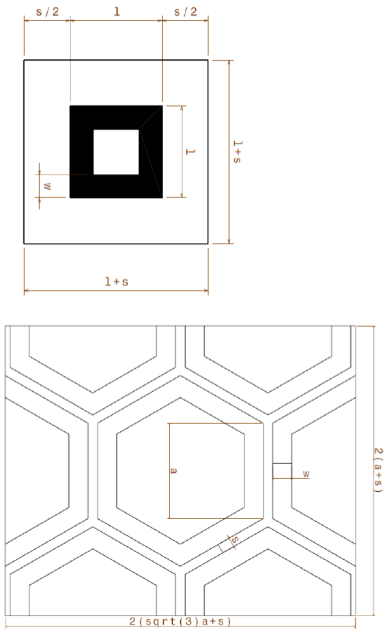

Figure 3.2: Basic dimensions and parameters used to define the two considered unit cells.

3.3 Unit Cell Design and Simulation

Once decided the geometrical representation of the configuration, it is time to chose the shape or unit cell. Among the different shapes existent and studied in this project, 2 of them will be tested in this section: the **square** and the **hexagonal** shapes. The first one has the advantages of being one of the most simple shapes, which allows to better control and understand how the different parameters affect its performance. In addition, since it is the shape used on the validation of the procedure, some information about this shape has already been studied. Hexagonal shapes, on the other hand, are a little bit more complex but are currently on trend on the field of FSSs (see, for example, [58], [59]). The main advantage of hexagonal shaped patches over square patches is that they are supposed to exhibit a boarder bandwidth [59].

Then, once **shape** and **frequency** have been established it is time to determine the initial dimensions from which starting the sweep and optimization. As seen before, for simple geometries as the ones studied dimensions are closely related to the wavelength. In addition, as results for a square-shaped optimizations are already available, this data can be used as a starting point, knowing that, for a frequency of $f = 9.45$ GHz the resonance point (considering a substrate with the properties given in [11] and the conductor used and whose properties are not given) is given for dimensions of $b = 9.7$ mm and $s = 5$ mm, with respect to Fig. 2.18 a first approximtion to the initial dimensions can be done.

For this case, two materials will be tested as substrates, and whose properties can be consulted in Table 3.1. It is important to point out, however, that since these textiles are not for electromagnetic purposes its actual properties may vary, causing this also some deviations from the expected results. The conductive yarn used will be regular textile yarn covered with silver, while the conductive ground will be copper.

Finally, in order to obtain the optimal parameters configuration the procedure will be as follows:

Textile	$\tan\delta$	ϵ_r	h
Cotton	0.0580	1.9	0.4 mm
Felt	0.0013	1.2	1.2 mm

Table 3.1: Electromagnetic properties of the textiles used as substrates.

3.3.1 5.55 GHz design

The first frequency for which the considered FSS will be optimized is $f = 5.55$ GHz. For the square shape, as the frequency is lower than the one given in [11] dimensions will be bigger. Since it is difficult to exactly determine the dimensions, the first step to do so will be carrying out a very coarse sweep for dimensions around the one of the example and bigger (it is important to recall that, since the substrate is not the same its electrical properties will be neither).

Then, with the obtained results, the sweep is gradually centered on the optimal point, up to reaching resonance, as depicted in the following pictures considering a dimensions of $w = 1$ with respect to the Fig. 3.1:

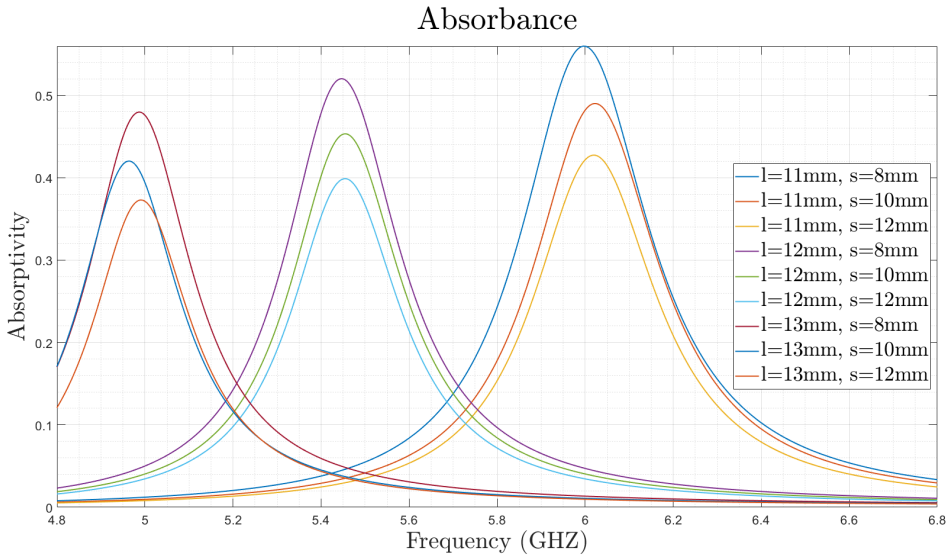

Figure 3.3: First sweep for the square geometry, $w = 1$ and f=5.55 GHz. Cotton.

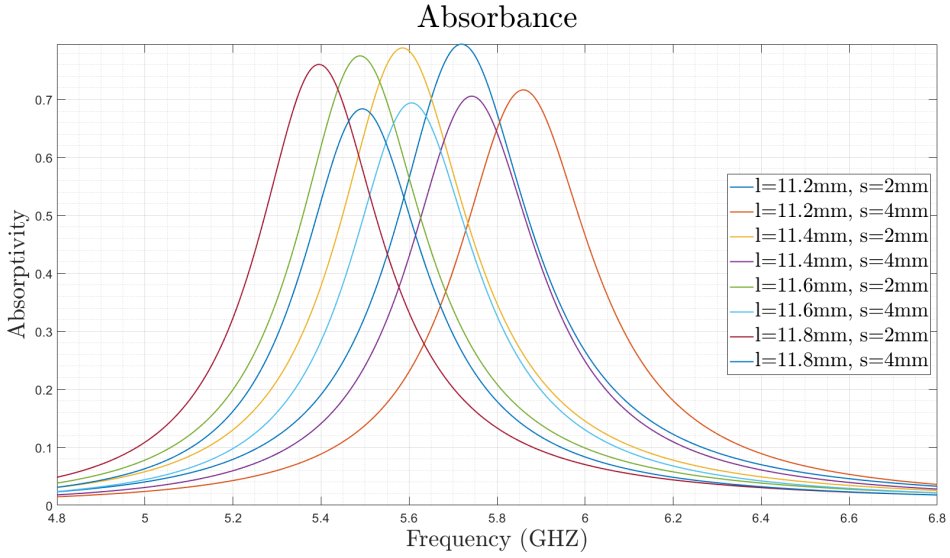

Figure 3.4: Second sweep for the square geometry, $w = 1$ and f=5.55 GHz. Cotton. Simulation.

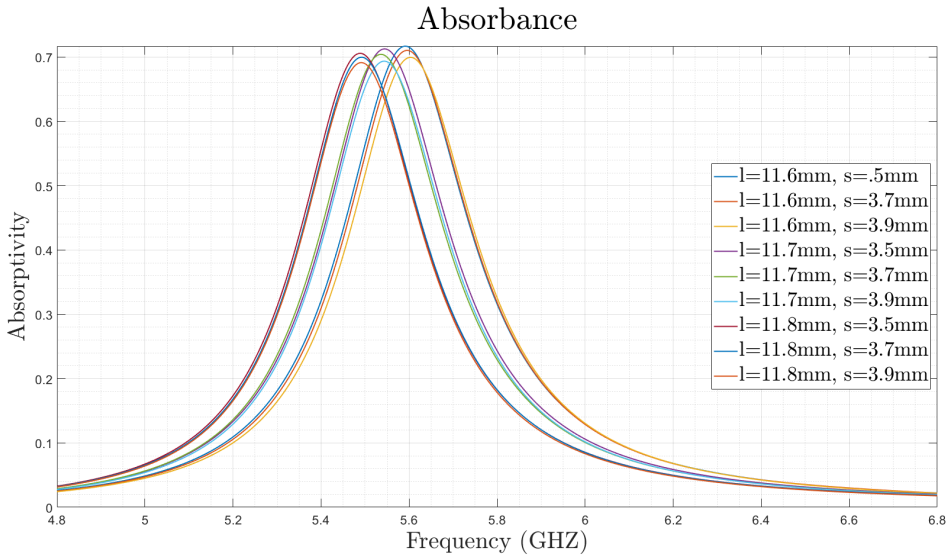

Figure 3.5: Third sweep for the square geometry, $w = 1$ and f=5.55 GHz. Cotton. Simulation.

Finally, repeating the same procedure for the different values of w the results are:

l	s	w	A_{max}
11.7	3.7	1	70%
12.1	0.9	2	86%
12.8	0.5	3	92%
14.1	0.6	4	94%
15.0	0.5	5	96%
16.5	0.5	7	98%

Table 3.2: Dimensions and absorbance for square unit cells and cotton as a substrate.

Note that the maximum value proposed for w has been 7. This is because higher values lead to unrealistic results due to the loss of the square geometry. Summarizing all the simulations, the obtained results considering a unit cell with the shape of a **square** and **cotton** as substrate are depicted in Fig. 3.6 and Table 3.2.

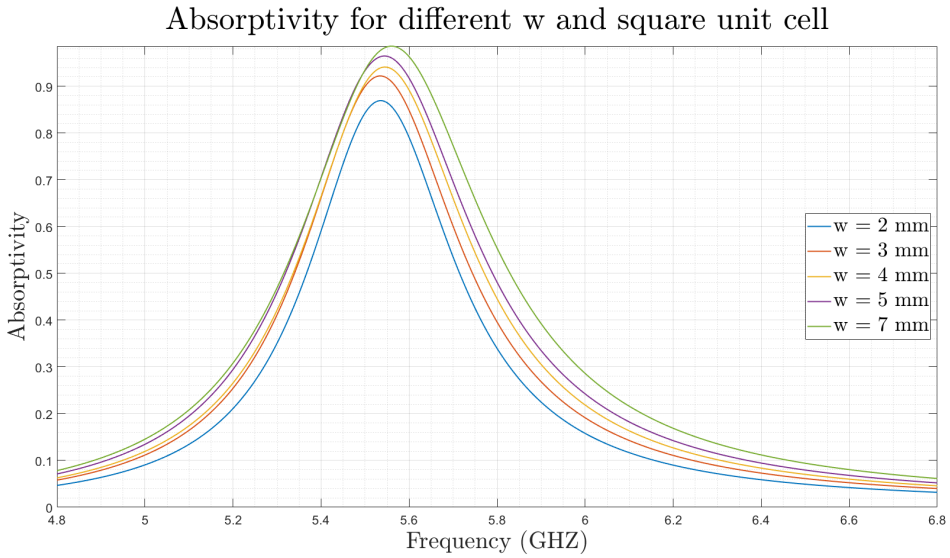

Figure 3.6: Absorbance for all the optimal configurations using a square shape. Cotton. Simulation.

Once determined the most optimal dimensions for the square shape, it is time to test the hexagonal shape. To do so the procedure will be the same, reaching the following design:

a	s	w	A_{max}
6.7	0.7	1	84%
7.9	1.6	2	83%
8.3	0.8	3	91%

Table 3.3: Dimensions and absorbance for hexagonal unit cells and cotton as a substrate.

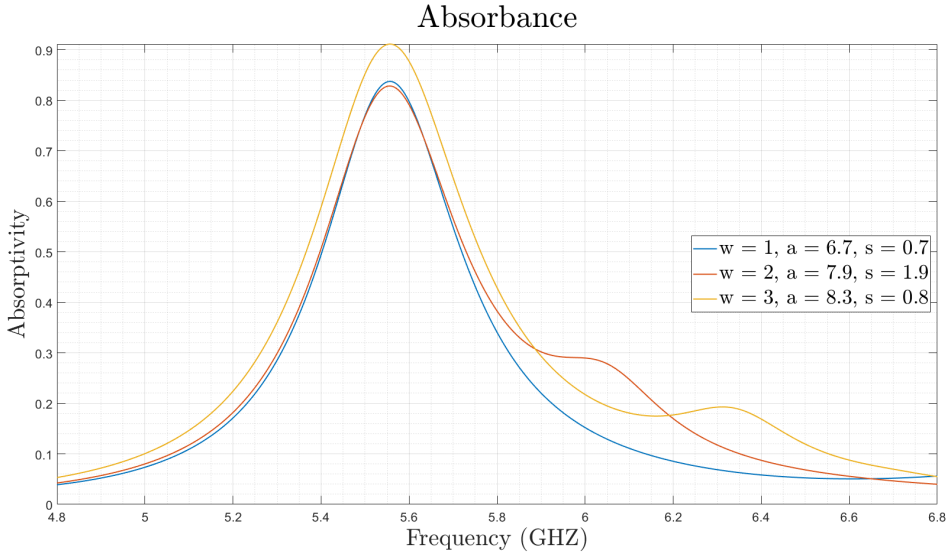

Figure 3.7: Absorbance for all the optimal configurations using an hexagonal shape. Cotton. Simulation.

All the simulation done up to the moment have been done considering cotton as a substrate. However, another substrate may be considered. In this case, felt. By doing the simulations considering this substrate it appeared that the optimal results did not reach significant values for

the square shape and only the hexagonal simulations lead to positive results, as depicted in Fig. 3.8 and Table 3.4.

a	s	w	A_{max}
4.4	0.5	1	87%
5.2	0.8	1	89%
5.8	1.2	1	88%

Table 3.4: Dimensions and absorbance for hexagonal unit cells and felt as a substrate.

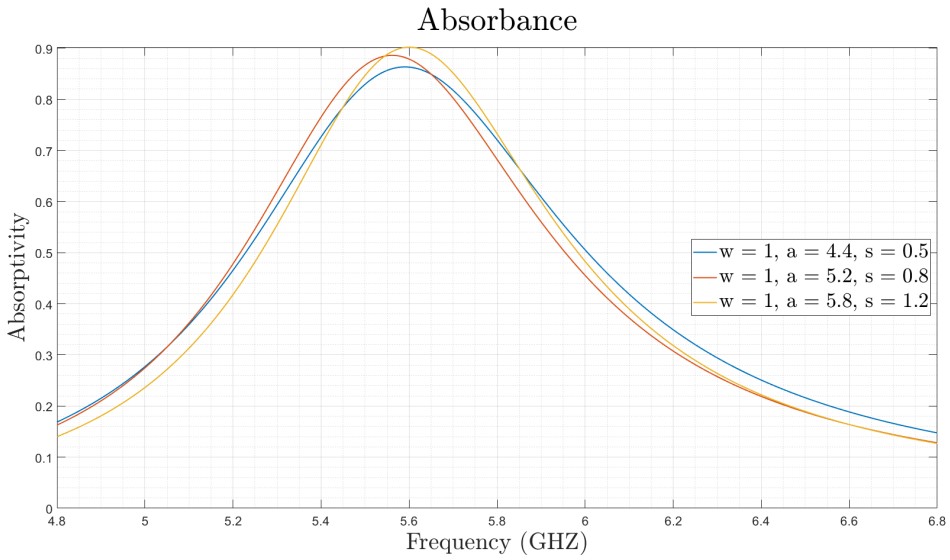

Figure 3.8: Absorbance for all the optimal configurations using an hexagonal shape. Felt. Simulation.

By observing both results, however, the first conclusion that can be drawn is that the electromagnetic properties of the felt make the unit cells smaller for the configurations that work but, unfortunately, these configurations are not a lot.

3.3.2 10.64 GHz design

Once optimised the structure for the frequency of 5.55 GHz the second considered frequency, 10.64 GHz is studied. First of all, it is easy to see how the increase in frequency will make the dimensions to decrease (since these are proportional to the wavelength and, hence, inversely proportional to the frequency).

Again, two shapes and two substrates have been considered, leading to the following results:

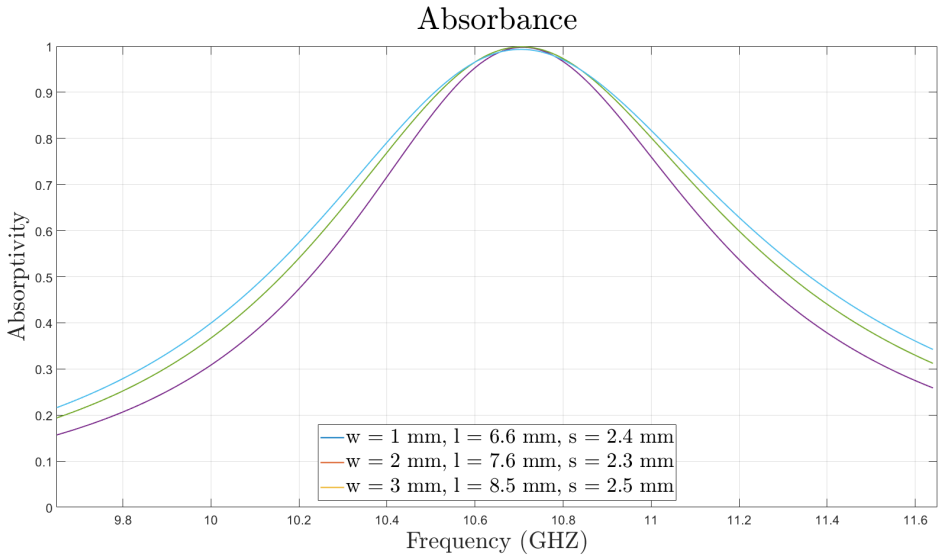

Figure 3.9: Absorbance for all the optimal configurations using squares as unit cell. Cotton. Simulation.

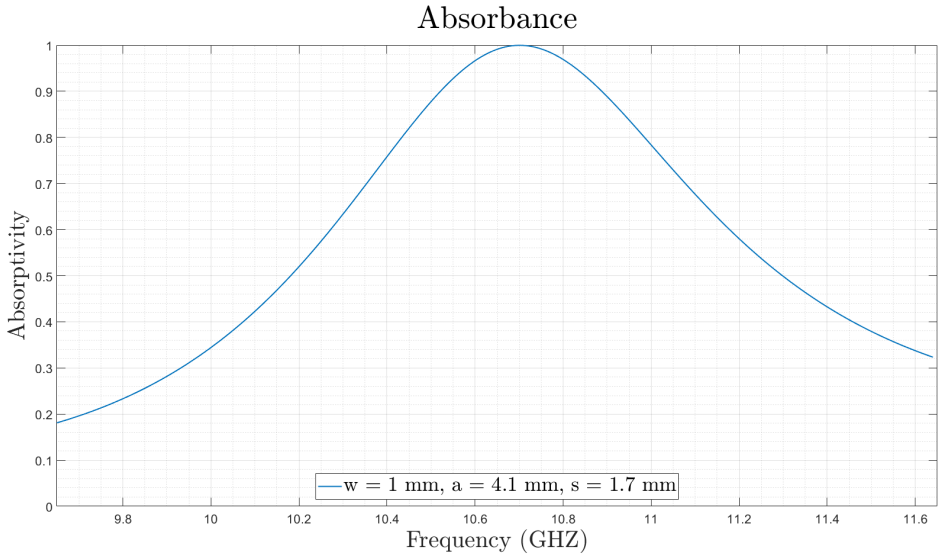

Figure 3.10: Absorbance for all the optimal configurations using an hexagonal shape. Cotton. Simulation.

Unit cell	l/a	s	w	A_{max}
Square	6.6	2.4	1	100%
Square	7.6	2.3	2	100%
Square	8.5	2.5	3	100%
Hexagonal	4.1	1.7	1	100%

Table 3.5: Dimensions and absorbance for square and hexagonal unit cells using cotton as a substrate.

3.4 Final Design

Once simulated the different considered unit cells for the proposed substrates, the final design used will be chosen considering the following criteria: First of all, it is necessary for the cell to be optimized at the desired frequency. Then, once this is achieved, the second parameter to be taken into account is the absorbance reached at this point. Finally, if the same absorbance is given, the one with the wider bandwidth will be considered to be more optimal.

By doing so, the best achieved designs are the ones shown in Table 3.6.

Frequency (GHz)	Unit cell	substrate	l/a	s	w	A_{max}
5.55	Square	cotton	16.5	0.5	7	98%
5.55	Hexagon	cotton	8.3	0.8	3	91%
5.55	Hexagon	felt	5.2	0.8	1	89%
10.64	Square	cotton	8.5	2.5	3	100%
10.64	Hexagon	cotton	4.1	1.7	1	100%

Table 3.6: Best reached designs through simulation optimization.

So, when comparing the most optimal designs using cotton as a substrate at both studied frequencies the following figures are obtained:

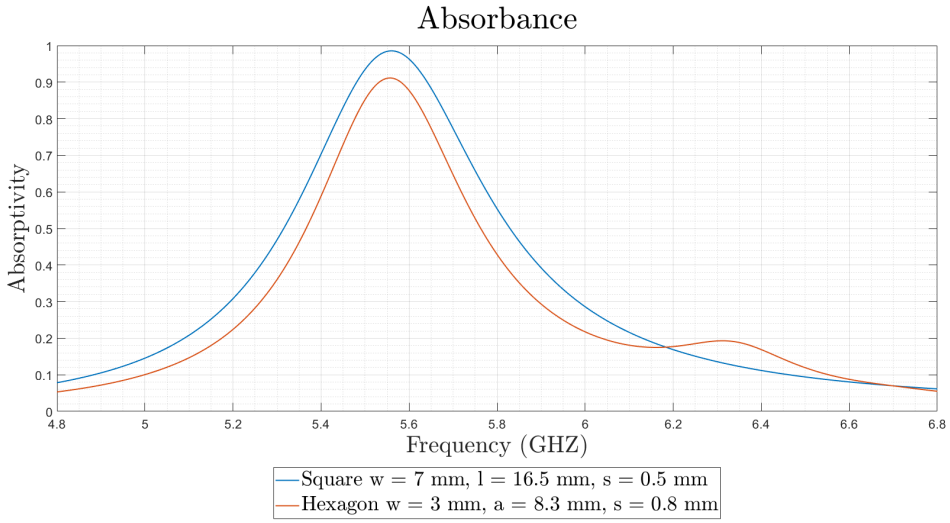

Figure 3.11: Absorbance for all the optimal configurations at a frequency of 5.55 GHz. Cotton. Simulation.

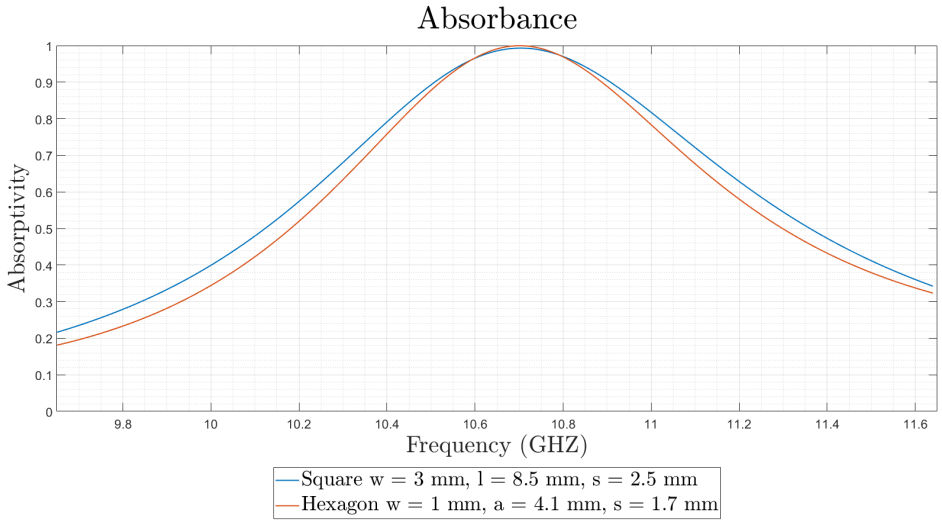

Figure 3.12: Absorbance for all the optimal configurations at a frequency of 10.64 GHz. Cotton. Simulation.

It seems clear that for the frequency of 5.55 GHz the square presents a better performance, since the absorbance peak is higher and the bandwidth is wider. In the frequency of 10.64 GHz, on the other hand, while the square stills offers a boarder bandwidth the highest peak in this situation is for the hexagonal shaped unit cells.

Another consideration to do, however, is that the simulations have been done using the approximation of infinite dimensions. Then, since it is not possible, the number of unit cells existent in the structure has to be also considered, since the higher the number of unit cells the closer to the infinite extent. Then, it is interesting to estimate how many unit cells will be in a structure of a given dimensions. In this case, the support that will be used will be of 16×16 cm^2, so the estimate number of cells that will fit are:

Frequency (GHz)	Unit cell	substrate	l/a	s	w	Number of cells
10.64	Square	cotton	8.5	2.5	3	196
10.64	Hexagon	cotton	4.1	1.7	1	80 (320 hexagons)

Table 3.7: Best reached designs through simulation optimization.

Obviously, and attending to the criteria of trying to reach the maximum amount of unit cells, the frequency chosen for testing will be 10.64 GHz, whose simulated current distributions on the unit cells for the given frequency are depicted in the following figure:

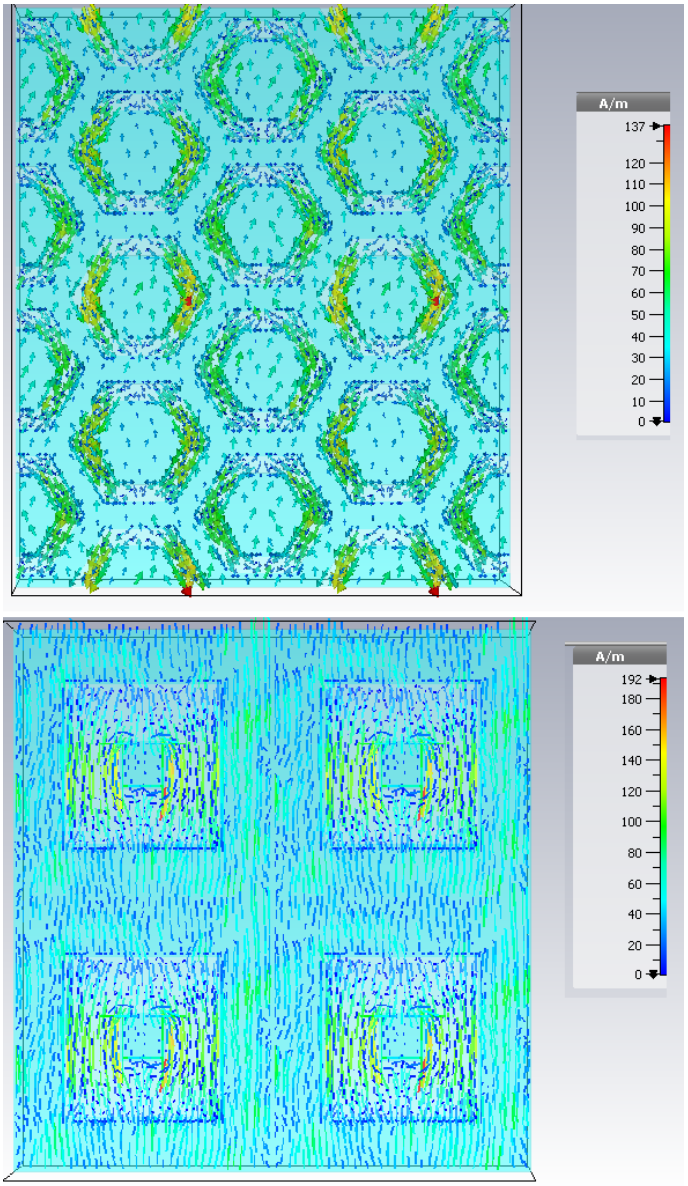

Figure 3.13: Simulated surface current distribution on the unit cells.

3.5 Crafting

For the construction of the samples to be tested the procedure will be as follows: First of all, using again CST a structure of the desired dimensions will be designed using the considered unit cell as a seed, as depicted in Fig. 3.14.

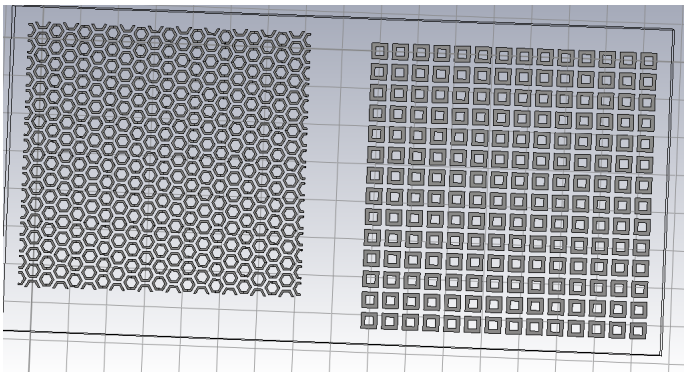

Figure 3.14: Geometrical configuration for the chosen geometries.

After creating these structures, it is necessary to export them as Gerber files. Once done that they can be converted to .png using the software Gerbv, making sure that dpi is set to 96 to preserve the correct dimensions. Then the .png file can be opened with any image editor to change the color scale to obtain a conductor in black and a white background. Once done that this can be exported to bmp format 24-bit.
This bmp file, then, has to be opened with the software of the embroidering machine: the Easy-DesignEX. This software allows to convert the bmp into the specific format fot he machine, in this case The Singer Model Singer XL 550, whose specifications can be found in the Attachment of this Report. The extension for this model is .XXX. This software also allows to choose the embroidery that will be used. In order to chose it two different criteria must be considered: on one hand the shape of the unit cell has to be respected and, on the other hand, the minimum amount of thread has to be used. Among the different options offered by the machine, the one that best suited this criteria was satin with density 20%.
Finally, once everything is set the file can be launched to the machine using the software linked to the machine Futura XL-550 (Fig. 3.15). Also the intensity of the machine was adjusted in order to make sure that the thread always had the appropriate tension and that it did not break.

Figure 3.15: embroidering machine Futura XL-550.

Once done that the embroidering machine will work elaborating the unit cells in the optimal order. During the process it is necessary to keep an eye on the machine since several errors may occur during the process that would lead to both a misalignment or the stop of the process. An example of the process and path followed for both the square and the hexagonal shapes can be seen in Figures 3.16 and 3.17 respectively.

Figure 3.16: Process of embroidering the squares.

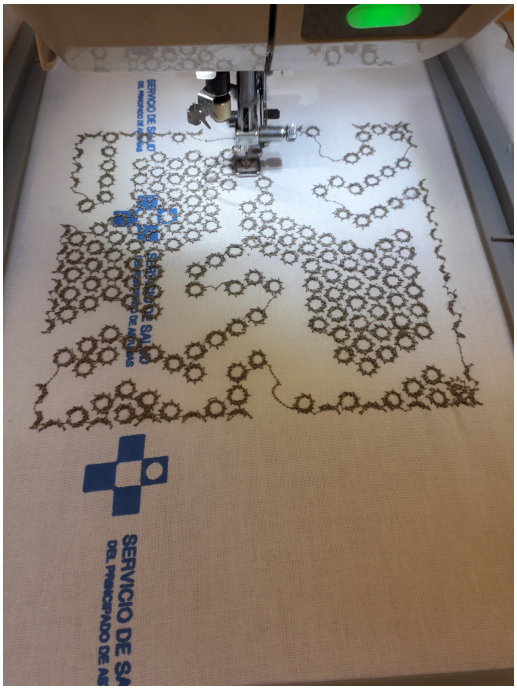

Figure 3.17: Process of embroidering the hexagons.

When the embroidering machine is done the next step is to attach the layer of substrate (Fig. 3.18) using an adhesive spray for fabric and the ground or conductive layer, which will be made of copper (Fig. 3.20).

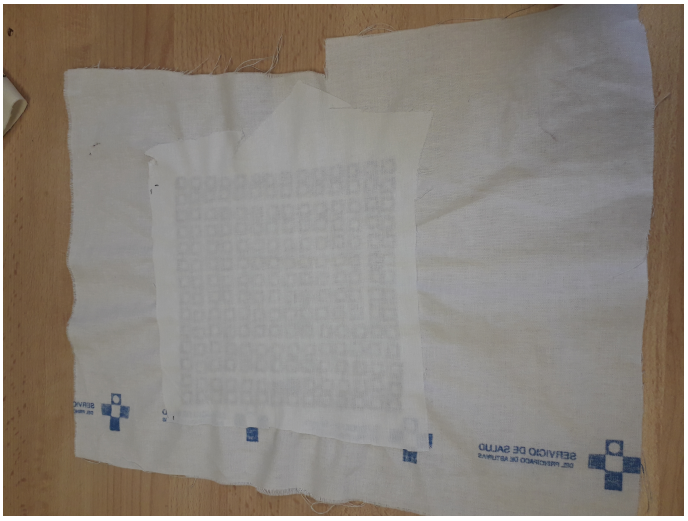

Figure 3.18: Layer of substrate attached on the back.

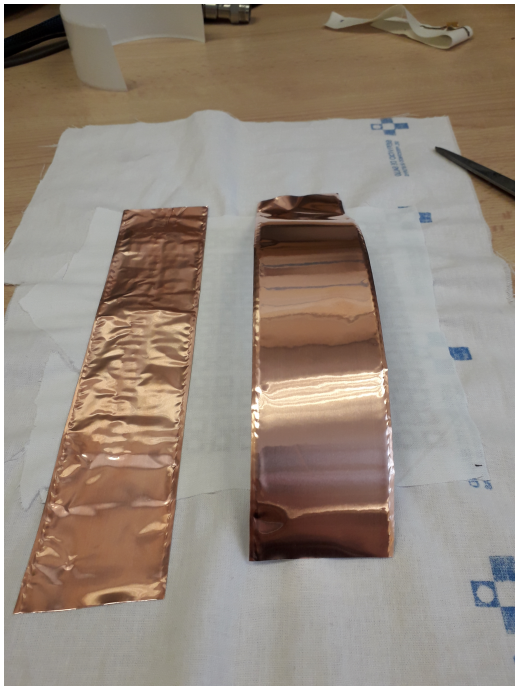

Figure 3.19: Construction of the ground in process.

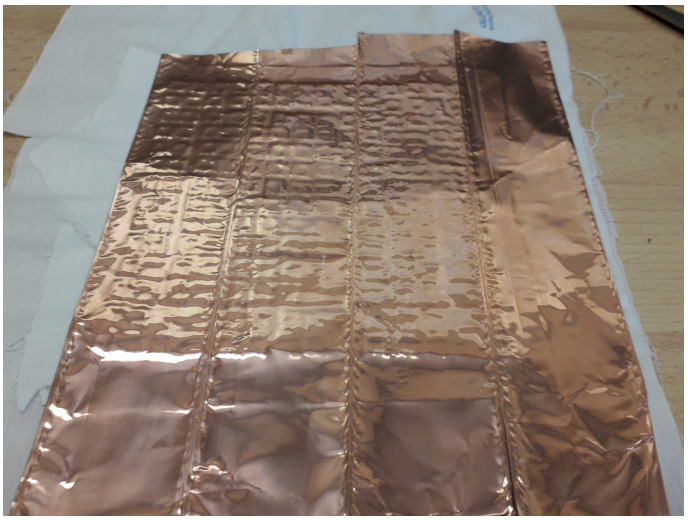

Figure 3.20: Ground layer.

So, the final result is as the one depicted in Fig. 3.21. In this same picture it is also possible to appreciate how the different sides have been labeled with a letter from A to H. This is because during the testing phase the two surfaces will be rotated in order to determine if the orientation affect the performance, especially because of the imperfections that appeared during the embroidering process (highlited in Fig. 3.22 and Fig. 3.23) and whose effect will be considered later. However, it is important to see that these imperfections are essentially concentrated on the edges of the surfaces making this way the virtual effect of just reducing the effective size of the surface.

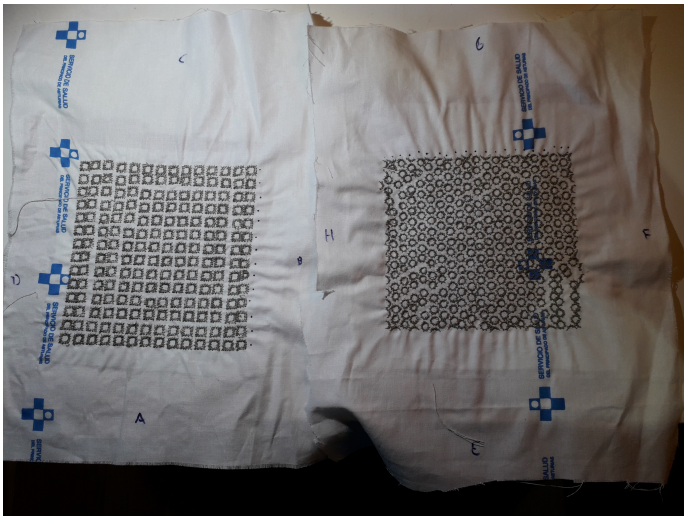

Figure 3.21: Final embroidered FSS.

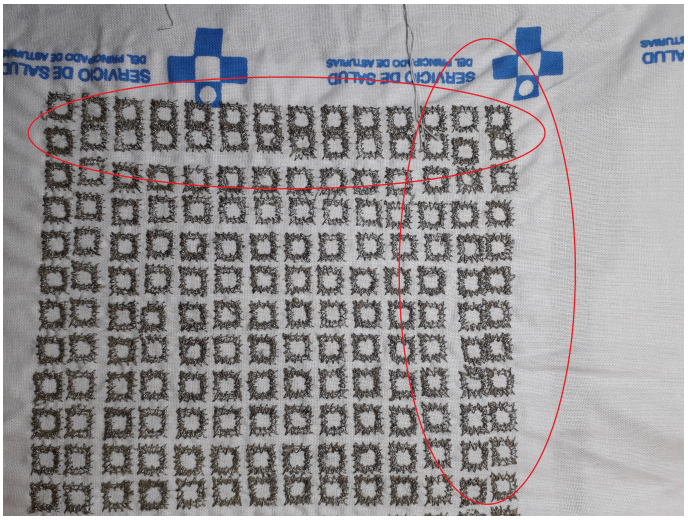

Figure 3.22: Imperfections of the FSS with square unit cells.

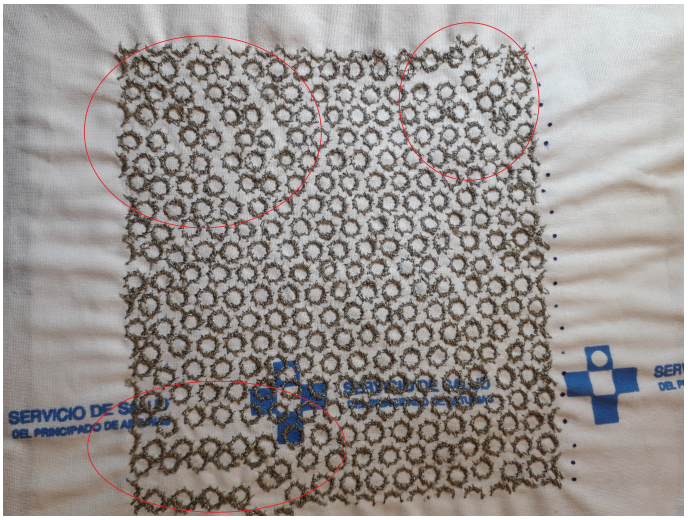

Figure 3.23: Imperfections of the FSS with hexagon unit cells.

3.6 Testing

Finally, the last step to assess if the simulations are correct is testing the crafted surfaces. To do so, the procedure will be as follows. First of all, the structure shown in Fig. 3.24 will be set. The structure is compound by a support fully made of wooden and plastic to avoid interference, a N9916A FieldFox Handheld Microwave Analyzer (whose specifications can be consulted in the Attachment to this Report) and two antennas placed in the same line and connected to the Microwave Analyzer.
One antenna works as the transmitter (tx) while the other is the receiver (rx) and both are centered with the FSS (Fig. 3.25). The small dimensions of the sample surface make this centering very important, because any small deviation may cause the result to vary since the surface would no longer be as simulated.

Figure 3.24: Structure used to test the sample surfaces.

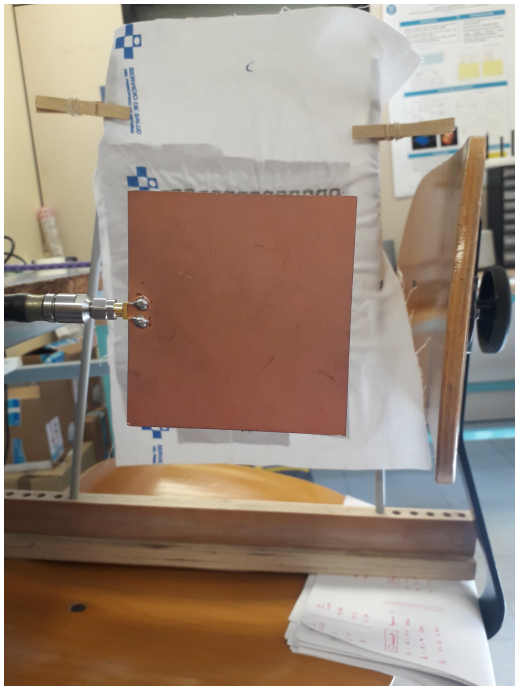

Figure 3.25: View of the relative position between the antenna and the surface on the structure.

Once prepared the system each surface is tested in its four possible orientations (referred as the letter which is in the bottom position in each specific case), as can be seen in Fig. 3.26 for the squares and Fig. 3.27 for the hexagons. In every situation the centering is done carefully and the dimensions depicted in Fig. 3.2 respected. The measured parameters are the S-Parameters S_{11} (related with the reflection) and the parameter S_{21}, related with the transmission. Both parameters are measured from 1 to 14 GHz taking 501 samples. The antennas were adapted at 2.4 GHz and, since the measures are relative, no calibration was done.

The dimensions of the full structure were: The antennas were separated 50 cm between them with the support centered at 25 cm. Also the antennas were 10 cm far from the table.

Figure 3.26: Sample with the square unit cell mounted in the structure.

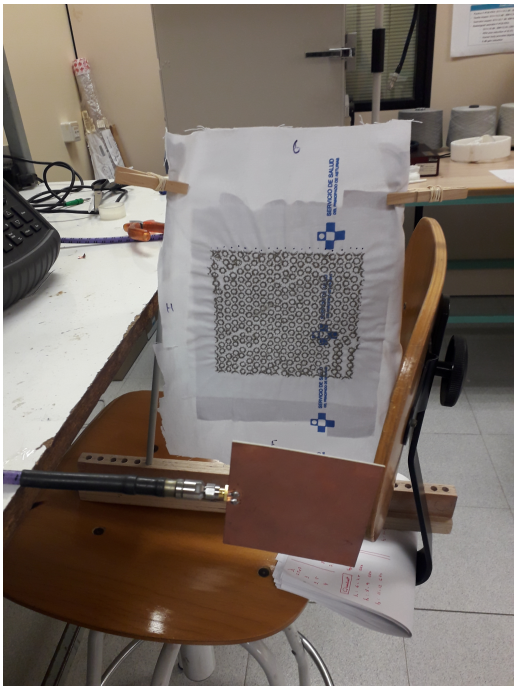

Figure 3.27: Sample with the square unit cell mounted in the structure.

Finally, in order to check what level of shielding was due to the circuit and what because of the ground layer a last test was performed just with the copper layer as depicted in Fig. 3.28.

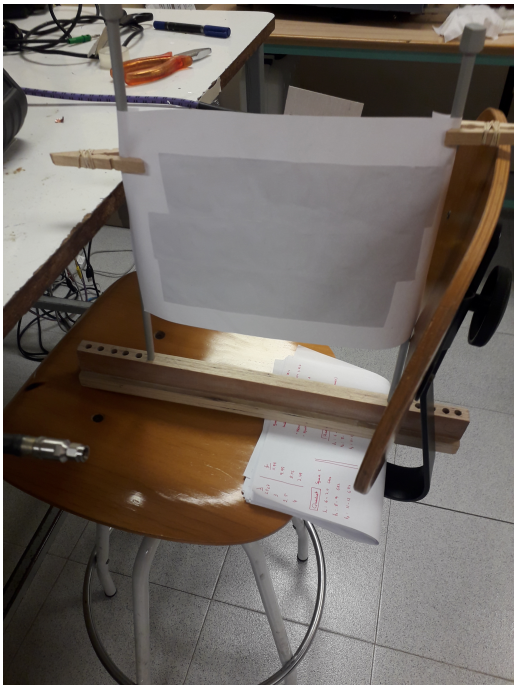

Figure 3.28: Test performed only with the metallic tape.

Results obtained with this simulations clearly showed a peak of attenuation around the expected frequencies, since S_{21} was clearly reduced. However, when computing the absorbance results made no sense, especially due to the wrong values obtained for the S_{11} parameter caused by the multiple reflections that appeared because of the fact that the testing was not being done surrounded by absorbent material.
To fix this, an alternative method of testing was proposed. To avoid extra reflections the testing was performed inside an electromagnetic diagnostic chamber Rohde & Schwarz DST 200 (Fig.

3.29). In addition to this, a calibration was done to improve the precision of the results. Finally, the antennas were changed for the one inside the chamber, Fig. 3.30, and a OmniLog 7600, Fig. 3.31, the specifications of which are also in the Attachment.

In spite of having different absolute value the relative values obtained for the transmission agreed with the previous testing done outside the chamber, while the improvement in the environment and the calibration made the values of S_{11} to become correct, leading to the final results shown in Chapter 4.

Figure 3.29: Exterior of the Electromagnetic Diagnostic chamber Rohde & Schwarz DST 200.

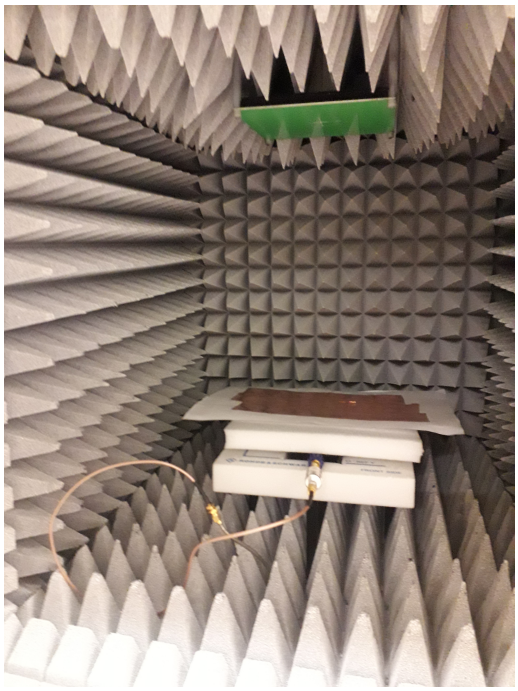

Figure 3.30: Exterior of the Electromagnetic Diagnostic chamber Rohde & Schwarz DST 200 with its antenna.

Figure 3.31: Antenna OmniLog 7600 used for the second part of the testing.

Chapter 4

Results

Although the system was tested from 1 to 14 GHz, the full graphs are only available in the Attachment of the Report, and here only the most relevant ones around the simulated frequency of resonance, going from 8 to 12 GHz, are shown.
Graphs are titled according to the measured parameters and the letter in the caption refers to the side that was on the bottom in each case, accounting this way to the orientation, which will be the way of assess the effect of the imperfections and irregularities (and, hence, asymmetries) that appeared during the crafting.

4.1 S-Parameters

The first evaluated parameters are the S_{11} and S_{21}. The expected performance is the reflection remain approximately constant while the transmission decreases. The results for the different configurations are shown in the Figures and Tables below:

Figure 4.1: S-Parameters for the A configuration around the frequency of interest. Experimental.

Figure 4.2: S-Parameters for the B configuration around the frequency of interest. Experimental.

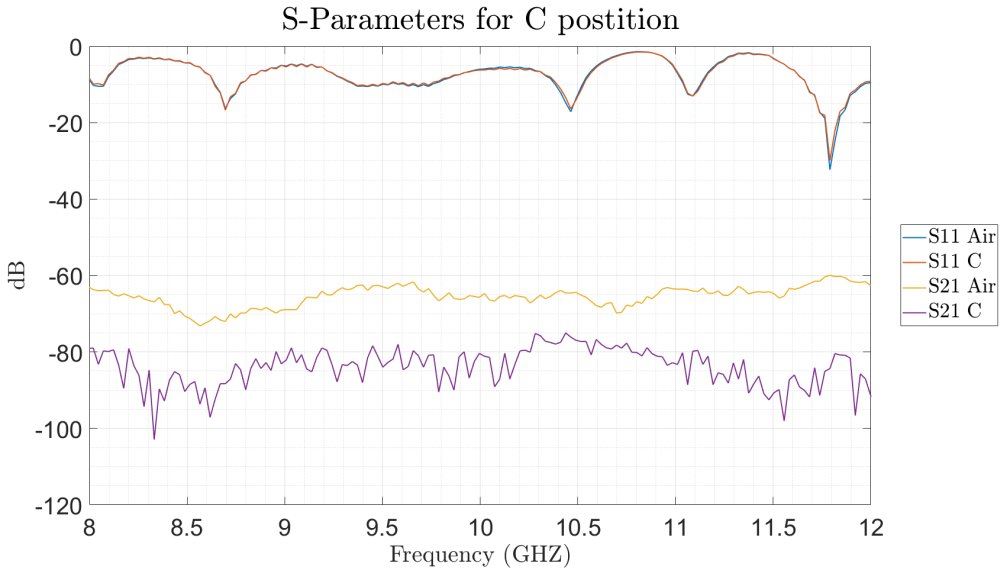

Figure 4.3: S-Parameters for the C configuration around the frequency of interest. Experimental.

Figure 4.4: S-Parameters for the D configuration around the frequency of interest. Experimental.

Figure 4.5: S-Parameters for the E configuration around the frequency of interest. Experimental.

Figure 4.6: S-Parameters for the F configuration around the frequency of interest. Experimental.

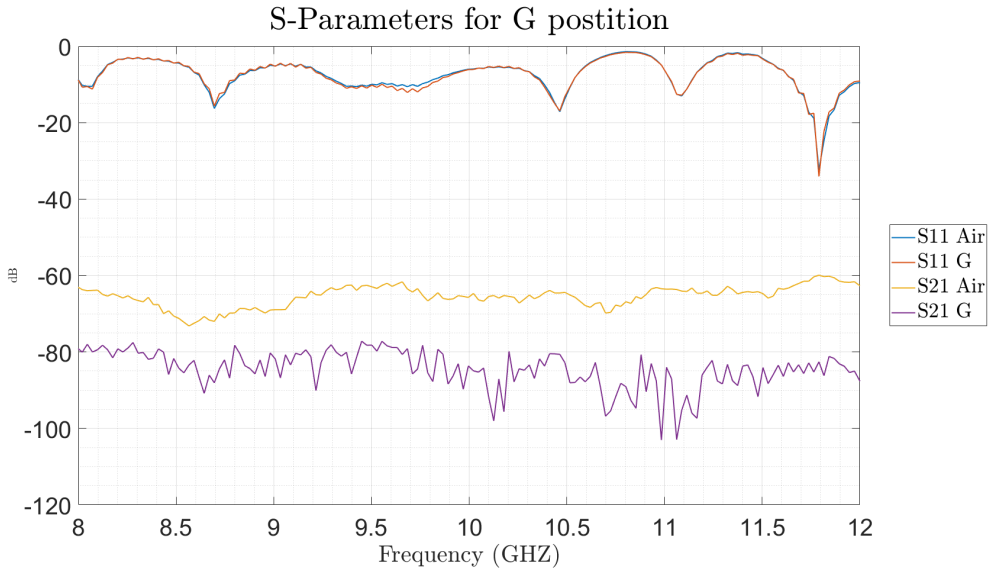

Figure 4.7: S-Parameters for the G configuration around the frequency of interest. Experimental.

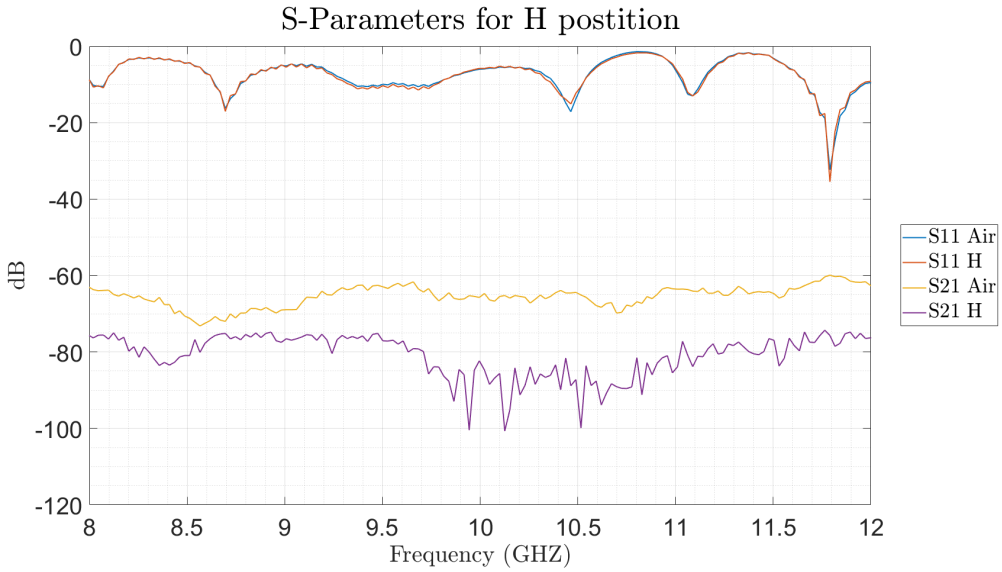

Figure 4.8: S-Parameters for the H configuration around the frequency of interest. Experimental.

Configuration	Frequency (GHz)	S_{21} (dB)
A	**11.89**	**-125.7**
A	11.53	-115.6
B	9.32	-107.7
B	10.15	-104.5
B	**11.66**	**-108.8**
C	**8.33**	**-102.9**
C	8.62	-97.1
C	11.56	-98.1
D	**9.74**	**-112.2**
D	10.10	-104.6
D	11.24	-104.4
D	11.43	-103.1
D	11.58	-100.5
E	8.51	-102.4
E	8.59	-101.6
E	9.89	-98.4
E	**10.20**	**-104.9**
F	9.42	-97.7
F	10.07	-98.2
F	10.78	-98.4
F	11.04	-100.3
F	11.22	-101.2
F	**11.58**	**-101.5**
G	10.13	-98.1
G	**10.98**	**-103.0**
G	11.06	-102.9
G	11.17	-97.3
H	9.94	-100.4
H	**10.13**	**-100.7**
H	10.52	-99.9

Table 4.1: Peaks of minimums for the S_{21} parameters for the different orientations.

In Table 4.1 the values in bold are the ones of maximum loss of transmission for each configu-

ration.

4.2 Difference

Although the value of the S_{21} parameter is a good way to assess the shielding (as it accounts for the loss of transmission) it makes no sense without a reference value, since it will always depend on the radiated power. For this reason, and with the purpose of determining the actual loss of power when the FSS is placed, the difference between the modulus of the S_{21} parameter with the FSS and without it (only air between the two antennas) will be calculated, allowing this way to determine the real effect of the surface on the performance of the system.

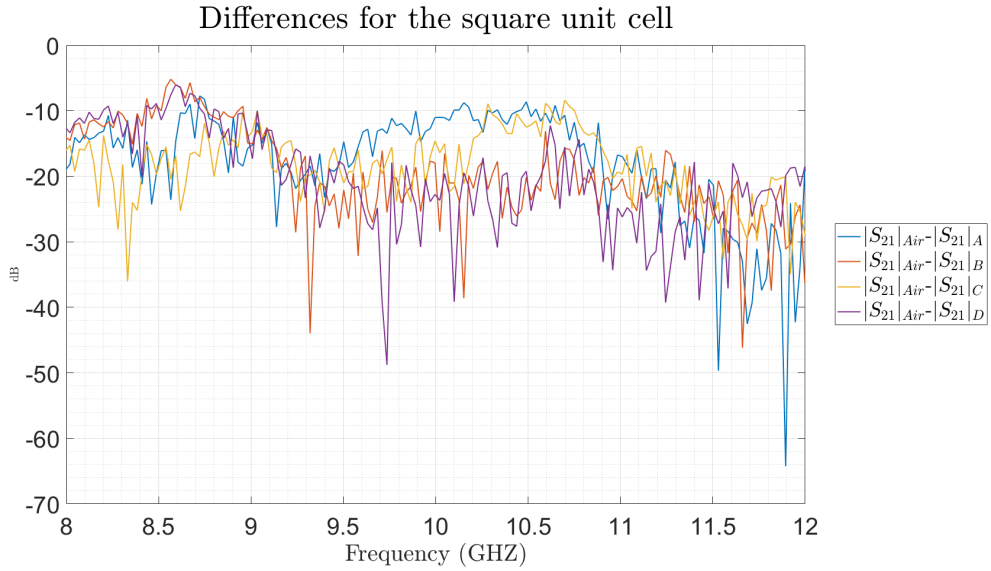

Figure 4.9: Difference on $|S_{21}|$ with and without the FSS made of square unit cells. Experimental.

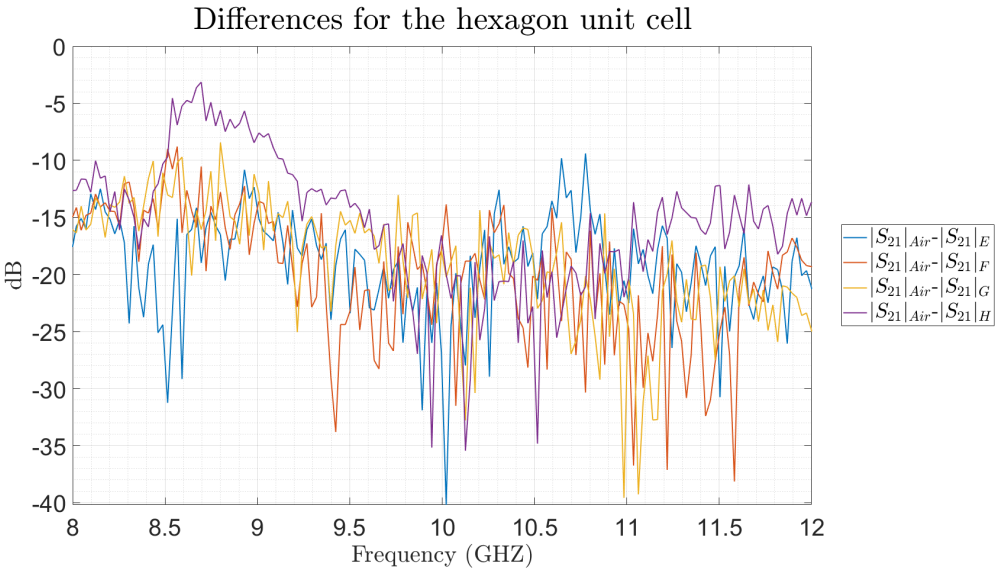

Figure 4.10: Difference on $|S_{21}|$ with and without the FSS made of square unit cells. Experimental.

The two maximum values for each configuration shown in Fig. 4.9 and Fig. 4.10 are shown in Table 4.2. These values are the points where the difference in the transmission that happens when the FSS is placed is maximum or, in other words, the frequencies that are attenuated the most by the material.

Configuration	Frequency (GHz)	$\|S_{21}\|_{Air} - \|S_{21}\|_{FSS}$ (dB)
A	11.53	-49.69
A	11.89	-64.24
B	9.32	-43.96
B	11.66	-46.16
C	8.33	-36.05
C	11.92	-34.91
D	9.74	-48.80
D	10.10	-39.17
E	9.90	-31.90
E	10.02	-40.19
F	11.22	-37.12
F	11.58	-38.14
G	10.98	-39.57
G	11.06	-39.26
H	9.94	-35.17
H	10.13	-35.44

Table 4.2: Maximum differences on the modulus of the transmission.

As expected the frequencies are the same or near to the ones of Table 4.1. In addition, now it is possible to see how the maximum of attenuation is between 35 and 65 dB.

4.3 Absorption

Finally, and as not only the transmission exist but also the reflection. Complex permittivity is related with the S_{11} parameter, while the complex permeability has to do with the S_{21} parameter both complex permittivity and permeability has been calculated based on the calculations given in the Nicholson-Ross-Weir (NRW) method. That is,

$$T = |\frac{E_t}{E_i}|^2 = |S_{21}|^2$$

$$\Gamma = |\frac{E_r}{E_i}|^2 = |S_{11}|^2$$

$$A = 1 - \Gamma - T = 1 - |S_{11}|^2 - |S_{21}|^2$$

So the absorption coefficient, A is given with respect to the power of the incident EM wave.

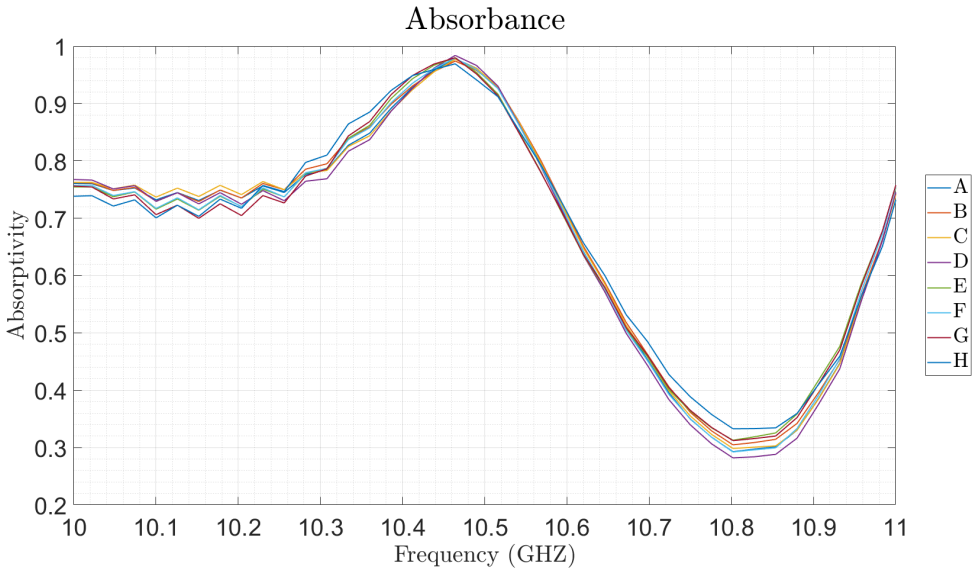

Figure 4.11: Absorbance around the desired frequency of 10.64 GHz. Experimental.

Configuration	Frequency (GHz)	A_{max} (%)
A	10.46	97.80
B	10.46	97.41
C	10.46	97.72
D	10.46	98.39
E	10.46	98.00
F	10.46	97.92
G	10.46	97.97
H	10.46	96.92

Table 4.3: Absorption around the frequency of optimization for the different configurations.

Looking at Table 4.3 it is possible to appreciate how the frequency of resonance has been slightly moved 0.2 GHz downwards, while the value of the absorption coefficient has reached the expected value of around 100%.

Before finishing this section, however, it is necessary to say that the thickness of the cotton used was 0.31 mm instead of the 0.4 mm considered for the simulations. Hence, it would be interesting to repeat the simulations with this new value of h to see if it helps justifying this shift in the frequency.

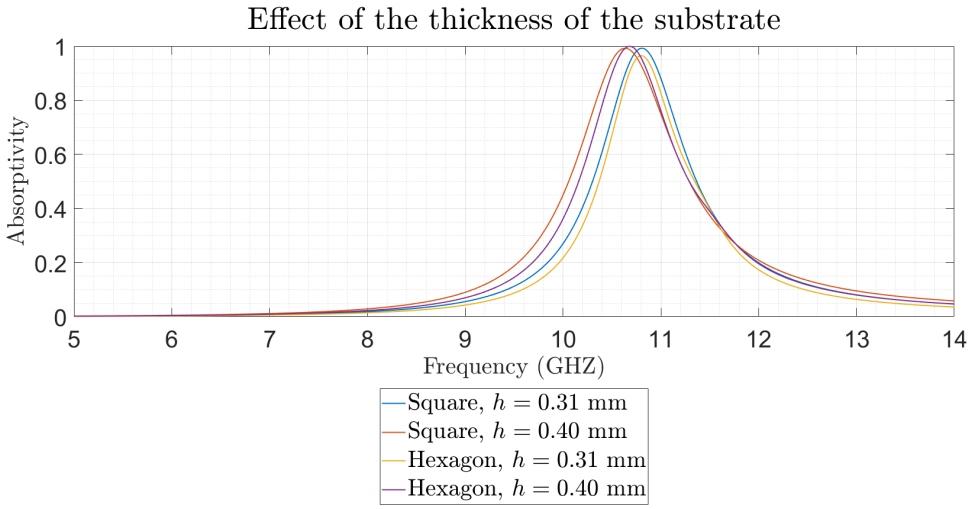

Figure 4.12: Absorbance considering different thickness of the substrate. Simulation.

In Fig. 4.12 it is possible to appreciate how, for the case of the square unit cell, a reduction in thickness leads to an increase of the frequency of resonance, while the maximum value of the absorption remains the same. For the case of the hexagon the frequency also increases and, in addition, the maximum absorption decreases.
So, in conclusion, although the change in the thickness of the substrate from the simulations to the reality may cause some deviations in both absorption (hexagonal shapes) and optimal frequency, it is not the main explanation of the observed shift in frequency, since the tendency is the opposite to the one observed.

4.4 Comparison with the simulation

When comparing the simulated and the measured values around the point of interest it is easy to appreciate how the measured frequencies have decreased around 0.24 GHz from the simulation, while the absorption has decreased just around 1%, which is negligible at all effects. The main differences, then, are the BW of the peak of absorption and the shape around it. These small differences, however, may be due to different effects, which will be broken down in the following lines: First of all, the materials used are not perfect. In order to reduce the computational time the material considered for the conductor on the simulations has been PEC (Perfect Electric Conductor). Although this should not make a huge difference it has some effect on the results. Another source of error are the fabrics. Values used for the fabric electric constants are measured each time, since as they are not materials designed for electronic purposes their electromagnetic properties may change depending on the piece used, making it necessary to measure them every time or use an approximation, being aware of the error that this may introduce. Some part of the error also comes from the fact that the real surface is not infinite. In the CST the calculations are done considering the surface as an infinite extension of unit cells, since it makes much easier for the computer to solve the system. This approximation causes, among others, the peak to be perfect and centered on the desired frequency. In the reality, however, the dimensions of the piece of fabric are limited and, the bigger they are, the closer they are to an infinite surface and, hence, more similar are the results. The fabric used for this thesis was relatively small and even despite this the results have been very similar to the expected ones. As has already been mentioned the weaving technique has not been considered neither in the simulations nor in the design, even though it has some degree of influence on the performance.

Nevertheless, the two factors that may have affected the most the final properties of the frequency selective surfaces are related to the embroidering machine. These are the precision and the perfection of the form. Since the embroidering machine moves in a discrete way there is a certain level of accuracy that can reach, being this way impossible to perfectly reproduce the simulated shapes, which had an accuracy up to tenths of a millimeter. In addition to that, the fact of using satin 20% has also made that the supposed conductor was not fully filled as was in the simulations. The main effect of distortion, however, was the misalignment of some unit cells. Mechanical frictions, undesired tensions, the use of some mechanical parts... All this facts that occur in the real world that are not taken into account in the simulations made that some unit cells were more away ones from the others than expected, while in other cases they were stuck together. This caused the pattern to break and, in fact, reduced the effective area of the FSS' making it less close to infinite.

So, to sum up, all the imperfections that happen when designs are brought to reality along with the inaccuracies that always appear when working at high frequencies made the results not to be perfect. However, they were really close to the ones of the simulations and, considering all the aforementioned, it proved that the assumptions, procedure and technology were correct.

It is important to note, in addition, that a more narrow peak of absorption has appeared for the measured textiles at 11.09 GHz (Fig. 4.15). Although this peak is not considered for the main conclusions its allocation, shape and values make of it another point of interest and whose main characteristics are written down in Table 4.5.

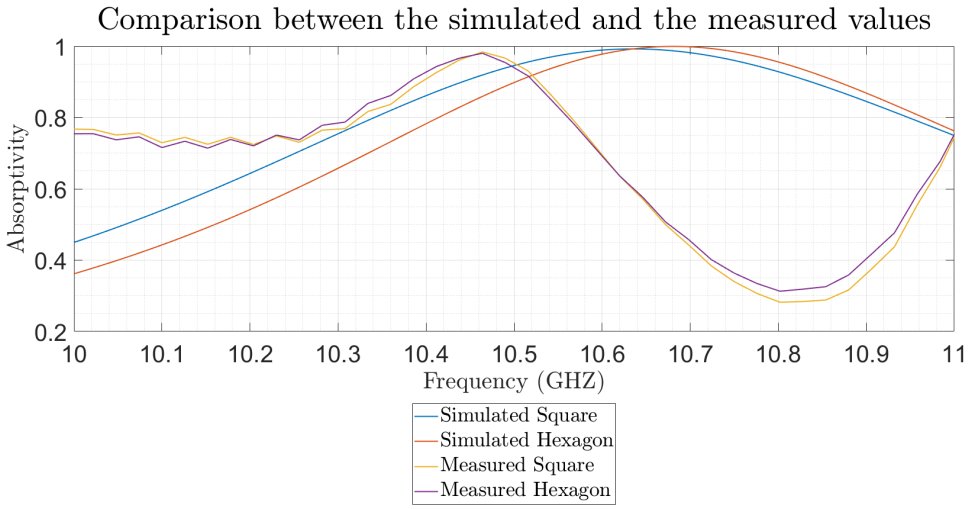

Figure 4.13: Absorbance for the measured and simulated configurations.

Shape	Case	Frequency (GHz)	A_{max} (%)
Square	Simulated	10.63	99.23
Hexagon	Simulated	10.68	99.94
Square	Measured	10.46	98.39
Hexagon	Measured	10.46	98.00

Table 4.4: Absorption around the frequency of optimization for the different configurations.

Shape	Case	Frequency (GHz)	A_{max} (%)
Square	Simulated	10.63	99.23
Hexagon	Simulated	10.68	99.94
Square	Measured	11.09	95.65
Hexagon	Measured	11.09	94.09

Table 4.5: Absorption around the alternative frequency of optimization for the different configurations.

Tables 4.4, 4.5 and Fig. 4.13 have been done considering the D and E orientations respectively.

Finally, regarding the bandwidth the usual way to measure it is the so called FWHM (Full-width at half-maximum), which is the range of frequency between two neighboring 50% absorption points, and is used as figure of merit for absorption bandwidth (see Fig. 4.15 and Table 4.7 and 4.8).
However, due to the complex shape of the experimental peak, in order to properly analyze the results and considering that just a 50% of absorption would not be enough for most of the possible applications, a second comparison considering 80% of absorption as the cut will be done (Fig. 4.14 and Table 4.6).

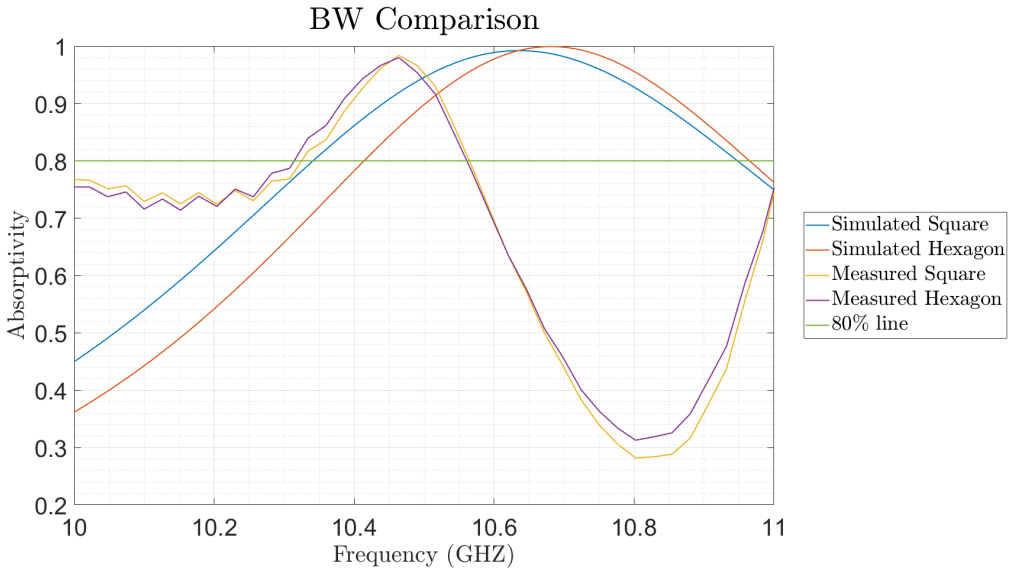

Figure 4.14: Comparison of the BW of the simulated and measured results.

Case	f_{min} (GHz)	f_{max} (GHz)	BW(GHz)
Sim. Square	10.34	10.95	0.61
Sim. Hexagon	10.41	10.97	0.56
Meas. Square	10.32	10.57	0.25
Meas. Hexagon	10.31	10.55	0.24

Table 4.6: BW comparison of 80%.

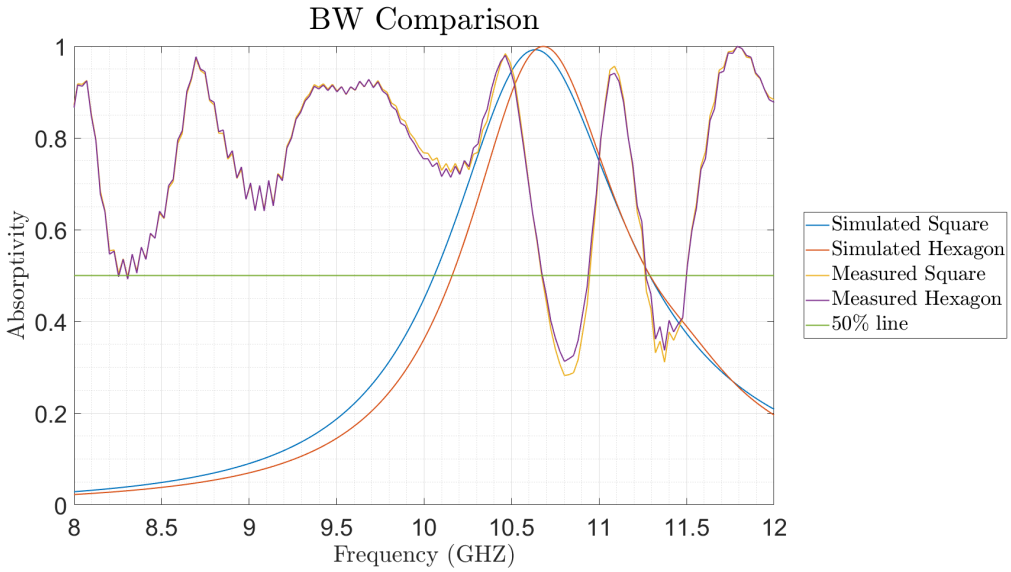

Figure 4.15: Comparison of the FWHM of the simulated and measured results.

Case	f_{min} Band 1 (GHz)	f_{max} Band 1 (GHz)	FWHM Band 1 (GHz)
Sim. Square	10.34	10.95	0.61
Sim. Hexagon	10.41	10.97	0.56
Meas. Square	8.31	10.57	2.26
Meas. Hexagon	8.31	10.55	2.24

Table 4.7: FWHM of the main absorption band.

Case	f_{min} Band 1 (GHz)	f_{max} Band 1 (GHz)	FWHM Band 1 (GHz)
Sim. Square	10.34	10.95	0.61
Sim. Hexagon	10.41	10.97	0.56
Meas. Square	10.93	11.27	0.34
Meas. Hexagon	10.93	11.27	0.34

Table 4.8: FWHM of the main absorption band.

Chapter 5

Conclusion

It has been demonstrated in this project that wearable metamaterials are a reality and that, by means of conventional fabrics and conductive thread, it is possible to reach surfaces with a high level of absorption, with all the implications that it has when it comes to new applications like vests, curtains and so, opening, at the same time, a new field of investigation to reduce the effect of electromagnetic radiation on the human body, since it is growing day by day and becoming a problem in some cases. Wearable FSSs made of cotton and silver thread have been demonstrated to be effective for reducing the impact of the electromagnetic radiation.

Specifically, tests and simulations in this thesis have been carried out in the X-Band, which goes from 8 to 12 GHz. In this range of frequency a maximum attenuation of 64.24 dB has been reached at the peak when the surface was placed.

In this thesis a first approximation for a FSSs adapted to 10.64 GHz, a frequency that offers real applications with good dimensions, using two different shapes has been simulated, crafted, and tested, and several conclusions have been drawn.
The computational requirements for simulating a FSS in its real extent are huge. For this reason the approximation of considering it a surface with infinite extension is done. This way the computational complexity diminishes but, since it is impossible, also introduces some errors. Using this approximation, however, carrying several sweeps changing some geometric variables have become possible, allowing to obtain the optimal values within the desired time.

Then, when crafting the optimal shapes some issues have appeared. First of all, the software considered the conductor as a block, while in the reality it was made of several stitches, which slightly changed the shape. In addition, computational optimizations were done with a precision up to tenths of millimeter, while it was impossible to obtain using a conventional embroidering machine. Besides, some tensions and the non-rigid nature of the fabric made the pattern to become irregular, making some distances to vary. Luckily, these errors were on the borders of the shape and did not cause a huge effect on the performance of the material, since their actual effect was to reduce the effective area.

In general, the main difference between the simulations and the experimental results was the bandwidth. While the frequency of resonance suffered just a small deviation due to the mentioned differences between the sample and the model and the peak of absorbance also were just diminished around 2%, the width of this peak was reduced below the half of the bandwidth of the one of the simulation.
In the simulations the peak of absorbance of the squares was at 10.63 GHz and had a value of 99.23%, while the one of the hexagons was at 10.69 GHz with a value of 99.94%. About the BW, if a 80% is considered it has a value of 0.61 GHz for the squares and 0.56 GHz for the hexagons.
Regarding the simulations, two peaks or bands appeared. The main one and the one that is used to extract the main conclusions has a peak situated at 10.46 GHz for both the hexagons and the squares, reaching a maximum value of absorption of 98.39% for the squares and 98.00% for the hexagons. With the consideration of the 80%, this peak has a bandwidth of 0.25 GHz in the case of the squares and 0.24 GHz for the hexagons. The secondary peak, at its turn, is centered at 11.09 GHz and is a little bit lower, giving a maximum value of 95.65% for the squares and 94.09% for the hexagons. The main difference between both peaks, however, is given when the FWHM is considered, since for the primary peak, which in fact is a wide band, it reaches a value of 2.26 GHz for the squares and 2.24 GHz for the hexagons, while the values for the second peak are much

lower: 0.34 GHz in both cases. So, to sum up, when comparing the simulated and the experimental results is easy to see how the frequency of resonance has slightly shifted 0.20 GHz downwards if the main peak (or band) is considered and 0.63 GHz upward if the secondary peak is considered. Besides, the resulting BW is also different. While the simulation gave as a result a very clear peak the experimental data was very different, since two peaks around the expected frequency appeared. If the 80% of absorption as a cut is considered both peaks are much narrow than the one of the simulation but, regarding the FWHM, the main peak becomes a very wide band. Then, the main conclusion that can be drawn of this behaviour is that, although the simulation is perfect and serves as a first approximation, there will always be some frequency shifts in the reality. In addition, the more complex shape of the peaks or bands of the experimental results also make necessary to decide which will be the cut frequency that will determine when the application is useful or not, because due to the irregular shape of the peaks the value of this cut frequency may make the BW to vary a lot or even make a secondary peak useful or not.

All these differences can be explained by the same means mentioned before, considering also some differences on the electric properties of the fabric, which is not a material designed for electromagnetic purposes.

So, in short, in this thesis has been proven that with some computer simulations and conventional textiles it is possible to obtain a frequency selective surface with good properties, showing this way that the technology and methodology are correct. However, in order to obtain a material with superb performance some considerations have to be done. Since regular textile materials are not meant for this kind of purposes some modifications should be done like, for instance, crafting them trying to keep constant electric properties. Apart from that, the equipment should be much more precise and allow to create bigger structures. At the same time, the weaving technique should also be considered.

Once the technology is proven effective, the next logical step is to improve it in order to try to obtain materials with superb electromagnetic properties fully operative. To do so, first of all is necessary to be able to simulate the structure with real dimensions and without the infinite approximation and considering the weaving technique. After that, embroidering it using high precision equipment to perfectly meet the simulation structure is also mandatory.

Finally, one last conclusion which is not from a main objective but may become important in the future is the environmental aspect, since fabrics like cotton are much easier to recycle than some polymers or other conventional electronic's materials.

Chapter 6

Planification

This section is devoted to the organization and administration of the project. First of all, a list with the different activities is given and, after that, the relationships between them are presented. Finally the amount of hours of dedication for each task is shown and, using all of this, the Gantt Diagram followed is presented.

6.1 List of Activities

ID	Activity	Description
1	**Bibliographic Research**	
1.1.	Metamaterials	Research of information of Metamaterials as a concept and their applications
1.2.	Frequency Selective Surfaces	Research of information about Frequency Selective Surfaces.
1.3.	Wearable Metamaterials	Understanding the concept of wearable metamaterial and its possible applications.
1.4.	Antenna Theory	Learning and understanding the basics on Antenna Theory in order to properly process and understand the results.
2	**CST Training**	
2.1.	Software Learning	Learning how the software works: its possibilities characteristics and options.
2.2.	First tests	Carrying out the first sample tests given by the developers of the software.
2.3.	Sample Case	Reproduction of a real case given in a paper in order to assess the correctness of the procedure followed and options chosen for the configuration of the solver.
3	**Unit Cell Design**	
3.1.	First Geometrical Approximation	Design of the initial measures based on previous experience and data given by the literature.
3.2.	Simulations and Optimization	Simulations sweeping the different geometrical parameters up to obtaining the most optimal one.
3.3.	Final Simulations	Simulations of the final geometries to obtain the information.
4	**Testing**	
4.1.	File creation	Convert the CST file in the one necessary for the sewing machine to work.
4.2.	Sewing	Sewing the different fabrics.
4.3.	Sample Construction	Construction of the surfaces to be tested.
4.4.	Support Building	Building of the support necessary to test the metamaterials.
4.5.	Testing	Testing the two surfaces made and extracting the desired parameters.
4.6.	Data handling and post-processing	Obtaining the necessary values from the data of the tests and comparing it with the ones from the simulations.
5	**Documentation Generation**	
5.1.	Report	Generation of the Report.
5.2.	Attachment	Generation of the Attachment.
5.3.	Budget	Generation of the Budget.

Table 6.1: Activity List.

6.2 Sequence Activities

ID	Activity	Predecessor	Relationship
1	**Bibliographic Research**		
1.1.	Metamaterials		
1.2.	Frequency Selective Surfaces	1.1.	FS
1.3.	Wearable Metamaterials	1.2.	FS
1.4.	Antenna Theory		
2	**CST Training**		
2.1.	Software Learning		
2.2.	First tests	2.1.	FS
2.3.	Sample Case	1.3. 2.2.	FS
3	**Unit Cell Design**		
3.1.	First Geometrical Approximation	1.3.	FS
3.2.	Simulations and Optimization	3.1. 2.3.	FS
3.3.	Final Simulations	3.2.	FS
4	**Testing**		
4.1.	File creation	3.3.	FS
4.2.	Sewing	4.1.	FS
4.3.	Sample Construction	4.2.	FS
4.4.	Support Building		
4.5.	Testing	4.3. 4.4.	FS
4.6.	Data handling and post-processing	4.5.	FS
5	**Documentation Generation**		
5.1.	Report		
5.2.	Attachment		
5.3.	Budget		

Table 6.2: Activities sequencing.

6.3 Resources Requirements

ID	Activity	time (h)
1	**Bibliographic Research**	**55**
1.1.	Metamaterials	22
1.2.	Frequency Selective Surfaces	22
1.3.	Wearable Metamaterials	6
1.4.	Antenna Theory	5
2	**CST Training**	65
2.1.	Software Learning	30
2.2.	First tests	10
2.3.	Sample Case	25
3	**Unit Cell Design**	93
3.1.	First Geometrical Approximation	5
3.2.	Simulations and Optimization	80
3.3.	Final Simulations	8
4	**Testing**	**67**
4.1.	File creation	2
4.2.	Sewing	10
4.3.	Sample Construction	3
4.4.	Support Building	4
4.5.	Testing	8
4.6.	Data handling and post-processing	40
5	**Documentation Generation**	**60**
5.1.	Report	50
5.2.	Attachment	5
5.3.	Budget	5

Table 6.3: Resources Requirements.

6.4 Gantt Diagram

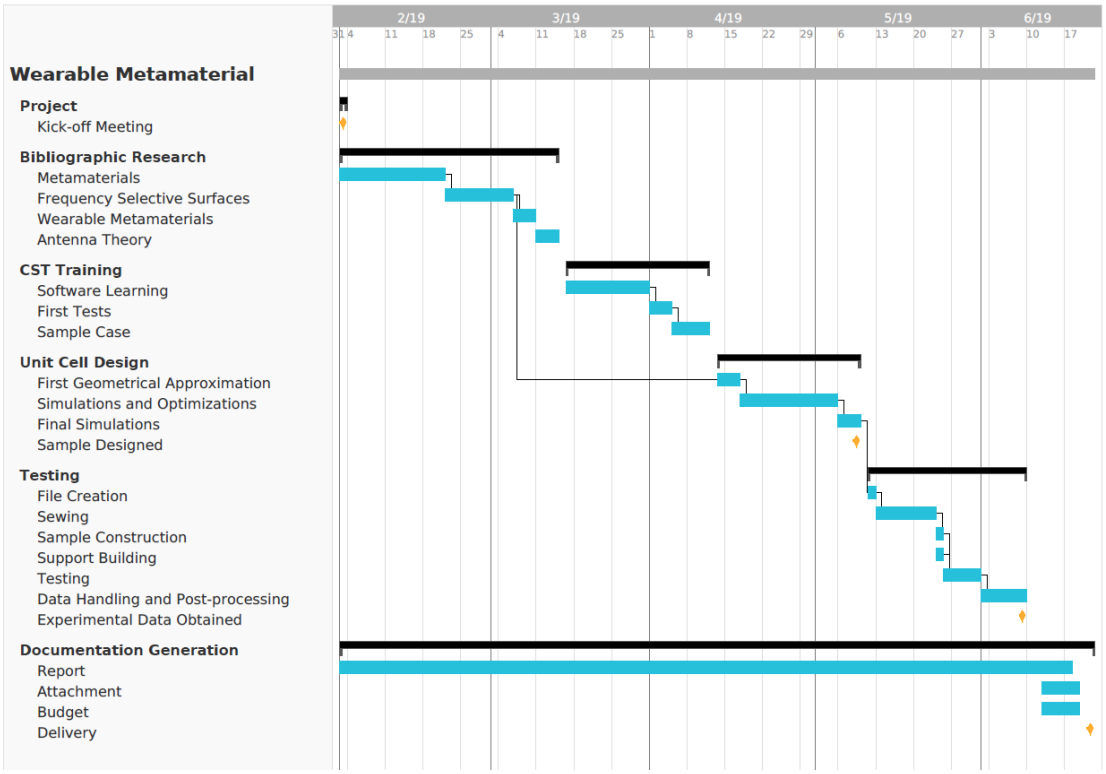

Figure 6.1: Gantt Diagram for the whole project.

Bibliography

[1] AIMME: Unidad de Materiales y Tratamientos Superficiales. *Aproximación a los metamateriales: Aproximación a tecnologías emergentes*, February 2011.

[2] Dr. Jeffrey D. Wilson. Metarefraction. Available at: https://commons.wikimedia.org/wiki/File:Metarefraction.svg. Last Access: 08/03/2019.

[3] Kirti Inamdar; Y. P. Kosta and Suprava Patnaik. Microwave applications of metamaterials concepts. *2010 International Conference on Advances in Recent Technologies in Communication and Computing*, pages 292–294, 2010.

[4] Daniel Binion et al. A metamaterial-enabled design enhancing decades-old short backfire antenna technology for space applications. *Nature Communications*, 10(108), 2019.

[5] Érico Cadineli Braz and Antonio Luiz Pereira de Siqueira Campos. Multiband frequency selective surfaces with a modified multifractal cantor geometry. *Journal of Microwaves, Optoelectronics and Electromagnetic Applications*, 13(2):111–121, December 2014.

[6] Wu Te-Kai. Frequency selective surfaces. *Encyclopedia of RF and Microwave Engineering*, 10.1002/0471654507.eme133, 2005.

[7] Rana Sadaf Anwar et al. Frequency selective surfaces: A review. *Applied Sciences*, 8(9), 2018.

[8] Pioneering 21st Century Electromagnetics and Photonics. Lecture 20: Frequency selective surfaces and metasurfaces. Available at: http://emlab.utep.edu/ee5390em21.htm. Last Access: 14/03/2019.

[9] Ben A. Munk. *Frequency Selective Surfaces: Theory and Design*, volume 29. John Wiley & Sons, Inc. Wiley Online Library: Hoboken, NJ, USA, 2000.

[10] CST GmbH–Computer Simulation Technology. *CST Microwave Studio - 3D EM for High Frequencies: Getting Started*. CST –Computer Simulation Technology, 2019.

[11] Jinpil Tak and Jaehoon Choi. A wearable metamaterial microwave absorber. *IEEE Antennas And Wireless Propagation Letters*, 16:784–787, 2017.

[12] CST GmbH–Computer Simulation Technology. Fss help - home - tutorials and examples - fss: Simulation of resonator array.

[13] Singer. Futura xl-550 sewing and embroidery machine. Available at: https://www.singer.com/Futura-XL-550-Sewing-Embroidery-Machine. Last Access: 13/06/2019, 2019.

[14] Rohde & Schwarz. R & s dst200 rf diagnostic chamber. Available at: https://www.rohde-schwarz.com/pk/product/dst200-productstartpage_63493-11087.html. Last Access: 13/06/2019, 2019.

[15] AARONIA AG. Ultra broadband antenna omnilog 70600. Available at: https://www.aaronia.com/products/antennas/OmniLOG-70600-Omni-Directional-Antenna/. Last Access: 13/06/2019, 2019.

[16] Keysight Technologies. N9916a fieldfox handheld microwave analyzer, 14 ghz. Available at: https://www.keysight.com/en/pdx-x201925-pn-N9916A/fieldfox-handheld-microwave-analyzer-14-ghz?cc=ES&lc=eng. Last Access: 13/06/2019, 2019.

[17] World Health Organization. Electromagnetic fields (emf). Available at: https://www.who.int/peh-emf/about/WhatisEMF/en/index1.html. Last Access: 08/06/2019, 2019.

[18] Wikipedia: The Free Encyclopedia. Electromagnetic radiation and health. Available at: https://en.wikipedia.org/wiki/Electromagnetic_radiation_and_health. Last Access: 09/06/2019, 2019.

[19] Li Yz et al. Effects of electromagnetic radiation on health and immune function of operators. *US National Library of Medicine National Institutes of Health*, 31(8):602–605, August 2013.

[20] National Research Council (US) Committee on Assessment of the Possible Health Effects of Ground Wave Emergency Network (GWEN). Effects of electromagnetic fields on organs and tissues. Available at: https://www.ncbi.nlm.nih.gov/books/NBK208983/. Last Access: 10/06/2019, 1993.

[21] M. Nauman et al. A miniaturized flexible frequency selective surface for x-band applications. *IEEE Transactions on Electromagnetic Compatibility*, 58(2):419–428, 2016.

[22] University of Oxford. English: Oxford living dictionaries. Available at: https://en.oxforddictionaries.com/definition/metamaterial. Last Access: 07/03/2019.

[23] Rakhesh Kshetrimayum. A brief intro to metamaterials. *IEEE Potentials*, 5(23):44–46, 2005.

[24] Andrés García Aguilar. *Análisis, diseño y prototipado de una lente plana basada en estructuras metamateriales para antenas*. PhD thesis, Universidad Politécnica de Madrid: Escuela Técnica Superior de Ingenieros de Telecomunicaciones, 2008.

[25] Sergey Antipov et al. Development of metamaterials for cherenkov radiation based particle detectors. In *Proceedings of the 23rd Particle Accelerator Conference*, volume T03 - Beam Diagnostics and Instrumentation, pages 3432–3434, 2010.

[26] Christophe Caloz; Tatsuo Itoh. Metamaterials for high-frequency electronics. *Proceedings of the IEEE*, 93(10):1744–1752, 2005.

[27] Pere Josep Ferrer González. *Multifunctional Metamaterial Designs for Antenna Applications*. PhD thesis, Universitat Politècnica de Catalunya: Department of Signal Theory and Communications, 2015.

[28] Lim Sungjoon; Christophe Caloz and Tatsuo Itoh. Metamaterial-based electronically controlled transmission-line structure as a novel leaky-wave antenna with tunable radiation angle and beamwidth. *Microwave Theory and Techniques, IEEE Transactions*, 53:161–173, 2005.

[29] George V. Eleftheriades; Ashwin K. Iyer and Peter C. Kremer. Planar negative refractive index media using periodically $l^{\smile}c$ loaded transmission lines. *IEEE Transactions on Microwave Theory and Techniques*, 50(12):2702–2712, 2002.

[30] A.K. Popov and V.M. Shalaev. Negative-index metamaterials: second-harmonic generation, manley–rowe relations and parametric amplification. *Applied Physics B: Lasers and Optics*, 84(131), 2006.

[31] Kazuo Sato. Metamaterials and automotive applications. *R&D review of Toyota CRDI*, 41(4), 2007.

[32] Pekka Alitalo and Sergei Tretyakov. Electromagnetic cloaking with metamaterials. *Materials today*, 12(3):22–29, 2009.

[33] F. Bilotti; S. Tricarico and L. Vegni. Design of invisibility cloaks for reduced observability of objects. In Jose M. Llorens and Luzi Bergamin, editors, *Metamaterials for Space Applications*. University Roma Tre, ESA, July 2008.

[34] D. P. Gaillot; C. Croënne and D. Lippens. Cloaking via a full dielectric metamaterial and transformation optics for high resolution focusing. In Jose M. Llorens and Luzi Bergamin, editors, *Metamaterials for Space Applications*. Institut d'Electronique de Microélectronique et de Nanotechnologie, Université des Sciences et Technologies de Lille, ESA, July 2008.

[35] Pekka Alitalo and Sergei Tretyakov. Chiral particles and transmission-line networks for cloaking applications. In Jose M. Llorens and Luzi Bergamin, editors, *Metamaterials for Space Applications*. Department of Radio Science and Engineering, TKK Helsinki, University of Technology, ESA, June 2008.

[36] Stanislav B. Glybovski et al. Metasurfaces: From microwaves to visible. *Physics Reports*, 634(24):1–72, May 2016.

[37] Filippo Costa; Agostino Monorchio and Giuliano Manara. An overview of equivalent circuit modeling techniques of frequency selective surfaces and metasurfaces. *The Applied Computational Electromagnetics Society Journal*, 29(12):960–976, 2014.

[38] F. Yang; Y. Rahmat-Samii. *Electromagnetic Band Gap Structures in Antenna Engineering*. Cambridge University Press: Cambridge, UK, 2009.

[39] I. Anderson. On the theory of self-resonant grids. *The Bell System Technical Journal*, 54(10):1725–1731, December 1975.

[40] R. J. Luebbers and B. A. Munk. Some effects of dielectric loading on periodic slot arrays. *IEEE Transactions on Antennas and propagation*, 26(4):536–542, July 1978.

[41] E.A. Parker et al. Frequency selectively screened office incorporating convoluted fss window. *Electronic Letters*, 46(5):317–318, March 2010.

[42] M. Yan et al. A novel miniaturized frequency selective surface with stable resonance. *IEEE Antennas and Wireless Propagation Letters*, 13:639–641, 2014.

[43] John P. Gianvittorio et al. Self-similar prefractal frequency selective surfaces for multiband and dual-polarized applications. *IEEE Transaction on Antennas and Propagation*, 51(11):3088–3096, November 2003.

[44] Jordi Romeu and Yahya Rahmat-Samii. Fractal fss: A novel dual-band frequency selective surface. *IEEE Transaction on Antennas and Propagation*, 48(7):1097–1105, July 2000.

[45] C. Puente et al. Fractal multiband antenna based on the sierpinski gasket. *Electronic Letters*, 32(1):1–2, January 1996.

[46] José I. A. Trindade et al. Analysis of stop-band frequency selective surfaces with dürer's pentagon pre-fractals patch elements. *IEEE Transactions on Magnetics*, 47(5):1518–1521, May 2011.

[47] T. Wu. Sharp transition frequency selective surface with concentric double fractal elements. *Microwave and Optical Technology Letters*, 58(6):1388–1390, June 2016.

[48] Benito Sanz-Izquierdo et al. Singly and dual polarized convoluted frequency selective structures. *IEEE Transactions on Antennas and Propagation*, 58(3):690–696, March 2010.

[49] Bora Döken and Mesut Kartal. Easily optimizable dual-band frequency-selective surface design. *IEEE Antennas and Wireless Propagation Letters*, 16:2979–2982, 2017.

[50] Shufeng Zheng et al. Analysis of miniature frequency selective surfaces based on fractal antenna–filter–antenna arrays. *IEEE Antennas and Wireless Propagation Letters*, 11:240–243, March 2012.

[51] Kamal Sarabandi Abbas Abbaspour-Tamijani and Gabriel M. Rebeiz. Antenna–filter–antenna arrays as a class of bandpass frequency-selective surfaces. *IEEE Transactions on Microwave Theory and Techniques*, 52(8):1781–1789, August 2004.

[52] Bo Li Amir K. Rashid and Zhongxiang Shen. An overview of three-dimensional frequency-selective structures. *IEEE Antennas and Propagation Magazine*, 56(3):43–67, June 2014.

[53] M. Silvia; A. Campos and L. Kretly. Design of thin microwave absorbers using lossy frequency selective surfaces. *Micfrowave and Optical Technology Letter*, 57(4):928–933, April 2015.

[54] Michael Ghebrebrhan et al. Textile frequency selective surface. *IEEE Microwave And Wireless Components Letters*, 27(11):989–991, November 2017.

[55] R. Seager et al. Fabric based frequency selective surfaces using weaving and screen printing. *Electronic Letters*, 49(24):1507–1508, November 2013.

[56] Leticia Alonso González. *Design, Simulation and Manufacturing Techniques for Fully Textile Integrated Microwave Circuits and Antennas.* PhD thesis, Universidad de Oviedo: Departamento de Ingeniería Eléctrica, Electrónica, de Computadores y Sistemas, 2018.

[57] International Telecommunication Union (ITU). Sharing of the 10.6-10.68 ghz band by the fixed and mobile services and the earth exploration-satellite service (passive). Technical Report RS.2096, International Telecommunication Union (ITU), 2007.

[58] G. Goncalves et al. Comparison of fss topologies for maximising the bandwidth of ultra-thin microwave absorbers. In *13th European Conference on Antennas and Propagation (EuCAP 2019)*, 2019.

[59] Weiwei Li and Atif Shamim. Silver nanowires based transparent, broadband fss microwave absorber. In *13th European Conference on Antennas and Propagation (EuCAP 2019)*, 2019.

Appendices

Appendix A

Attachment

A.1 Equipment

This section is devoted to give a short explanation of the equipment used for the tests, giving its main parameters in order to better understand how the experimental measures were taken.

A.1.1 Singer Futura XL-550 Sewing and Embroidery Machine

The sewing machine used during this project was the Singer Futura XL-550 Sewing and Embroidery Machine (Fig. A.1).
This machine offers a combination of sewing, embroidery designs, and software that makes it really ewasy to use. Among other features, it includes [13]:

- 125 Designs + 20 Fonts for embroidery.
- Function SwiftSmart Automatic Needle Threader.
- Multiple Hoop Capability for oversized designs.
- 215 Buil-in Stitches-basic, stretch, decorative.
- Bonus software to create designs and fonts.

Estimated cost: 1399.99 €.

Figure A.1: Singer Futura XL-550 Sewing and Embroidery Machine [13].

A.1.2 Rohde & Schwarz DST200 RF Diagnostic Chamber

Some of the measures were taken in a Rohde & Schwarz DST200 RF Diagnostic Chamber, which allows accurate radiated testing of wireless devices 400 MHz to 18 GHz.

The R&S DST200 RF diagnostic chamber is the ideal environment for RF analysis during development. It supports a wide range of radiated test applications for wireless devices and fits on any R & D lab bench, where it can be used at all times during the product design and optimization phase. The R & S DST200 effectively assists in achieving high first-time pass rates during final type approval, which saves time and money.

High-quality wireless devices have to pass special radiated tests such as desense and coexistence tests to ensure operation without self-interference. Verifying over-the-air (OTA) performance and measuring radiated spurious emissions (RSE) are also mandatory.
The R&S DST200 provides support for the radiated tests that are required in R & D, quality assurance, production and service. Compared with applications using large EMC anechoic chambers, test setups with the R&S DST200 are compact and easy to use and generate consistent, comparable results [14].

Its key facts are [14]:

- Anechoic RF chamber with highly effective shielding > 110 dB for interference-free testing in unshielded environments.
- Wide frequency range from 400 MHz to 18 GHz covering all important wireless standards.
- High reproducibility of measurements due to excellent field uniformity at location of equipment under test (EUT).
- Compact dimensions suitable for any lab environment.
- Unique mechanical design provides long-term stability and maintains high shielding effectiveness.
- Simple and effective front door locking mechanism without pneumatic components.
- Automated 3D positioner for OTA and RSE precompliance measurements.

In Tables A.1 to A.3 the main characteristics are specified.

RF Specifications		
Frequency range		400 MHz to 18 GHz
Antenna polarization		right-hand circular polarized
Shielding effectiveness	400 MHz to 700 MHz	>95 dB (meas.)
	700 MHz to 3 GHz	>110 dB
	3 GHz to 6 GHz	>100 dB
	6 GHz to 18 GHz	>75 dB (meas.)
Quiet zone	above EUT table, ⌀× L (cylindrical)	200 mm × 30 mm
Field uniformity	max. field variation in quiet zone	<3.2 dB (meas.)

Table A.1: RF Specifications of the Rohde & Schwarz DST200 RF Diagnostic Chamber [14].

RF connectors		
Test antenna	R&S DST-B220 option	1 × N, female

Table A.2: RF connectors of the Rohde & Schwarz DST200 RF Diagnostic Chamber [14].

General data		
Dimensions	W × H × D, with locking handle	770 mm × 760 mm × 695 mm
Weight		approx. 55 kg
Max. EUT dimensions	W × H × D	400 mm × 330 mm × 400 mm
Operating cycles		min. 66 000 cycles

Table A.3: General data of the Rohde & Schwarz DST200 RF Diagnostic Chamber [14].

Figure A.2: Rohde & Schwarz DST200 RF Diagnostic Chamber, exterior [14].

Figure A.3: Rohde & Schwarz DST200 RF Diagnostic Chamber, interior [14].

A.1.3 Ultra Broadband Antenna OmniLOG 70600

The OmniLOG® 70600 Antenna is specially developed as small and compact, broadband omni-directional antenna.
Despite its small size it covers an extremely wide frequency range of 680MHz to 6GHz. Within the most important frequency bands the antenna reaches very high gain up to 6.5dBi. It fits perfectly to the SPECTRAN Handheld Spectrum Analyzers but can also be used with any other Spectrum Analyzer brand.

The Antenna offers a heavy-duty 90° knuckle base with SMA connector. The knuckle base is freely adjustable into each position and fixed by two special ball pressure screws.

Every OmniLOG antenna goes through rigorous testing in our laboratories before dispatch. Its high-tech antenna-case (radome) offers protection against mechanical damage and environmental influence.

Figure A.4: Antenna OmniLOG 70600 [15].

In Table A.4 its technical data is presented:

Compatible with any Spectrum Analyzer brand	
Design	Omni-Directional (radial isotropic)
Frequency range	680MHz to 6GHz
Nominal impedance	50 Ohm
Peak Gain	6.5dBi
Avg. Gain	3.5dB
Avg. VSWR	2.5
RF connection	MA (m) or N (see optional adapter)
Temperature range	-20°C bis +70°C
Shock	40G at 10msec
Thermal Shock	-20°C bis +70°C
Dimensions (L/W/D)	173×62×9mm
Weight	54 g
Warranty	10 years
Estimated price	249.95 €

Table A.4: Technical data of the antenna [15]

And its main parameters are depicted in the following graphs:

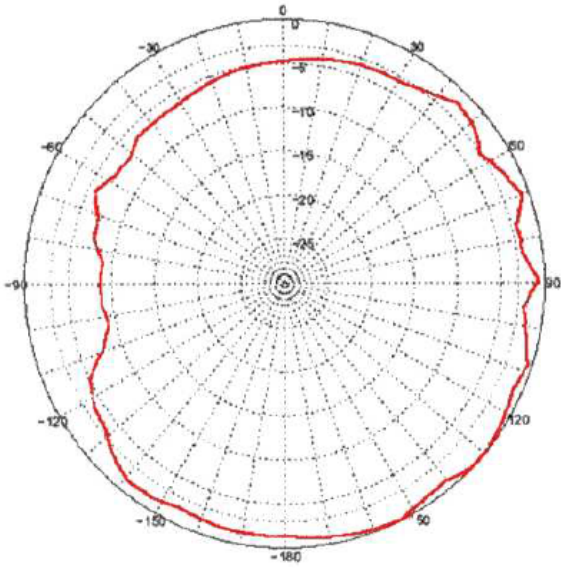

Figure A.5: Horizontal pattern of the OmniLOG 70600 [15].

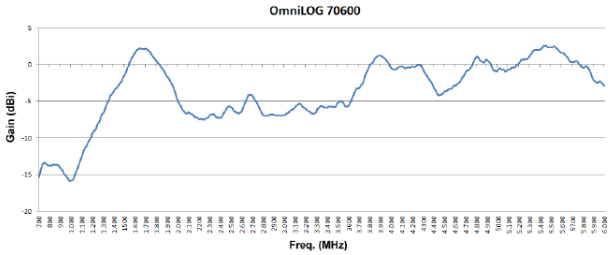

Figure A.6: Gain of the OmniLOG 70600 [15].

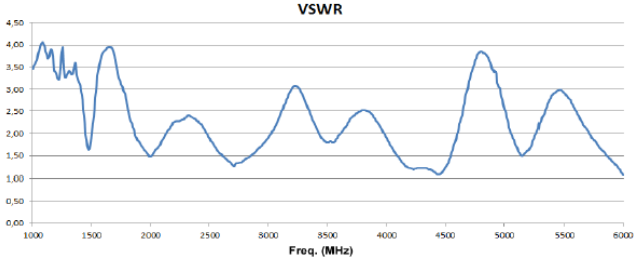

Figure A.7: VSWR of the OmniLOG 70600 [15].

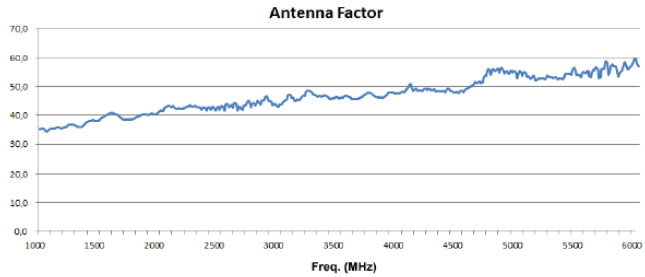

Figure A.8: Antenna Factor of the OmniLOG 70600 [15].

Estimated cost: 249.95 €.

A.1.4 N9916A FieldFox Handheld Microwave Analyzer

The main parameters of the Microwave Analyzer used to measure the S parameters are [16]:

- Maximum frequency: 14 GHz
- CAT/VNA Start Frequency: 30 kHz
- SA Start Frequency: 5 kHz
- Dynamic Range: 91 dB
- Output Power: -4 dBm
- Number of Built-In Ports: 2 ports
- Instrument Type: Combination Analyzer
- Cable and Antenna Analyzer: Yes-Standard
- Spectrum Analyzer: Yes-Optional
- Vector Network Analyzer: Yes-Optional
- Additional CAT/VNA Based Features: QuickCal (Subset), Vector Voltimeter, Mixed-Mode S-Parameters, DTF/DR Cable Measurements
- Additional SA Based Features: Built-In Power Meter, Extended Range Transmission Analysis (ERTA)
- System Features: Built-In DC Source and GPS Receiver-Internal Only
- Standard Attenuator Range: 30 dB
- Standard Attenuator Step: 5 dB
- DANL @1 GHz: -155 dBm
- Maximum Analysis Bandwidth: n/a
- Phase Noise @1 GHz (1 MHz offset): -113 dBc/Hz
- Phase Noise @1 GHz (10 kHz offset): -111 dBc/Hz
- Phase Noise @1 GHz (30 kHz offset): n/a
- TOI @1 GHz (3rd Order Intercept): +15 dBm
- Overall Amplitude Accuracy: ±0.5 dB
- Bandwidth Options: 5 MHz

- Applications-General Purpose: AM/FM Tune and Listen, Cable and Antenna Analysis, Field Strength Measurement, SCPI Code Compatibility, Spectrogram, Stimulus Response.

Estimated cost: 14874,70 €.

Figure A.9: N9916A FieldFox Handheld Microwave Analyzer [16].

A.2 Graphs

In this section the graphs of the S parameters and the absorption for the whole range of tested frequencies are shown. It is important to note that some peaks appear far from the optimization frequency. This could be due to different reason, which in any case fall out of the scope of this thesis.

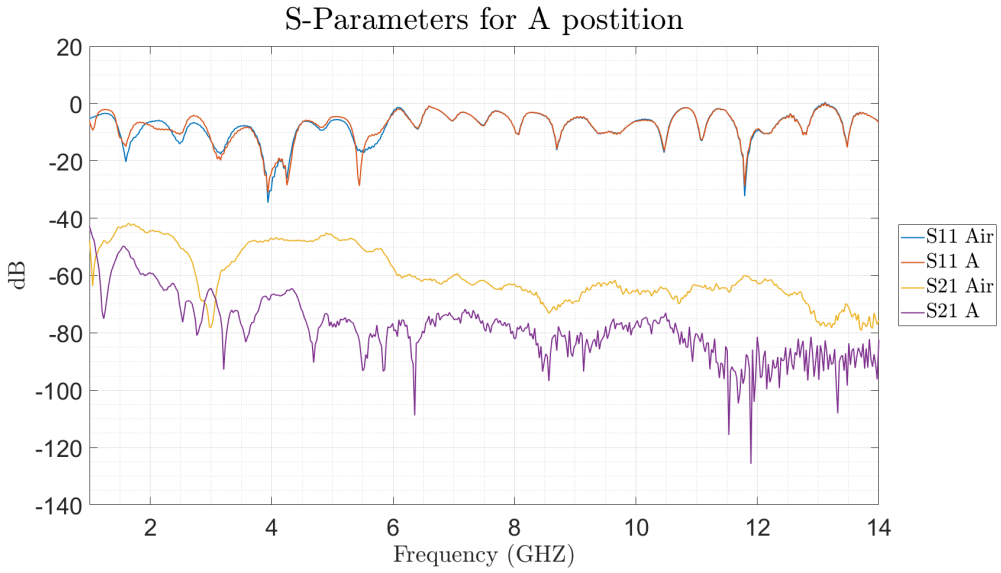

Figure A.10: S_{11} and S_{21} measured for the squares in A orientation. Experimental.

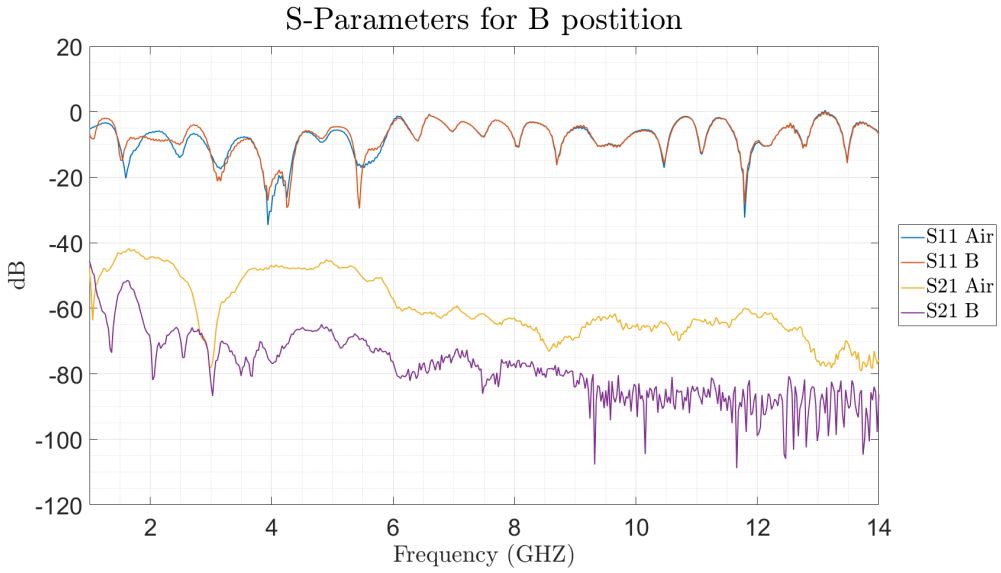

Figure A.11: S_{11} and S_{21} measured for the squares in B orientation. Experimental.

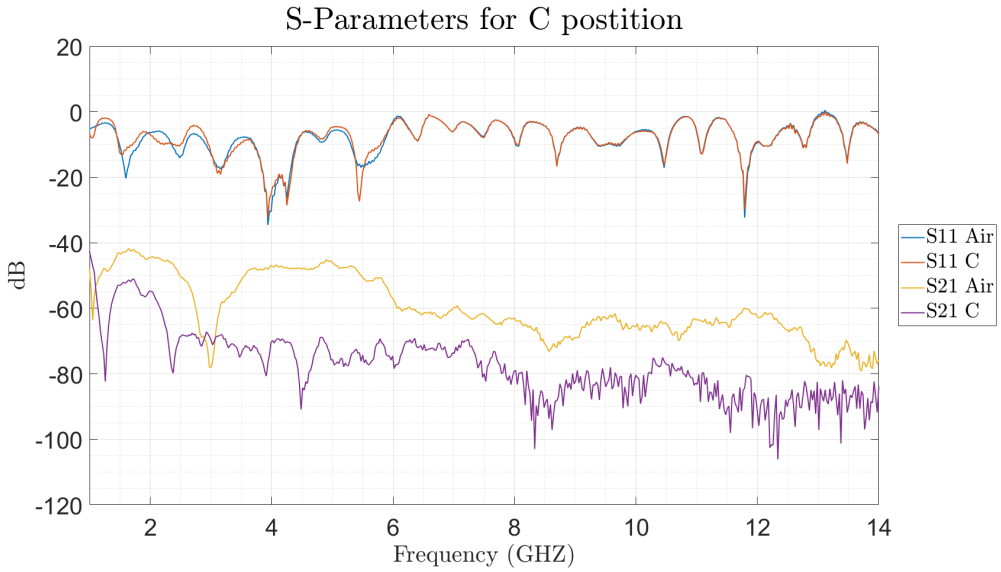

Figure A.12: S_{11} and S_{21} measured for the squares in C orientation. Experimental.

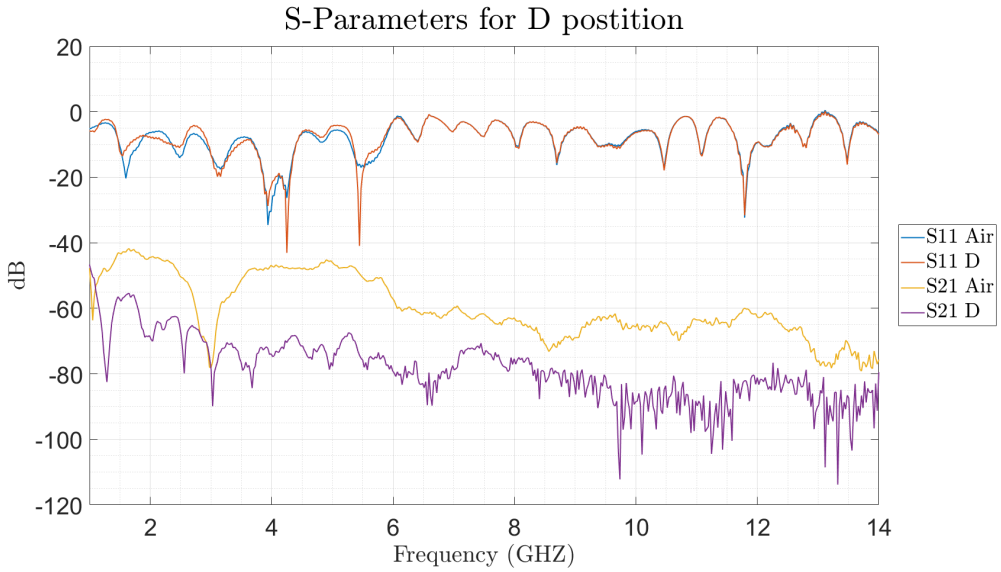

Figure A.13: S_{11} and S_{21} measured for the squares in D orientation. Experimental.

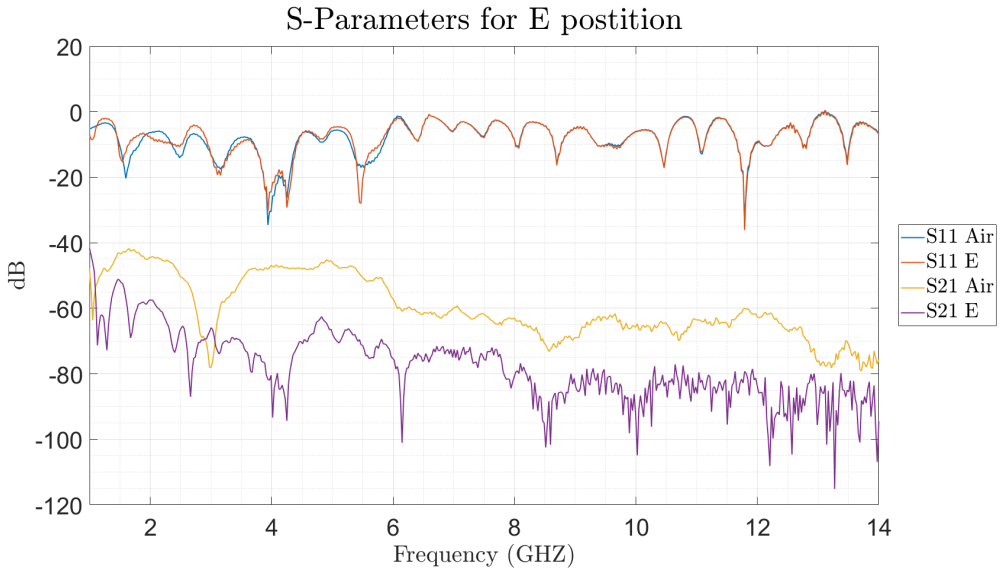

Figure A.14: S_{11} and S_{21} measured for the hexagons in E orientation. Experimental.

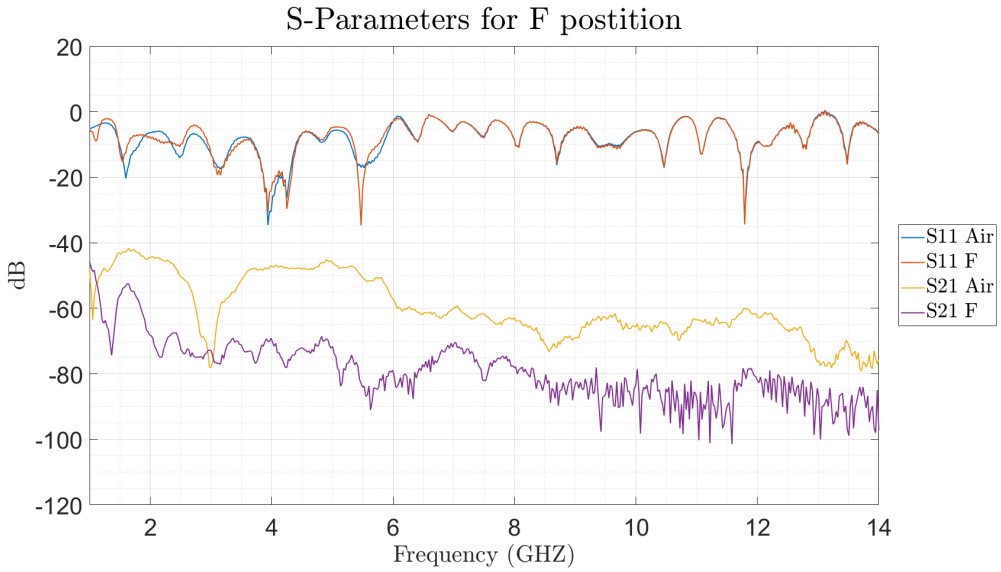

Figure A.15: S_{11} and S_{21} measured for the hexagons in F orientation. Experimental.

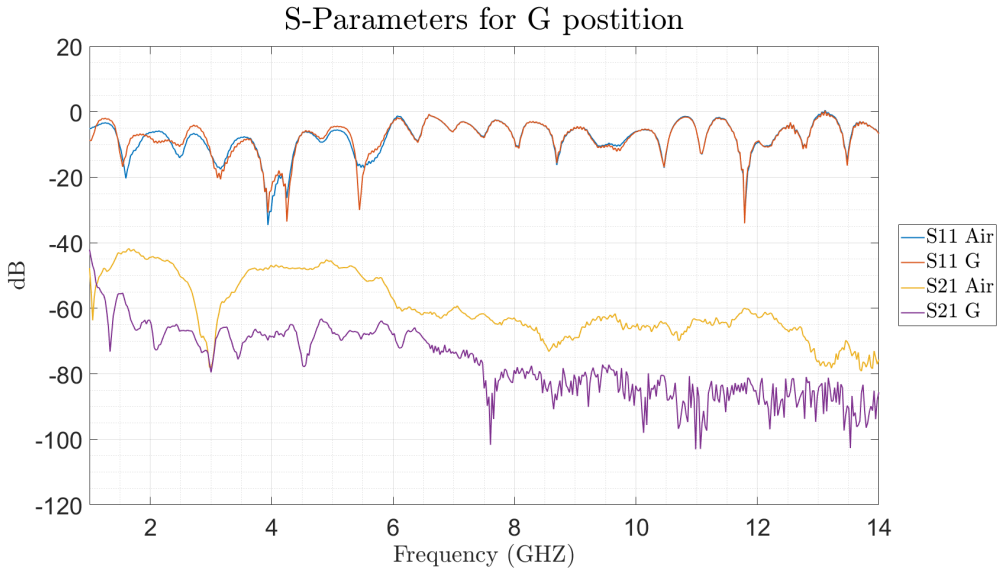

Figure A.16: S_{11} and S_{21} measured for the hexagons in G orientation. Experimental.

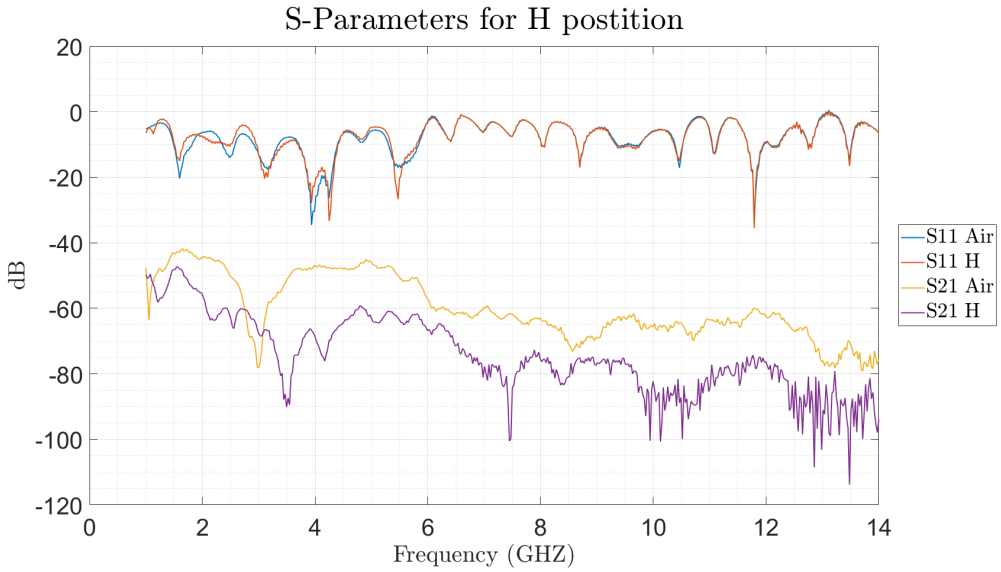

Figure A.17: S_{11} and S_{21} measured for the hexagons in H orientation. Experimental.

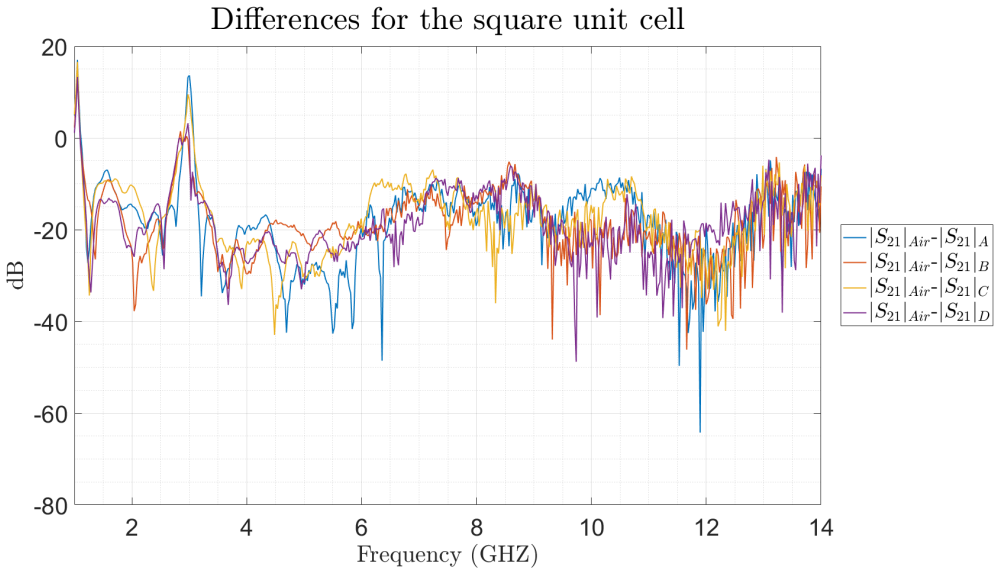

Figure A.18: Difference of the S_{21} parameter when the FSS with square unit cells is placed. Experimental.

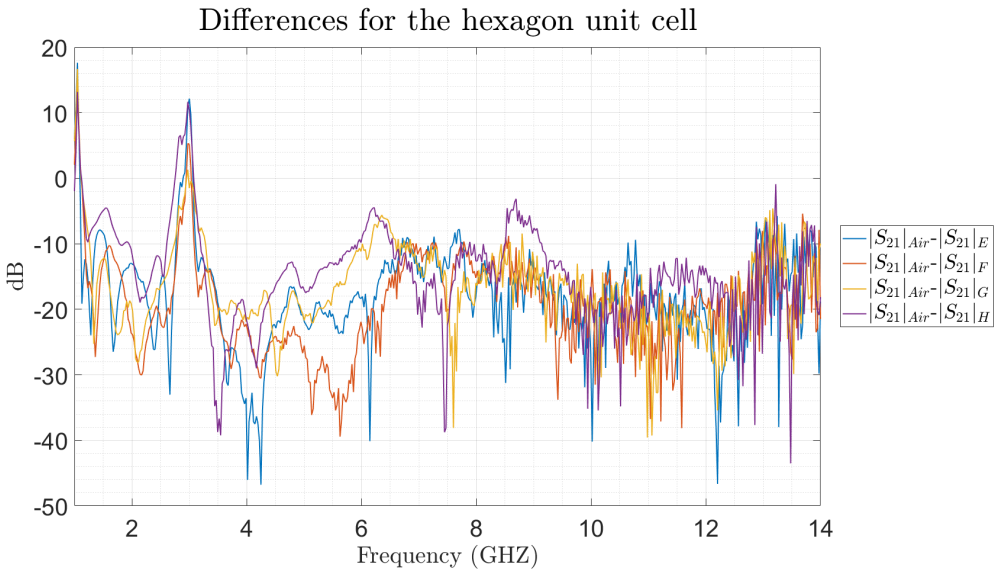

Figure A.19: Difference of the S_{21} parameter when the FSS with hexagon unit cells is placed. Experimental.